A study on the ORC for OTEC applications

Performance analysis for a changed configuration

J. J. Stelwagen

Master of Science Thesis

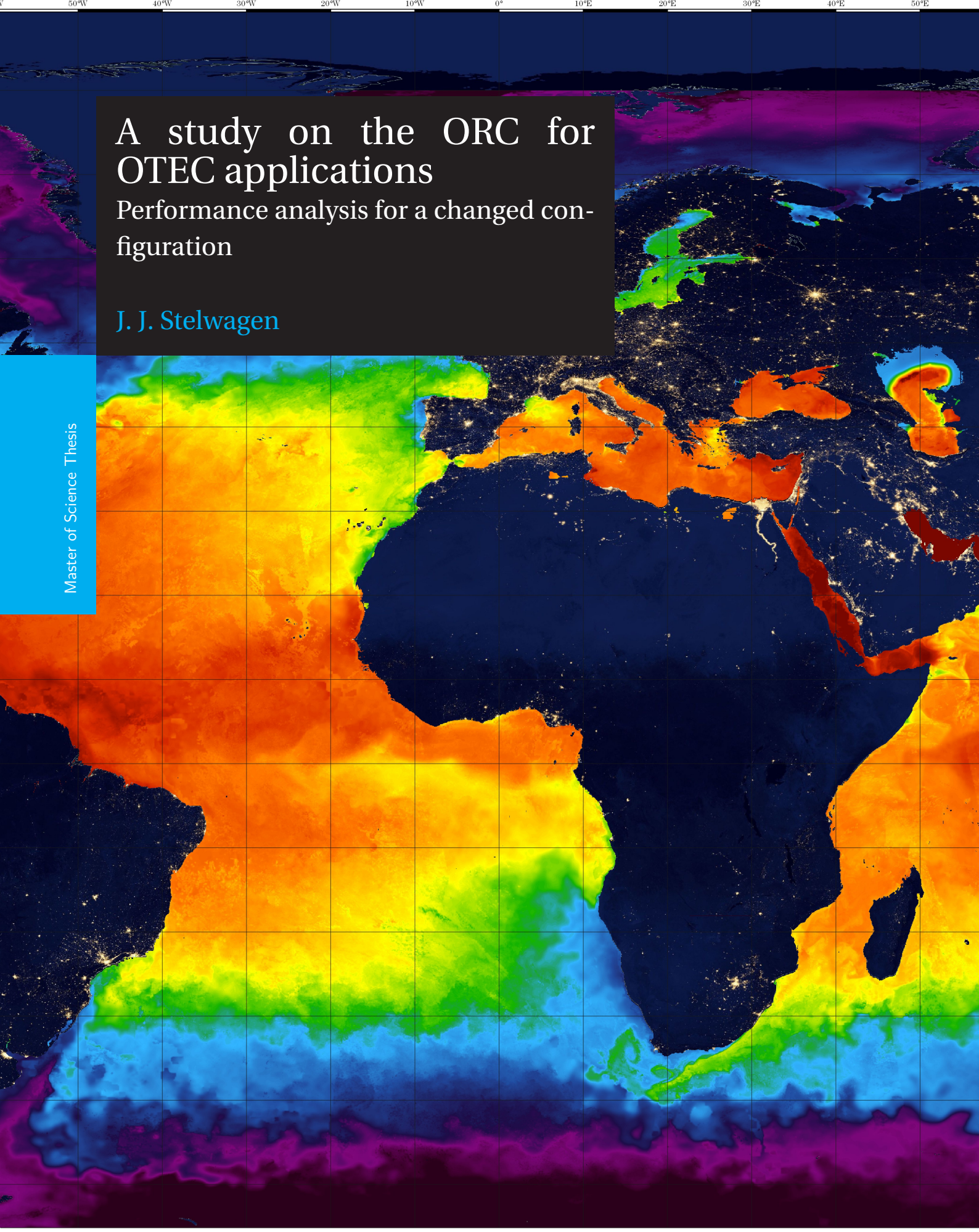

TU Delft Delft University of Technology

Challenge the future

A STUDY ON THE ORC FOR OTEC APPLICATIONS

PERFORMANCE ANALYSIS FOR A CHANGED CONFIGURATION

by

J. J. Stelwagen

in partial fulfillment of the requirements for the degree of

Master of Science
in Mechanical Engineering

at the Delft University of Technology,
to be defended publicly on 03-07-2019, 2019 at 11:00 AM.

Supervisor:	Dr. ir. C.A. Infante Ferreira,	TU Delft
Thesis committee:	Dr. ir. H. Polinder,	TU Delft
	Dr. O. Moultos,	TU Delft
	Ir. X. Tao,	TU Delft
	Ir. B. Harmsen,	Bluerise B.V.

An electronic version of this thesis is available at http://repository.tudelft.nl/.

TU Delft Delft University of Technology

The work in this thesis was supported by Bluerise B.V. Their cooperation is hereby gratefully acknowledged.

ABSTRACT

This thesis project aims to enable Bluerise to create a 3 [MW] plant for their OTEC system. The current model and lab setup used to create insight into the systems working mechanisms are based on a Kalina cycle configuration. This method uses a working fluid mixture of water and ammonia. After evaporation, the liquid and vapor are separated and the heated liquid is used in a recuperator to retain (some of) the heat and increase the efficiency of the system.

The first 3 [MW] test plant that is planned to be built will be using an ORC configuration. This method solely uses ammonia as a working fluid and doesn't use a recuperator to retain heat. Understanding the effects of liquid separation and re-circulation are important aspects while using this configuration.

The working method of the current OTEC off-design model and lab setup will have to be altered to accommodate the ORC configuration. An extensive study on both available literature, the current OTEC off-design model and OTEC Demo lab setup lead to conclude that a gear pump will be implemented to drive the liquid re-circulation from the separator back to the evaporator. Parallel to the gear pump, a one-way valve is installed into the cycle so natural re-circulation experiments can also be conducted. From literature, a hypothesis is made on what the effect on the evaporator heat transfer rate could be by changing the re-circulation rate. The re-circulation rate must not be too high, because increased amounts of vapor bubbles increase fluid mixing and thus heat transfer. The re-circulation rate also must not be too low, because dry-out in the evaporator will occur, reducing the heat transfer rate.

The OTEC off-design model that currently exists at Bluerise B.V. is used and expanded upon to accommodate the ORC configuration. The evaporator is changed in more detail, adding a heat transfer correlation and the possibility to calculate the evaporator pressure drop through two phase pressure drop correlations.
After implementing the gear pump liquid re-circulation technique, the OTEC Demo can be used to create experimental data.

From experiments, it is found that the re-circulation rate does not significantly change the evaporator heat transfer rate between 1.2 to 2.9 re-circulation rate. This is a remarkable result but can be explained by the low flow velocities in the evaporator, which indicate that the heat transfer process in the evaporator is mostly driven by pool boiling heat transfer mechanisms over flow boiling heat transfer mechanisms. Knowing that the re-circulation rate does not affect the evaporator heat transfer rate, liquid re-circulation can also happen naturally, by the liquid column driving force in the separator. Using this technique, a comparison with the Kalina cycle configuration using pure ammonia is made. The evaporator performance is higher in the Kalina cycle configuration, but the ORC configuration net power output is slightly higher. The main reason for this phenomenon is a lower required pumping power for the ORC configuration. The OTEC off-design model in ORC configuration is validated to the experimental data collected. The two phase heat transfer correlations used show to be very mass flux dependent, and applicable to flow boiling evaporative heat transfer. The correlations proposed by Taboas and Han et al. have the best fit to the experimental data. The correlation proposed by Taboas is used to validate the full cycle model. This two phase heat transfer correlation has a consistent negative deviation from the experimental data, causing the full cycle model to be conservative in the cycle performance it calculates.

Finally, a scaling analysis is made in support of the efforts by Bluerise to create a 3 [MW] OTEC plant. Using the geometries supplied by Bluerise it is concluded that a 3 [MW] net power output could be achieved, but it heavily depends on the water side pump power needed and the turbine efficiency, which are not investigated in the current research.

PREFACE

With rising energy demands and an increased interest in renewable heating and energy solutions, innovative ideas and technologies are being developed more and more. The OTEC system as designed by Bluerise B.V. will enable developing societies in tropical oceanic context to gain access to a renewable, abundant and consistent energy source. Using the ocean as a thermal battery, renewable solar energy can be utilized year round, 24 hours a day.

The subject of this thesis came to mind after discussing the current road map towards the first 250 [kW] prototype system to be constructed. The current model and lab system are based on a Kalina cycle. The first 3 [MW] power plant will be based on the ORC. These methods both impose different characteristics upon the system and to predict the performance of the first 3 [MW] prototype, research will have to be done. This opened up an opportunity for this master thesis to commence.

ACKNOWLEDGEMENTS

I would like to thank my supervisor Dr. Ir. Carlos Infante Ferreira for his assistance and feedback during the writing of this thesis, being ever so patient with my stubbornness.

I would like to thank PhD student Xuan Tao who helped me implement and commission the changes I made to the OTEC Demo test setup at the 3mE faculty.

Also my thanks go out to everybody at Bluerise B.V. who've helped and supported me during the full duration of this thesis project. Special thanks go out to Joost Kirkenier, for helping set up this thesis project and creating the opportunity for me to conduct research at Bluerise B.V. Special thanks also go out to Bram Harmsen, for being my thesis supervisor at Bluerise B.V., helping me overcome all obstacles, small or large.

J. J. Stelwagen
Delft, June 2019

"**The proper use of science is not to conquer nature but to live in it.**"
"I think the environmental crisis is a grim and terrible challenge. But on this day, this earth's new birthday, we accept this challenge. We declare that the proper use of science is not to conquer nature, but to live in it, that to save ourselves we must save the world that is our habitat. On this day we shall begin, by our own acts, to dedicate the wisdom of science and the power of technology to the welfare of man. We shall survive."

— Barry Commoner,
CBS news special: "Earth day, a question of survival", 22 April 1970

CONTENTS

NOMENCLATURE

Symbols

A	Surface area	[m^2]
Bd	Bond number	
Bo	Boiling number	
c_p	Specific heat capacity at constant pressure	[J/kgK]
c_v	Specific heat capacity at constant volume	[J/kgK]
D	Deviation	
d	Certain dimension or diameter, depending on subscript	[m]
E	Energy	[kg/s]
f	Fanning friction factor	
G	Mass flux	[kg/m^2s]
h	Enthalpy	[J/kg]
k	Thermal conductivity	[W/mK]
KE	Kinetic energy	[J]
L	Length	[m]
L_p	Plate length	[m]
L_w	Effective plate width	[m]
M	Mass	[kg]
$\dot{m}$	Mass flow rate	[kg/s]
N_e	Effective number of channels	[kg]
Nu	Nusselt number	
p	Pressure	[Pa]
P_c	Corrugation pitch	[m]
Pr	Prandtl number	
$\dot{Q}$	Heat transfer rate	[W]
q	Vapor quality	
$q"$	Heat flux per unit area	[W/m^2]
r	re-circulation rate	
Re	Reynolds number	
std	Standard deviation	

Symbols

t	Wall thickness	[m]
T	Temperature	[K]
U	Overall heat transfer coefficient	[W/m^{2}K]
u	velocity	[m/s]
$\dot{V}$	Volumetric flow rate	[m^3/s]
V	Unit volume	[m^3]
v	specific volume	[m^3/kg]
W	Work	[W]
We	Weber number	
X	Lockhart-Martinelli parameter	
y	Vertical column height (liquid)	[m]

Subscripts

a	Acceleration
avg	Average
$cold$	The stream with lowest inlet temperature
$conv$	Convective
$crit$	A critical state
cv	control volume
$duty$	An imposed amount by geometry
eq	Equivalent
f	Friction
g	Gravitational
$head$	Pressure built up by vertical height
hex	Heat exchanger
in	The inlet stream
is	Isentropic
liq	The liquid state
liq,o	Property calculated as if the two phase stream is liquid only
$LMTD$	The logarithmic mean temperature difference
$load$	An imposed amount by cold/ warm source
lv	A phase change from liquid to vapor
man	Manifolds
out	The outlet stream
sl	from subcooled to saturated liquid state
tp	A two phase state
vap	The vapor state
vap,o	Property calculated as if the two phase stream is vapor only
$warm$	The stream with highest inlet temperature

Greek

α	Heat transfer coefficient	[W/m^{2}K]
β	Chevron angle	[°]
γ	ratio between specific heat capacity at constant pressure over specific heat capacity at constant volume	
Δ	Difference	
η	Efficiency	
θ	Bubble contact angle	[°]
μ	Kinematic viscosity	[Pa s]
ρ	Density	[kg/m^3]
Φ	Surface enhancement factor	
ϕ	Liquid or gas two phase friction multiplier, depending on subscript	

GLOSSARY

CHF Critical Heat Flux. 22

GMTD Generalized Mean Temperature Difference. 36

LMTD Logarithmic Mean Temperature Difference. 10

MHF Minimum Heat Flux. 22

ONB Onset of Nucleate Boiling. 22

ORC Organic Rankine Cycle. iii

OTEC Ocean Thermal Energy Converter. iii

P&ID Piping & Instrumentation Diagram. 28

PFD Process Flow Diagram. 27

SWAC Sea Water Air Conditioning. 1

1

INTRODUCTION

1.1. BACKGROUND

In recent years, the demand and interest in sustainable energy technologies have seen a rise, following the increase in understanding of climate change and its consequences. Climate change is already having an impact on several economies, communities, and ecosystems around the planet [1]. The use of fossil fuels to power and provide heating and cooling for our dwellings and industries will have to be reduced. Providing safe, reliable and sustainable energy to all people is one of the greatest challenges thrust upon humanity in this day and age [2].

With current developments in technologies, policies, and understanding, sustainable energy sources are starting to compete economically with fossil energy sources. Sustainable energy sources will be able to provide our energy demand in a cost-efficient way more and more in the (near) future.

The OTEC system, as designed by Bluerise B.V. will be able to provide the energy demand in the context of tropical oceanic communities. An OTEC system utilizes the temperature difference in oceanic water to generate electricity. Figure 1.1 shows the areas on the planet where the ocean surface temperature is high enough (minimum 25 °C) for OTEC systems to be applicable. Using the temperature difference between surface and deep seawater, many different applications can be provided, see Figure 1.2.

According to Bluerise B.V., more than 50% of the energy used in tropical oceanic communities, is put into air conditioning. By pumping up cold deep seawater this cooling demand can be met while reducing the energy used for air conditioning by 90%. This technique is called SWAC.

The temperature difference between surface and deep seawater can also be used to generate electricity. OTEC is the name given to systems specifically designed to convert this temperature difference into usable work (or electricity) [3]. The combination of both SWAC and OTEC systems can create the opportunity for tropical oceanic communities to completely switch to renewable energy sources and become independent of fossil fuels.

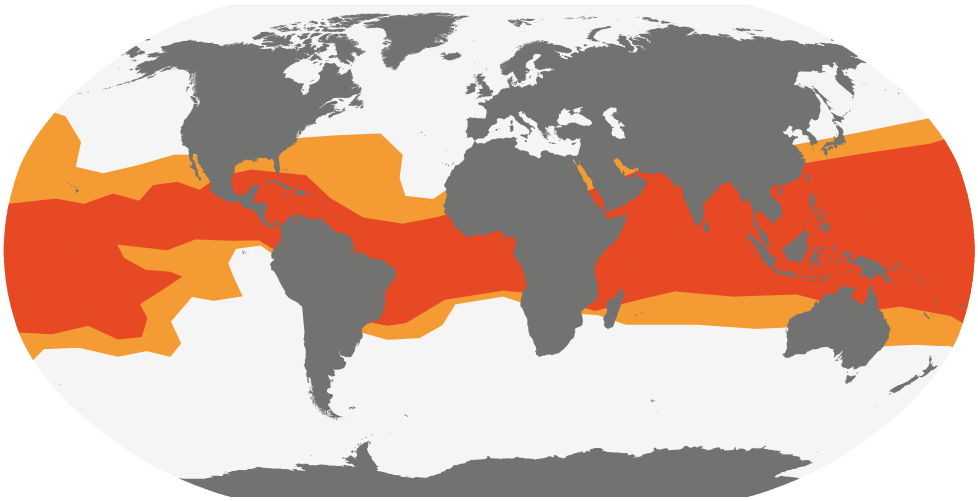

Figure 1.1: Ocean surface water temperature. Orange indicates surface water of at least 20 °C, while darker orange indicates surface water of 25 °C and higher. Source [3]

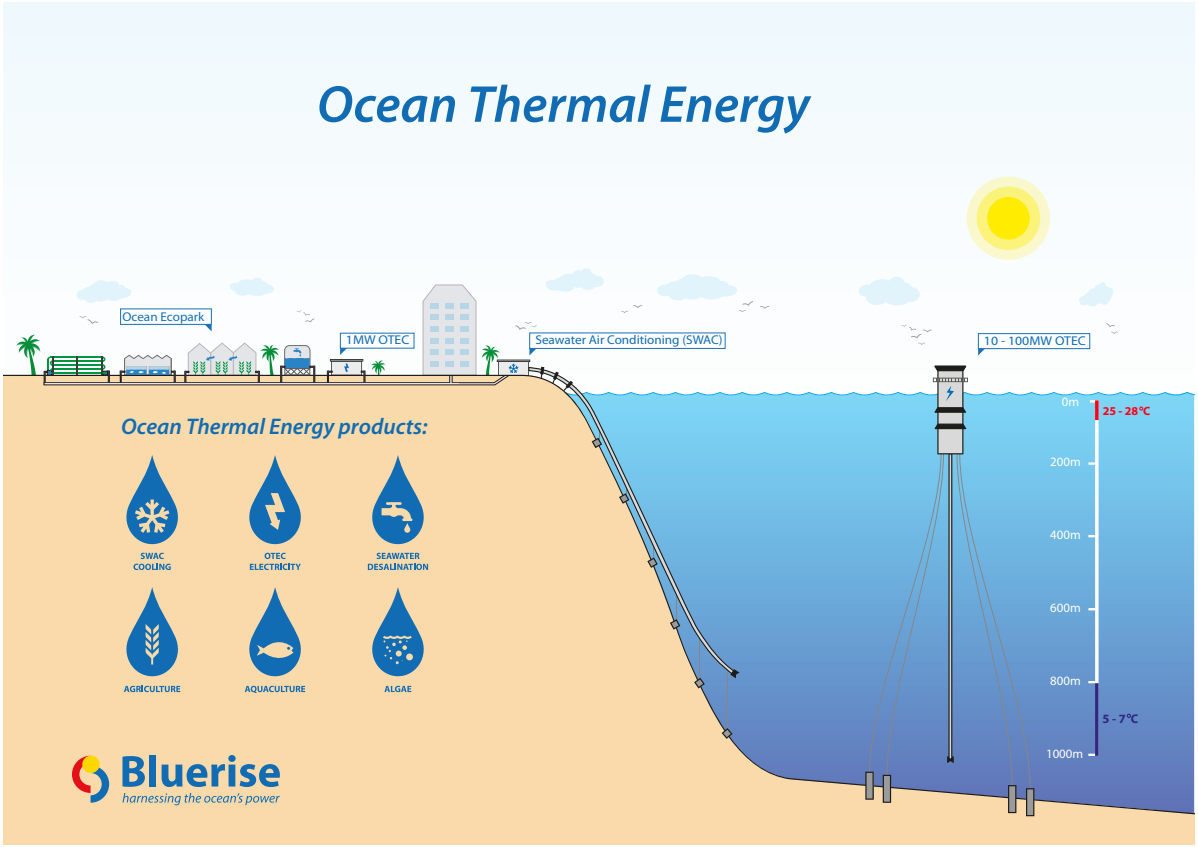

Figure 1.2: Applications for ocean thermal energy. Source Bluerise B.V.

1.2. ORC VS KALINA

1.2.1. BASIC WORKING PRINCIPLES

The basic ORC configuration of the OTEC system can be seen in Figure 1.3. Warm surface water is being pumped through the evaporator (step 2-3), transferring heat to the working fluid causing it to evaporate. This high pressure vapor is then fed through a turbine (step 3-4) generating electricity and reducing the pressure. After leaving the turbine, the working fluid is condensed in the condenser (step 4-1), by transferring heat to the cold deep seawater that is being pumped up. A pump that increases the pressure of the working fluid (step 1-2) closes the loop. [3]

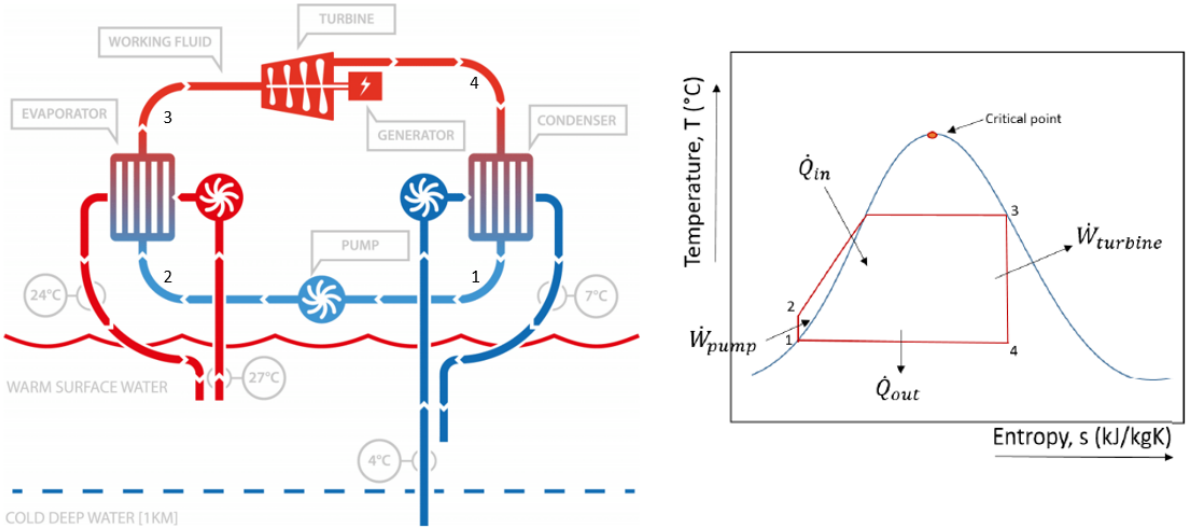

Figure 1.3: Schematic representation of the simple ORC cycle that forms the basis for the OTEC system designed by Bluerise B.V. including the corresponding T-S diagram. Source [4] & [5]

The T-S diagram in Figure 1.3 shows the thermodynamic cycle that represents the ORC. The steps between 1-2 (over the pump) and 3-4 (over the turbine) represent adiabatic processes. The steps between 2-3 (over the evaporator) and 1-4 (over the condenser) represent isobaric processes [5].

The first law of thermodynamics dictates for any system (or cycle) that the energy going into the system has to be equal to the energy leaving the system:

$$\Delta E = E_{out} - E_{in} = 0 \tag{1.1}$$

For any point in this closed cycle, the mass and energy equations hold:

$$\frac{dM}{dt} = \dot{m}_{in} - \dot{m}_{out} \tag{1.2a}$$

$$\frac{dE}{dt} = \dot{m}_{in} * h_{in} - \dot{m}_{out} * h_{out} + \dot{Q}_{total} - W_{total} \tag{1.2b}$$

In these equations, $\dot{m}$ is the mass flow and $\frac{dM}{dt}$ is the rate of change of mass, both in [kg/s]. h_i is the enthalpy of the respective stream in [J/kg]. $\frac{dE}{dt}$ is the rate of change of energy, $\dot{Q}_{total}$ is the rate of heat to the system and W_{total} is the rate of useful work produced by the system, all three in [W].

The OTEC model and test setup designed by Bluerise B.V. is currently using a Kalina cycle as a working principle. A schematic representation of this cycle can be seen in Figure 1.4. This method uses a mixture of water and ammonia as a working fluid.

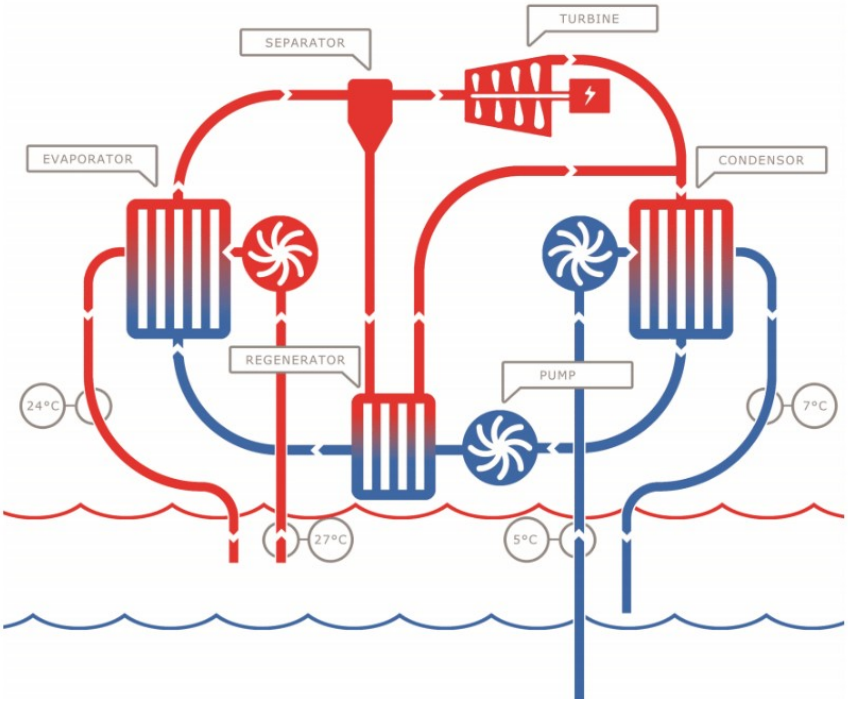

Figure 1.4: Schematic representation of the Kalina cycle used in the Bluerise B.V. OTEC system. Source [4]

The main reason for using a mixture in the Kalina cycle is that it benefits the performance of the evaporator. This does, however, create the need for an additional separator after the evaporator. Using a mixture of ammonia and water causes the working fluid to only partially evaporate inside the evaporator. To prevent liquid from going into the turbine, which would quickly destroy the turbine, a separator is installed. The separator separates the working fluid liquid phase from the working fluid vapor phase. The liquid phase is then passed through a recuperator, before returning to the condenser. The vapor phase is expanded over the turbine and then fed to the condenser.

The separator that's currently being used is a vertical wire-mesh separator, where gravity is the main driver for separation. The function of the recuperator is to ensure the highest amount of thermal energy to be taken from the seawater, so less seawater will have to be pumped into the system, increasing efficiency [5].

1.2.2. WORKING FLUID

According to the research of Ganic and Wu [6], ammonia is the best working fluid for OTEC applications, requiring the lowest heat exchanger surface area in both the evaporator and the condenser. This low heat exchanger surface area requirement is a result of the relatively high thermal conductivity and large latent heat of vaporization of ammonia. Even though ammonia has some toxic and corrosive properties, it is still considered the best working fluid for the OTEC installation.

In Figure 1.5 the temperature glide of a non-azeotropic mixture can be seen. If the temperature glide can follow the temperature profile of the cold and warm source, an increase in the surface area of the cycle within the T-S diagram can be realized. This increase in surface area within the T-S diagram results in a higher heat exchanger performance, compared to the pure fluid, while maintaining the same characteristics for the cold and warm source flow.

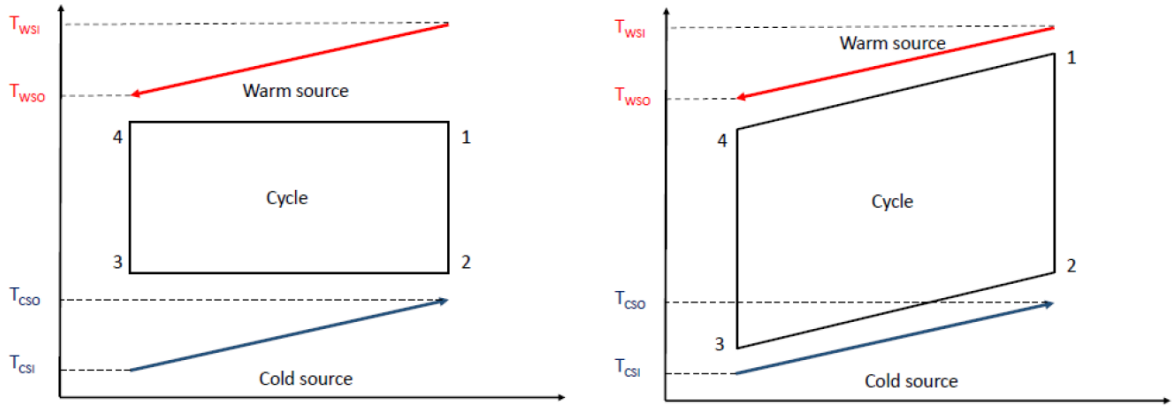

Figure 1.5: T-S diagram for a pure fluid ORC (left) and a non-azeotropic mixture Kalina cycle (right). Source [5]

1.3. RELEVANCE

In the previous section, a short introduction towards the difference between a Kalina cycle and an ORC has been given. This difference forms the basis for the research discussed in this thesis report. Currently, the Bluerise B.V. model and lab setup are based on the Kalina cycle method. The first 3 [MW] prototype to be built will, however, be based on an ORC method. Changing from the Kalina cycle configuration to an ORC configuration will, without doubt, affect the cycle layout, operation characteristics, and performance.

The reason behind changing the design from a Kalina cycle configuration to an ORC configuration is explained by costs. Proving the feasibility for OTEC systems to (potential) investors, it's all dependent on cost-effective means of power generation, able to compete with fossil fuel technologies from an economic perspective. The bulk of the costs for an OTEC system are caused by the heat exchangers. Because the temperature difference between the warm source (roughly 27 °C water) and the cold source (roughly 5 °C water) is so small, a large heat exchanger surface area will be required. Even though the Kalina cycle has better evaporator performance with the same warm and cold source characteristics, it is likely that a much larger total heat exchanger surface area is required. One of the reasons for this is the use of a recuperator, which is a full additional heat exchanger. Mancini et al. [7] also discuss heat transfer degradation caused by the working fluid being a mixture, which will be discussed in more detail in Chapter 2.

The relevance of this research for Bluerise B.V. will be in determining an optimized working method for the ORC configuration. The basic ORC configuration as explained before is a very simple system where the working fluid runs through the system in a loop. This can only be done provided that all the working fluid evaporates in the evaporator, so no separation is required. But superheating the working fluid in the evaporator will cause a decrease in the total heat transferred in the evaporator. When superheating the working fluid, heat is transferred to the vapor phase and will just raise the vapor phase temperature. The heat transfer rate to a vapor phase only working fluid is significantly lower than the heat transfer rate to a two phase working fluid state.

Superheating the working fluid is undesirable, however, this doesn't tell us anything on the desired degree of vaporization to achieve the highest heat transfer. Determining how to achieve the highest possible heat transfer rate in the evaporator is key to achieve the highest performing OTEC ORC configuration.

If the working fluid inlet temperature, heat exchanger characteristics and all warm side characteristics remain the same, the only variable that determines the degree of evaporation on the working fluid side is the working fluid mass flow rate through the evaporator. Literature suggests that increasing the mass flow rate through the evaporator will have a small effect on the evaporator heat transfer coefficient for pure ammonia. At higher mass flow rates, a lower vapor quality outlet can be expected to leave the evaporator. The vapor quality inside the heat exchanger also affects the local heat transfer coefficient. In Figure 1.6 a plot can be seen of the local heat transfer coefficient vs the vapor quality for an ammonia/ water mixture and pure ammonia at different mass fluxes.

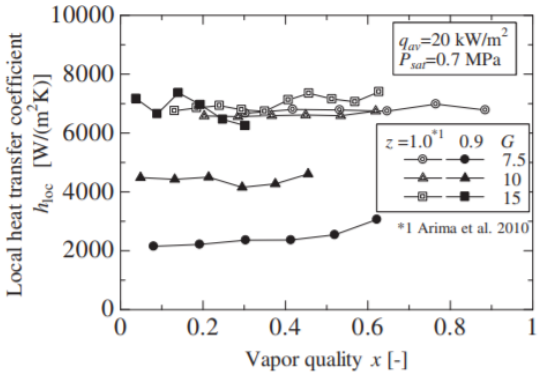

Figure 1.6: Comparisons of local heat transfer coefficient in vertical plate heat exchangers for an ammonia/ water mixture (black lines) and pure ammonia (grey lines) at different mass fluxes. Source [8]

For the ammonia water mixture, the rise in local heat transfer coefficient with increasing mass flow is evident, but for pure ammonia, the difference is not that clear. How the vapor quality affects the local heat transfer coefficient also looks inconsistent, as there is no clear increase or decrease over differing vapor fractions.

Partial vaporization of the working fluid in the evaporator will cause the need for separation of the working fluid vapor phase from the working fluid liquid phase after the evaporator. The separator, as used in the Kalina cycle configuration, will also be implemented in the ORC configuration. The liquid working fluid fraction will be re-circulated to the evaporator, joining the working fluid stream coming from the main cycle pump, as can be seen in Figure 1.7. The re-circulation rate and mass flow through the evaporator are dependent on one another. When the mass flow rate through the evaporator increases, the vapor fraction in the evaporator outlet decreases and the liquid fraction in the evaporator outlet increases. Consequently, the liquid mass flow coming from the separator is increased until a new balance is created.

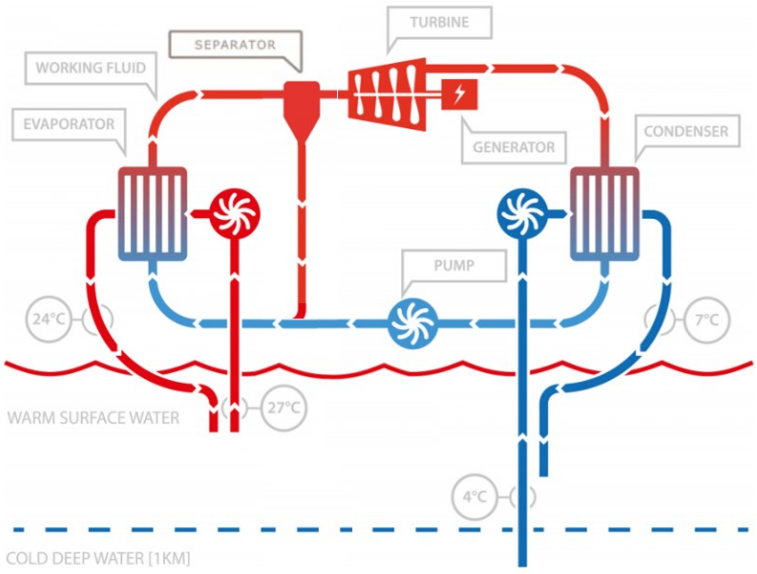

Figure 1.7: Schematic representation of the OTEC ORC lay-out including separation and re-circulation of the overfed evaporator

1.4. OBJECTIVE

The main objective of this thesis research is to identify the differences in performance and operating characteristics between a Kalina cycle configuration and an ORC configuration for the Bluerise B.V. OTEC system. The scope is narrowed down on the evaporator, where the effect of re-circulation and operating pressure on the evaporator performance will be modeled and tested. This research will be executed to support the first 3 [MW] ORC OTEC system that is planned to be built. The main research question then follows:

How will changing the OTEC system working principle from a Kalina cycle configuration to an ORC configuration influence the system performance and operating characteristics?

Accompanying sub-questions for this research assignment will be:

1. What is the working mechanism of the current system and how are working fluid states calculated in the Kalina cycle configuration?
2. How can liquid separation and re-circulation be applied to the OTEC cycle?
3. What is known from literature on evaporator performance dependent on evaporator re-circulation?
4. How can the current OTEC Demo configuration be adjusted to implement an ORC configuration?
5. How can the current OTEC off-design model be adjusted to implement an ORC configuration?
6. How is the evaporator performance in the ORC configuration influenced by its re-circulation rate?
7. How is the evaporator performance in the ORC configuration and Kalina cycle configuration influenced by the evaporator operating pressure?
8. How is the full cycle performance in the ORC configuration and Kalina cycle configuration influenced by the orifice pressure drop?
9. How well does the ORC configuration perform compared to the Kalina cycle configuration?
10. How can the results of the performance analysis be scaled to a 3 [MW] system?

1.5. METHODOLOGY

To achieve a satisfactory result for this thesis research a clear vision on the structure of the work has to be created. To prevent doing work that has already been done in the past, getting false results and drawing premature conclusions, the methodology for the research has to be correct and followed throughout the research.

The sections below shortly describe the different means of acquiring knowledge on the subject in a structured and thorough manner.

1.5.1. LITERATURE REVIEW

A literature review is needed to create a solid foundation of knowledge on which to base the research. Proposed correlations, assumptions and methods can be applied and don't have to be reinvented to prevent re-doing what has already been done by others. The literature review also creates a frame of reference on the state of technology concerning the subject to understand the severity of the challenge of this research. The goal of the literature study is to answer the first three sub-questions posed above.

1.5.2. OTEC DEMO ADJUSTMENTS

The OTEC test setup called the "OTEC Demo" has been in use for many years and has already proven its worth to Bluerise B.V. Understanding its working mechanisms, sensor layout and constraints is important before making adjustments to create the ORC configuration. Another constraint considering the OTEC Demo is the fact that multiple people are using this setup at the same time. Adjustments need to be made in such a way that they're easily implemented but just as easily reversed. This way the setup can be reset to its old configuration in a relatively short time frame. The goal of the OTEC Demo adjustments is to answer sub-question four.

1.5.3. MODEL ADJUSTMENTS
The current off-design model for the Bluerise OTEC system can be used to create insight into the working method and working fluid states for the Kalina cycle configuration. The model has been used for many years and though being successfully tested, it has become quite complex and large. An extensive study on the working mechanism of this model is needed, after which changes can be implemented to facilitate an ORC configuration of the OTEC system in the model. The goal of the Model Adjustments is to answer sub-question five.

1.5.4. VALIDATION, VERIFICATION & EXPERIMENTAL PROCEDURE
The created model will need to be validated before a certain amount of confidence in the results can be established. This validation will be done by using the OTEC Demo and comparing data sets from both the model and the OTEC Demo. Only if validation of the model has been done correctly, any claims on the performance of the 3 [MW] OTEC plant can be made. Experiments will also be executed to test the performance of the cycle and the evaporator on varying re-circulation rates and turbine pressure drops. These experimental results will be compared to the OTEC model. The results from these experiments will also be used to make a comparison between the performance of the ORC configuration and Kalina cycle configuration. The goal of the Validation, Verification & Experimental Procedure is to answer sub-question six, seven, eight and nine.

1.5.5. SCALING ANALYSIS
Using the result of the Validation, Verification & Experimental Procedure, an off-design scaling analysis towards a 3 [MW] OTEC ORC system can be made. The design of this system is made by Bluerise and will be tested in the validated OTEC model. The results can then be compared by Bluerise B.V. to the results of other simulation tools they're using. The goal of the Scaling Analysis is to answer sub-question ten.

1.5.6. CONCLUSIONS & RECOMMENDATIONS
The work done during this thesis assignment will be summarized and conclusions on the results will be formulated. Recommendations on improvements or interesting subjects for follow-up studies will also be given.

2

LITERATURE STUDY

2.1. WORKING FLUID STATE CALCULATIONS

As stated before, according to the research of Ganic and Wu [6] ammonia is the best working fluid for the OTEC application. In this chapter, some properties and the calculation of different states of ammonia in the system will be discussed.
The thermodynamic properties of ammonia are taken from REFPROP [9]. REFPROP is one of the most complete fluid libraries available. CoolProp [10] offers the ability to directly link the REFPROP database to the Python model.
The following sections are divided into separate components that make up the OTEC cycle. For each component, some design and operating equations are given that have been used in the off-design system model that is created at Bluerise B.V. Most of these design and operating equations will be used in the re-designed ORC OTEC system and will therefore be discussed in this chapter.

2.1.1. HEAT EXCHANGERS

The heat exchangers are the main interest in the scope of this thesis assignment. When re-designing the OTEC system from a Kalina cycle configuration to an ORC configuration, the heat transfer and evaporation/ condensation characteristics will change. This section will shortly discuss the way the heat exchangers are defined and how the heat transfer is calculated. The focus will be on the evaporator.

PLATE HEAT EXCHANGER GEOMETRY AND FLOW ARRANGEMENT

Plate heat exchangers have been chosen in a previous design phase of the system [11] and will still be used in the current re-designing of the system. Plate heat exchangers provide a compact solution with a good heat transfer to cost ratio. Titanium plate heat exchangers are currently used as seawater and especially ammonia can be corrosive to other materials. Research is also being done on the possibility of using polymer heat exchangers but they are not being used at the time of writing [12].
The heat exchangers operate in countercurrent flow arrangement with Chevron type plates. The basic geometrical parameters for this type of plate heat exchanger can be seen in Figure A.1 in Appendix A. To calculate the heat transfer for a plate heat exchanger, the effective heat transfer surface area has to be calculated. How this is done can also be seen in Appendix A.

DESIGN EQUATIONS

For the design of the ORC, it can be assumed that the heat exchanger geometries are known and with these fixed parameters, the outlet working fluid states can be calculated. Following this guideline, general mass and energy conservation over the heat exchangers can be applied, as can be seen in Goudriaan [11].

The heat transferred from the warm water side to the working fluid side can be calculated as follows:

$$\dot{Q}_{load} = \dot{m}_{warm}(h_{warm,in} - h_{warm,out}) \tag{2.1a}$$

$$\dot{Q}_{load} = \dot{m}_{warm} c_{p,warm}(T_{warm,in} - T_{warm,out}) \tag{2.1b}$$

Where $\dot{Q}_{load}$ is the heat load of the water flow to the evaporator in [W]. $\dot{m}_{warm}$ is the mass flow of the warm water in [kg/s]. $h_{warm,in}$ and $h_{warm,out}$ are the respective in- and outlet enthalpies of the warm water in [J/kg]. $c_{p,warm}$ is the specific heat coefficient of the warm water in [J/kgK]. $T_{warm,in}$ and $T_{warm,out}$ are the respective in- and outlet temperatures of the warm water in [K]. The subscript $warm$ changes to $cold$ when applied to the condenser heat exchanger.

The amount of heat that can be transferred to the working fluid is mainly determined by the heat exchanger geometry and is described by the following equation:

$$\dot{Q}_{duty} = U_{hex} A_{hex} \Delta T_{LMTD} \tag{2.2}$$

Where $\dot{Q}_{duty}$ is the heat duty of the evaporator or condenser in [W]. U_{hex} is the overall heat transfer coefficient of the heat exchanger in [W/m^{2}K]. A_{hex} is the total heat transfer area in [m^2]. ΔT_{LMTD} is the LMTD between the in- and outlet of the heat exchanger in [K].

The LMTD is calculated as follows:

$$\Delta T_{LMTD} = \frac{(T_{warm,in} - T_{cold,out}) - (T_{warm,out} - T_{cold,in})}{ln \frac{T_{warm,in} - T_{cold,out}}{T_{warm,out} - T_{cold,in}}} \tag{2.3}$$

The overall heat transfer coefficient of the heat exchangers is calculated as follows [11]:

$$\frac{1}{U_{hex}} = \frac{1}{\alpha_{fouling}} + \frac{1}{\alpha_{conv,warm}} + \frac{1}{\alpha_{conv,cold}} + \frac{t}{k_{wall}} \tag{2.4}$$

Where $\alpha_{fouling}$ is the fouling resistance, $\alpha_{conv,warm}$ and $\alpha_{conv,cold}$ are the convective heat transfer coefficient of the warm and the cold stream respectively, all three in [W/m^{2}K]. t is the plate thickness in [m]. k_{wall} is the thermal conductivity of the plate material in [W/mK].

HEAT TRANSFER CORRELATIONS

To date, multiple correlations have been created to define the heat transfer rate in plate heat exchangers for boiling and condensing purposes. The methods vary in their methodology and the results they produce [11]. At Bluerise B.V., several assessments on these correlations have been made by graduation students. In this section, the heat transfer correlations for the evaporator will be discussed.

Evaporation is the phase-change process where the saturated or subcooled working fluid liquid turns partially or fully into a vapor. A general overview and explanation for this process can be seen in Appendix B. In plate heat exchangers, the flow regime is assumed to be comparable to the one displayed in Figure B.1.

For plate heat exchangers, consensus about the dominant heat transfer mechanism has not been reached in recent years [13]. In general, there are two different transfer mechanisms that both get pointed out by literature to have the greatest impact. Panchal et al. [14], Engelhorn and Reinhart [15], Oserberger and Slipcevic [16], Pelletier [17], and Hsieh and Lin [18] all found nucleate pool boiling to be of dominant influence. Convective flow boiling was found to be dominant by Margat et al. [19] and Han et al [20].
Nucleate pool boiling occurs in a static liquid when the heat flux is below the critical heat flux and vapor bubbles slowly appear on the liquid surface. Convective boiling shares a lot of characteristics with nucleate pool boiling, however, forced convection imposes some specific conditions on how the vapor bubbles are formed and how they breakaway into the bulk of the liquid [21].

Over the years, several heat transfer correlations have been created to determine the heat transfer in a single phase and a two phase flow for plate heat exchangers. In previous research done at Bluerise B.V., these heat transfer correlations have been assessed and tested, but for the validity of the research done in this thesis assignment, they will be re-evaluated.

Gudjónsdóttir [22] showed in her research that the correlation developed by Yan & Lin [23] predicted the two phase evaporating heat transfer the best in combination with the correlation by Donowski & Kandlikar [24] for the single phase heat transfer. Following up on the research done by Gudjónsdóttir, Goudriaan [11] and Kuikhoven [25] developed an additional single phase heat transfer correlation suited for the water side of the

plate heat exchanger. This correlation is based on experiments done on the OTEC demo and provides higher accuracy than the one created by Donowski & Kandlikar. In the following two sections these single and two phase heat transfer correlations will be discussed.

The basis for the heat transfer correlations is the following expression of the convective heat transfer coefficient in terms of the Nusselt number:

$$\alpha_{conv} = Nu \frac{k_{liq}}{d_{eq}} \tag{2.5}$$

Where k_{liq} is the thermal conductivity of the liquid phase working fluid in [W/mK]. d_{eq} is the equivalent diameter in [m]. The heat transfer correlations proposed in the coming section will be expressed in terms of the Nusselt number, which can, in turn, be translated to the convective heat transfer coefficient.

SINGLE PHASE

Single-phase heat transfer correlations make use of some dimensionless numbers to calculate the single phase heat transfer over a plate heat exchanger. These dimensionless numbers (what they represent and how they are calculated) can be found in Appendix C.0.1.

An overview of all single-phase heat transfer correlations implemented in the OTEC model can be found in Appendix D. The single phase heat transfer correlation found to have the best fit on the water side heat transfer is the "GoudKuik correlation". The single phase heat transfer correlation found to have the best fit on the ammonia side is the correlation developed by Donowski & Kandlikar [24].

TWO PHASE

The process of evaporation is dependent on the imposed heat flux, the working fluid mass flux, the vapor quality, the thickness of the film, dry-out and the flow regime. Different two phase heat transfer correlations have been developed in the past. These correlations all take the before mentioned physical phenomena into account in a different way. Some two phase heat transfer correlations use additional non-dimensional numbers to calculate the two phase heat transfer. These dimensionless numbers (what they represent and how they are calculated) can be found in Appendix C.0.2.

An overview of all two phase heat transfer correlations implemented in the OTEC model can be seen in Table 2.1. The two phase heat transfer correlation used will dictate what the calculated heat transfer in the evaporator will be under different conditions. These correlations and their accuracy are consequently crucial to the correct prediction of the performance of the evaporator. All two phase heat transfer correlations will be tested and validated in Chapter 5.

Table 2.1: Overview of the selected two phase heat transfer correlations for the plate heat exchanger evaporator

Author	Two phase heat transfer correlation	Validation range
Amalfi [26]	$Nu_{tp} = 982\beta_r^{1.101} We^{0.315} Bo^{0.320} \rho^{-0.224}$	$Bd < 4$
	$Nu_{tp} = 18.495\beta_r^{0.248} Re_{vap}^{0.135} Re_{liq}^{0.351} Bd^{0.235} Bo^{0.198} \rho^{-0.223}$	$Bd \geqslant 4$
	$\beta_r = \frac{\beta}{\beta_{evap,max}}$	$\beta_{evap,max} = 70.0$
Yan & Lin [27]	$Nu_{tp} = 19.26 Re_{eq} Re^{-0.5} Pr_{liq}^{1/3} Bo_{eq}^{-0.3}$	$2,000 \leqslant Re_{eq} \leqslant 10,000$ $55 \leqslant G \leqslant 70$ $11 \leqslant q" \leqslant 16$
Longo et al. [28]	$Nu_{tp} = 0.122 \Phi Re_{eq}^{0.8} Pr_{liq}^{1/3}$	$5.7 \leqslant G \leqslant 125$ for convective boiling
Khan et al. [29]	$Nu_{tp} = (-173.52\frac{\beta}{60} + 257.12)(Bo_{eq} Re_{eq})^{-0.09\frac{\beta}{60}+0.0005} \left(\frac{p}{p_{crit}}\right)^{-0.624\frac{\beta}{60}+0.822}$	
Palmer et al. [30]	$Nu_{tp} = 2.7 Re_{liq}^{0.55} Pr_{liq}^{0.5}$	$13 \leqslant Re_{eq} \leqslant 230$ $1.6 \leqslant G \leqslant 19$ $1.3 \leqslant q" \leqslant 8.3$
Huang et al. [31]	$Nu_{tp} = 1.87 \cdot 10^{-3} \left(\frac{q" d_0}{k_{liq} T_{sat}}\right)^{0.56} \left(\frac{\Delta h_{lv} d_0}{\alpha_{liq}^2}\right)^{0.31} Pr_{liq}^{0.33}$	$\theta = 35°$
	$d_0 = 0.0146 \cdot \theta \left(\frac{2\sigma}{g(\rho_{liq} - \rho_{vap})}\right)^{0.5}$, $\alpha_{liq} = \frac{k_{liq}}{\rho_{liq} c_{p,liq}}$	
Arima et al. [8]	$\alpha_{tp} = 16.4 \alpha_{liq,eq} \left(\frac{1}{X_{vv}}\right)^{1.08}$	$40 \leqslant Re \leqslant 3600$
	$\alpha_{liq,eq} = 0.023 \frac{\lambda_{liq}}{d_h} \left(\frac{G(1-q) d_h}{\mu_{liq}}\right)^{0.8} Pr_{liq}^{0.4}$	$7.4 \leqslant G \leqslant 15$
	$X_{vv} = \left(\frac{1-q}{q}\right)^{0.5} \left(\frac{\rho_{vap}}{\rho_{liq}}\right)^{0.5} \left(\frac{\mu_{liq}}{\mu_{vap}}\right)^{0.5}$ (laminar-laminar)	$15.4 \leqslant q" \leqslant 24.5$

Table 2.1: Continued

Author	Two phase heat transfer correlation	Validation range
Han et al. [20]	$Nu_{tp} = Ge_1 Re_{eq}^{Ge_2} Bo_{eq}^{0.3} Pr_l^{0.4}$ $Ge_1 = 2.81\left(\frac{P_c}{d_h}\right)^{-0.041}\left(\frac{\pi\beta}{180}\right)^{-2.83}$ $Ge_2 = 0.746\left(\frac{P_c}{d_h}\right)^{-0.082}\left(\frac{\pi\beta}{180}\right)^{0.61}$	
Ayub [32]	$Nu_{tp} = C\left(\frac{Re_{liq}^2 \Delta h_{lv}}{L_p}\right)^{0.4124}\left(\frac{p}{p_{crit}}\right)^{0.12}\left(\frac{65}{90-\beta}\right)^{0.35}$ $C = 0.0675$ for thermosyphon evaporators $C = 0.1121$ for flooded evaporators	
Taboas [33]	If $u_V < -111.88u_L + 11.848$, $\alpha_{tp} = 5Bo^{0.15}h_{lo}$ If $u_V > -111.88u_L + 11.848$, α_{tp} = greatest value of $\begin{cases} 5Bo^{0.15}h_{lo} \\ \left(1+\frac{3}{X_{tt}}+\frac{1}{X_{tt}^2}\right)^{0.2}h_{lo} \end{cases}$ $u_V = \frac{Gq}{\rho_{vap}}$ $u_L = \frac{G(1-q)}{\rho_{liq}}$ $X_{tt} = \frac{(1-q)\dot{m}}{q\dot{m}}\left(\frac{\rho_{vap}}{\rho_{liq}}\right)^{0.5}$	

2.1.2. TURBINE

In previous research and models created (by for example Goudriaan [11] and Kuikhoven [25]) for the Bluerise B.V. OTEC system the turbine was modeled as an ideal orifice. This means no enthalpy loss over the expansion. Together with a mass balance, these two equations determine the characteristics of the turbine.

$$h_{in} = h_{out} \tag{2.6a}$$
$$\dot{m}_{in} = \dot{m}_{out} \tag{2.6b}$$

This simple representation of the turbine was replaced by the work done by van Strijp [34]. He stated that the power output of the turbine could be determined by:

$$\dot{W}_t = \dot{m}(h_{in} - h_{out}) \tag{2.7}$$

Where $\dot{W}_t$ is the power delivered by the turbine in [W]. $\dot{m}$ is the mass flow through the turbine in [kg/s]. h_{in} and h_{out} are the respective in and outgoing enthalpies of the working fluid in [J/kg].

In the current research project, the turbine will be represented by an ideal orifice in both the off-design model and the lab setup. This means equations 2.6 will hold and the pressure drop over the orifice will be a given input to the system.

To assess the performance of the turbine, the turbine work can be calculated using the following equation [35]:

$$\dot{W}_T = \eta_{is}\dot{m}_{vap}c_p T_{in}\left[1 - \left(\frac{p_{turb,out}}{p_{turb_in}}\right)^{\frac{\gamma-1}{\gamma}}\right] \tag{2.8}$$

In which η_{is} is the isentropic efficiency of the turbine and γ is a ratio between the ammonia vapor heat capacity at constant pressure, c_p, to the heat capacity at constant volume, c_v, both in [J/kgK].

2.1.3. PUMPS

In the OTEC cycle, three pumps can be identified. There are two water pumps, one for the warm and one for the cold side, and there's one working fluid pump. The water pumps are not included in any of the analyses presented in this thesis work. An additional pump might be needed to successfully implement the liquid recirculation around the evaporator.

The efficiencies of the pumps can be calculated as follows:

$$\eta_p = \frac{\dot{V}(p_{out} - p_{in})}{\dot{W}_p} \tag{2.9}$$

Where η_p is the pump efficiency. $\dot{V}$ is the volumetric flow rate in [m^3/s]. p_{in} is the entering pressure in [Pa]. $\dot{W}_p$ is the work done by the pump in [W].

This efficiency is also called the isentropic efficiency. It comprises a comparison between the actual performance of a device and the performance that would be achieved if it would be able to perform with an efficiency of 100%.

2.1.4. SEPARATOR

The function of the separator is to separate the vapor phase working fluid from the liquid phase working fluid coming out of the evaporator. This is done to prevent liquid phase working fluid from entering the turbine, which would be detrimental to its lifetime.

The current separator installed at the OTEC demo setup is a vertical wire-mesh separator. It uses gravity to separate the vapor from the liquid and the fine wire-mesh ensures that absolutely no liquid phase working fluid is transported to the turbine.

The pressure drop of the separator is the only effect that depends on the geometry of the separator. The pressure drop should be as small as possible, it depends on the areas of the in and outlet ports of the separator. To ensure that the pressure drop over the separator is the same for both scales, the areas have to be scaled to compensate for the mass flow. The scale factor of the area ports is given in the following equation [34]:

$$d_{new} = d_{old} * \sqrt{\frac{\dot{m}_{new}}{\dot{m}_{old}}} \tag{2.10}$$

2.2. LIQUID SEPARATION & RE-CIRCULATION

To create a working ORC configuration in the current system, the best method for working fluid re-circulation has to be identified. According to literature, there are multiple design possibilities to obtain the desired result. Some of these design possibilities will be discussed in this chapter.

2.2.1. REBOILERS & VAPORIZERS

The design for the OTEC ORC configuration requires an evaporator with re-circulation to be implemented into the system, as shown in Figure 1.7. According to Sinnott & Towler [36], a system with partial evaporation of the feed (and re-circulation) is called a reboiler and a system with full evaporation of the feed is called a vaporizer. Three principal types of reboilers can be identified.

- Forced circulation
- Thermosiphon (natural circulation)
- Kettle type

To determine which type of reboiler is best suited to be implemented in the OTEC system designed by Bluerise B.V. a rating for the three options on several design criteria can be found in Appendix G. Following the results of this rating, the thermosiphon reboiler would be the preferred option. In Figure 2.1 the working method of a thermosiphon reboiler is displayed.

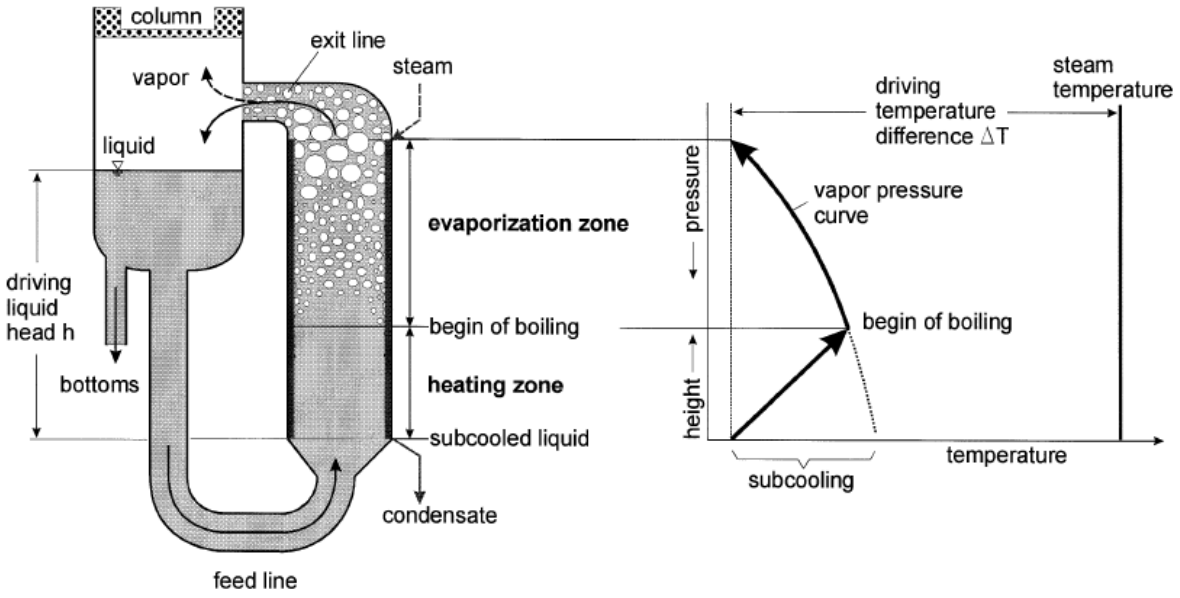

Figure 2.1: Working mechanism of a thermosiphon reboiler. Source [37]

The working principle of a thermosiphon reboiler is based on a complex interaction between heat transfer and two phase flow. The reboiler can be divided into two zones in which different processes are taking place:

1. Heating Zone: The working fluid inside the heating zone is heated up to the working fluid boiling temperature until it starts to evaporate.

2. Evaporation Zone: The working fluid entering the evaporation zone from the heating zone starts to evaporate and rises further through the thermosiphon reboiler. A combination of further heating and the pressure drop in the thermosiphon reboiler (flash) will cause the working fluid to evaporate more and more towards the exit line/ outlet.

Upon exiting the thermosiphon reboiler the vapor and liquid phases of the working fluid are separated and the liquid fraction is re-circulated. In a classic thermosiphon reboiler, it is the heat transferred to the working fluid that also causes the driving force for re-circulation

2.2.2. DESIGN

The design of a thermosiphon reboiler is complicated by the fact that the fluid circulation rate, heat-transfer rate, and pressure drop are all interrelated. To design a thermosiphon reboiler, iterative design procedures must be used. According to Sinnott & Towler [36], a typical design procedure will look as follows:

1. Calculate the vaporization rate required, from the specified duty.

2. Estimate the exchanger area from an assumed value for the overall heat transfer coefficient. Decide the exchanger layout and piping dimensions.

3. Assume a value for the re-circulation rate through the heat exchanger.

4. Calculate the pressure drop in the inlet piping (single phase).

5. Divide the exchanger tube into sections and calculate the pressure drop section-by-section up the tube. Use suitable methods for the sections in which the flow is two phase. Include the pressure loss due to the fluid acceleration as the vapor rate increases. For a horizontal reboiler, calculate the pressure drop in the shell, using a method suitable for two phase flow.

6. Calculate the pressure drop in the outlet piping (two phase).

7. Compare the calculated pressure drop with the available differential head, which will depend on the vapor voidage, and hence the assumed circulation rate. If a satisfactory balance has been achieved, proceed. If not, return to step 3 and repeat the calculations with a new assumed circulation rate.

8. Calculate the heat transfer coefficient and heat transfer rate section-by-section up the tubes. Use a suitable method for the sections in which the boiling is occurring.

9. Calculate the rate of vaporization from the total heat transfer rate and compare it with the value assumed in step 1. If the values are sufficiently close, proceed. If not, return to step 2 and repeat the calculations for a new design.

10. Check that the critical heat flux is not exceeded at any point up the tubes.

11. Repeat the complete procedure as necessary to optimize the design.

The design procedure shows that to know the dimensions of the heat exchanger, the required heat duty, the re-circulation rate, and the heat exchanger pressure drop have to be calculated. These three values determine the required dimensions of the heat exchanger which in turn affects these three values. This iterative process needs to be solved to design a heat exchanger which is following some required specifications.

For the OTEC Demo, this process is reversed. The evaporator plate heat exchanger is already installed and will not be changed anymore. The dimensions of this heat exchanger will thus affect the evaporator pressure drop, heat duty, and re-circulation rate. The variable that will be the result of testing will be the heat duty, with fixed heat exchanger dimensions and thus a fixed pressure drop. The variable that can be changed to see what effect it has on the heat duty, is the re-circulation rate through the evaporator.

2.3. EVAPORATOR PRESSURE DROP

Like stated before, considering that in the OTEC Demo the size of the evaporator plate heat exchanger is fixed, the only property to vary is the re-circulation rate. To properly model what would happen at different re-circulation rates, it's imperative to successfully model the properties that are imposed by the heat exchanger geometry. The variables that are imposed by the heat exchanger geometry are the heat transfer, but also the pressure drop in the plate heat exchanger. In Appendix D and Section 2.1.1 the heat transfer correlations for single and two phase heat transfer in a plate heat exchanger have been given, respectively. In the current section, some light is shed on methods to calculate the pressure drop in a plate heat exchanger.

The pressure drop calculations over a plate heat exchanger evaporator suffer from the same difficulties as the heat transfer correlations do: discrepancy in different data sets and difficulty in creating prediction models that are generally valid for plate heat exchangers [7]. In the past, different methods have been created and tested. Some of these methods will be discussed in this section.
Mancini et al. [7] discussed the pressure drop of the working fluid in a heat exchanger as the sum of the contributions of acceleration, friction, gravity, and manifolds.

$$\Delta p_{tot} = \Delta p_a + \Delta p_f + \Delta p_g + \Delta p_{man} \tag{2.11}$$

The contributions of the acceleration, gravity, and manifolds are considered to be very small compared to the frictional pressure drop and are thus assumed to be zero. In Appendix H a short explanation on how to calculate these is given as a reference.

2.3.1. FRICTIONAL PRESSURE DROP

In literature, three different methods are proposed to calculate the frictional pressure drop, based on different correlations:

- Correlations calculating the two phase Fanning Friction Factor.
- The Lockhart and Martinelli [38] method, consisting in the estimation of two phase multipliers correlating the single phase liquid and vapor pressure drops to the two phase pressure drop. Palm and Claesson [13] coefficients can be used in this method.
- The kinetic energy model, assuming proportionality between the kinetic energy per unit volume and the frictional pressure losses, as proposed by Longo and Gasparella [28]

FANNING FRICTION FACTOR

When calculating the frictional pressure drop according to the Fanning Friction Factor method, the following equation is used [39]:

$$\Delta p_f = f \frac{2G^2 L}{d_h \rho_m} \tag{2.12}$$

Where f is the Fanning Friction Factor, which is correlated in terms of the Reynolds number. Many researchers proposed single and two phase pressure drop correlations for plate heat exchangers. Table 2.2 and Table 2.3 show the correlations that will be implemented in the off-design model.

This pressure drop calculation method can also be applied to a control volume analysis. Taking the mass flux through the control volume, the length of the control volume ($L = \Delta z$) and the Fanning Friction Factor correlated to the values of the relative dimensionless numbers in the control volume.

Table 2.2: Overview of the selected single phase Fanning Friction Factor correlations for plate heat exchanger evaporator pressure drop.

Author	Fanning Friction Factor correlation	Validation Range
Martin [40]	$\zeta = 4f$ $\frac{1}{\sqrt{\zeta}} = \frac{cos\beta}{\sqrt{0.18tan\beta+0.36sin\beta+\zeta_0/cos\beta}} + \frac{1-cos/\beta}{\sqrt{3.8\zeta_1}}$ $\zeta_0 = \frac{64}{Re}$ and $\zeta_1 = \frac{597}{Re} + 3.85$	$Re < 2000$
Winkelmann [41]	$f_{sp} = 0.30 + 53Re^{-10}$ $f_{sp} = 1.0Re^{-0.135}$	$10 < Re < 1700$ $1700 \leq Re < 50000$
Kumar [42]	$f = 19.40Re^{-0.589}$ $f = 2.990Re^{-0.183}$	$10 < Re < 1700$ $1700 \leq Re < 50000$
Focke et al. [43]	$4f = 5.03 + \frac{7.55}{Re}$ $4f = 26.8Re^{-0.209}$	$90 < Re < 400$ $400 \leq Re < 16000$ For both: $\beta = 60°$
Thonon [44]	$f = 45Re^{-0.670}$ $f = 0.370Re^{-0.172}$	$Re < 160$ $Re > 160$ For both: $\beta = 60°$
Khan et al. [45]	$f = 34.43Re^{-0.5}$	$500 < Re < 2500$ $\beta = 60°$
Luan et al. [46]	$f = 0.2Re^{-0.23}$	$1500 \leq Re \leq 15000$

Table 2.3: Overview of the selected two phase Fanning Friction Factor correlations for plate heat exchanger evaporator pressure drop.

Author	Fanning Friction Factor correlation	Validation Range
Dahlgren [12]	$f_{tp} = 270000 Re_{eq}^{-1.5}$	$52 < G < 84$
Ayub [47]	$f_{tp} = \frac{n}{Re^m}(-1.89 + 6.56R - 3.69R^2)$	$30 \leq \beta \leq 65$
	$R = \frac{\beta}{30}$	
	$m = 0.137,\ n = 2.99$	for $Re \leq 4000$
	$m = 0.172,\ n = 2.99$	for $4000 \leq Re \leq 8000$
	$m = 0.161,\ n = 3.15$	for $8000 \leq Re \leq 16000$
	$m = 0.195,\ n = 2.99$	for $Re > 16000$
Khan et al. [48]	$f_{tp} = 212 Re_{eq}^{-0.51} \frac{p}{p_{crit}}^{0.53}$	$1387 < Re_{eq} < 2200$
Yan and Lin [27]	$f_{tp} Re^{0.5} = 6.947 * 10^5 Re_{eq}^{-1.109}$	$Re_{eq} < 6000$
	$f_{tp} Re^{0.5} = 31.21 Re_{eq}^{0.04557}$	$Re_{eq} \geq 6000$
Kuo et al. [49]	$f_{tp} = 21500 Re_{eq}^{-1.14} Bo^{-0.085}$	
Yan et al. [50]	$f_{tp} = 94.75 Re_{eq}^{-0.0467} Bo^{0.5} Re^{-0.4} \left(\frac{p}{p_{crit}}\right)^{0.8}$	
Hsieh and Lin [51]	$f_{tp} = 23820 Re_{eq}^{-1.12}$	$2000 < Re < 12000$ $0.0002 < Bo < 0.002$
Jokar et al. [52]	$f_{tp} = 5.474 * 10^3 Re_{eq}^{-1.35}$	$70 \leq Re_{eq} \leq 420$
Tao [53]	$f_{tp} = (4.207 - 2.673\beta^{-0.46})(1815 - 5.41 Bd^{1.358}) Re_{eq}^{-0.793} \left(\frac{p}{p_{crit}}\right)^{0.3}$	
	p_{sat}: pressure at saturated conditions	

Dahlgren [12] compared single phase pressure drop correlations through experiments and conceived a new correlation, based on the correlation proposed by Martin [40] in the VDI Heat Atlas [54]. In Figure 2.2 the comparison made by Dahlgren on the single phase pressure drops to his experimental data on the OTEC Demo can be seen. As can be concluded from this image, the correlation proposed by Martin has the highest fit. The correlation by Martin has also been validated over a wider range than the correlation proposed by Dahlgren, so it will be the preferred option in this research.

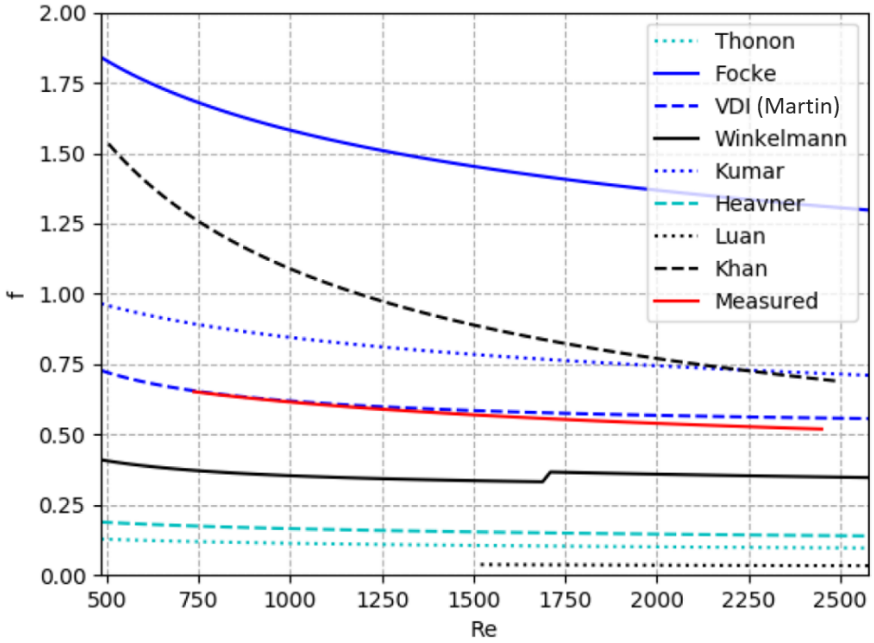

Figure 2.2: Single phase pressure drop correlations comparison. Source [12]

LOCKHART AND MARTINELLI METHOD

To calculate the frictional pressure drop according to the Lockhart and Martinelli method [38], the Lockhart-Martinelli parameter, X, and the two phase friction multipliers, ϕ_l^2 or ϕ_v^2, have to be determined. They are defined as:

$$X^2 = \frac{\Delta p_l}{\Delta p_v} \tag{2.13a}$$

$$\phi_l^2 = \frac{\Delta p_{tp}}{\Delta p_l} \tag{2.13b}$$

$$\phi_v^2 = \frac{\Delta p_{tp}}{\Delta p_v} \tag{2.13c}$$

Where Δp_l is the liquid phase frictional pressure drop calculated as if the liquid phase was flowing alone, Δp_v is the vapor phase frictional pressure drop calculated as if the vapor phase was flowing alone and Δp_{tp} is the resulting two phase frictional pressure drop.

The relationship between the Lockhart-Martinelli Parameter and liquid two phase friction multiplier was originally illustrated graphically by Lockhart and Martinelli. Chisholm [55] came up with a correlation to represent this relationship:

$$for \quad Re_L > 4000 \quad \phi_l^2 = 1 + \frac{C}{X} + \frac{1}{X^2} \tag{2.14a}$$

$$for \quad Re_L < 4000 \quad \phi_v^2 = 1 + CX + X^2 \tag{2.14b}$$

The value of constant C is usually determined from experimental data for different situations. In previous research, different values were found for the numerous chevron angles in plate heat exchangers. Thonon et

al. [44] suggested using $C = 8$, although no information on the experiments or the channel geometry was included. The same group later reported a value of $C = 3$ based on the experimental work of Margat et al. [56] [19]. Holt et al. [57] investigated pressure drop in ducts with different channel cross sections and fluids and found (like Mishika and Hibiki [58]) that the value of C is a function of the hydraulic diameter d_h. From literature, it can be concluded that the value of C is hard to determine and very inconsistent. Typical values depend on the hydraulic diameter and can thus be correlated to the flow regime. Typical values for C depending on the liquid-vapor flow regime can be seen in table 2.4.

Table 2.4: Typical C values depending on liquid-vapor flow regime

Liquid	Vapor	C value
Turbulent	Turbulent	20
Laminar	Turbulent	12
Turbulent	Laminar	10
Laminar	Laminar	5

This method of calculating the frictional pressure drop can also be applied to a control volume analysis. By taking the quality inside the control volume and looking at the flow regime in the control volume.

KINETIC ENERGY MODEL

Longo and Gasparella investigated the frictional pressure drop for evaporation in a corrugated plate heat exchanger. They determined the frictional pressure drop experimentally by subtracting the acceleration pressure drop, the gravity pressure drop and the manifolds pressure drop from the total measured pressure drop.

$$\Delta p_f = \Delta p_{tot,measured} - \Delta p_a - \Delta p_g - \Delta p_{man} \tag{2.15}$$

According to the data that was obtained from these experiments, a plot of the saturated boiling frictional pressure drop vs. the kinetic energy per unit volume was made. From the experimental data a best fitting equation was derived:

$$\Delta p_f = 1.49 \frac{KE}{V} \tag{2.16}$$

Where $\frac{KE}{V}$ is the kinetic energy per unit volume in [J/m^3].
This method can also be applied to a control volume analysis. By calculating the frictional pressure drop per control volume according to the kinetic energy of the working fluid in that control volume.

2.4. WORKING FLUID MIXING

Working fluid mixing at the mixing point between the separator, main working fluid pump and the evaporator could simply be done joining piping through a T-section. By using a regular T-section, the pressure losses in the evaporator have to be overcome by either a tall column height or a gear pump between the column and the T-section.
Another possibility for the working fluid mixing point would be the use of an ejector. This is not the scope of this thesis research but could be an interesting follow-up study. An introduction to the working mechanism of an ejector is given in Appendix I

2.5. EVAPORATOR HEAT TRANSFER PREDICTION

To get a grasp of resulting heat transfer under different re-circulation rates, a survey among existing literature is done. First, a comparison of evaporator heat transfer between working fluid mixtures and pure working fluids is made. Secondly, some insight is given in two phase heat transfer for evaporators depending on the mass flow through the evaporator.

2.5.1. MIXTURE VS PURE WORKING FLUID HEAT TRANSFER

Mancini et al. [7] discuss the differences in heat transfer and pressure drop for evaporation of zeotropic mixtures compared to pure fluids in plate heat exchangers. Even though zeotropic mixtures offer the advantage of a temperature glide, which can match the temperature glide of the warm source (See Figure 1.5), additional

heat transfer area is needed for a mixture working fluid. This need for additional heat transfer area is caused by heat transfer degradation.

In general, the boiling process can be characterized by and divided into three different forms, which can be seen in Figure 2.3. Understanding these boiling phenomena helps to understand why heat transfer degradation is caused in working fluid mixtures.

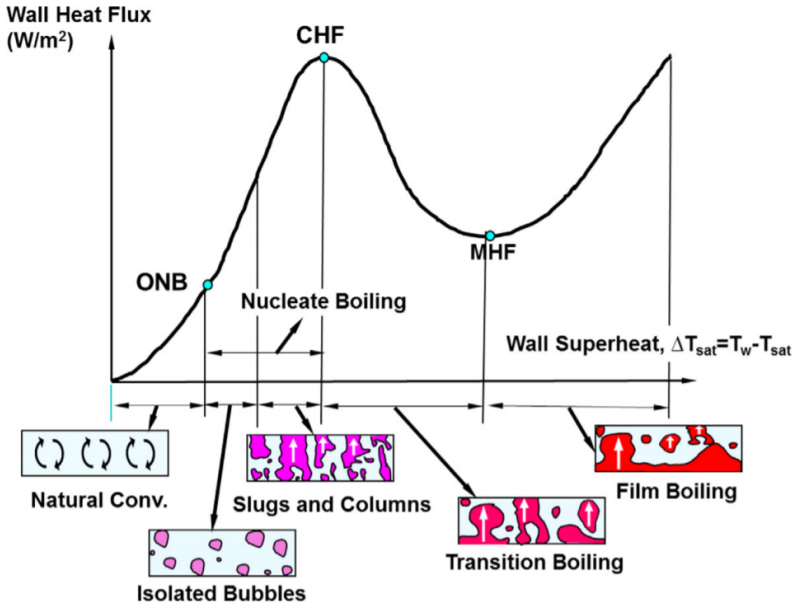

Figure 2.3: Boiling characteristics. Source [59]

As can be seen in Figure 2.3, boiling within a liquid starts when the wall superheat (which is the difference between the wall temperature and the liquid saturated temperature) reaches a certain level at the ONB point. Before this degree of wall superheat is reached, natural convection within the liquid causes the heat to spread throughout the liquid and no vapor is formed yet. When the wall superheat surpasses the ONB point, nucleate boiling starts to occur. At first, isolated vapor bubbles form within the liquid and start breaking away from the wall. When the wall superheat is increased even further, vapor bubbles start to merge and form larger slugs and columns of vapor within the liquid. Heat transfer increases throughout this process. This is caused by increased mixing and turbulence within the liquid, caused by the increasing amount of bubbles being formed. When the wall superheat is increased even further, the CHF will be reached. When the wall superheat is increased beyond the CHF point, transition boiling will start to occur. In this phase, vapor will form too fast for new liquid to flow to the wall surface and "dried out" patches of wall surface area where no liquid is touching the wall will start to appear. The dry-out of the wall reduces wall heat flux, causing the wall to increase in temperature even more until the MHF point is reached. Beyond the MHF point, film boiling occurs, where none of the wall surface is wetted anymore and completely covered in vapor.

According to Radermacher & Hwang [60] heat transfer degradation in working fluid mixtures is mainly caused by the following two phenomena:

- *"Increase of the local saturation temperature."*
  In working fluid mixtures, nucleate boiling heat transfer is suppressed at much lower qualities than in pure working fluids. Van Wijk et al. [61] noted that the more volatile component of the mixture disappears from the liquid surrounding a vapor bubble, simply because it evaporates into the growing bubble. Thus, for the volatile component, the fraction of it in the liquid close to the liquid-vapor interface is lower than in the bulk of the liquid. When the fraction of the volatile component in a liquid decreases, the bubble point temperature of the mixture as a whole increases, according to phase equilibrium. When the bubble point temperature increases, the effective wall superheat decreases. With a lower effective wall superheat, the wall heat flux is also lower.

- *"Formation of a mass diffusion resistance due to the more readily evaporation of the more volatile component."*
  Jung and Radermacher [62] explain this phenomenon by looking at local bubble dynamics. As stated before, the concentration of the volatile component in the liquid closely surrounding the forming vapor bubble is lower than in the bulk of the liquid. From the bulk of the liquid, some of the more volatile component diffuses towards the liquid-vapor interface to restore the concentration. The diffusion of the volatile component towards the liquid-vapor causes a mass transfer resistance to heat transfer since the heat transfer is affected by how quickly the concentration of the more volatile component near the liquid-vapor interface can be replenished.

Next to these main phenomena, several other reasons are mentioned.

- Changes in the physical properties of the mixture with changing mass fractions
- An increase in wall superheating causes lower boiling site densities
- The main heat transport mechanisms are delayed in working fluid mixtures.
- The physical transport properties are degraded in working fluid mixtures compared to pure fluids.

2.5.2. MASS TRANSFER INFLUENCE ON HEAT TRANSFER

Evaporator heat transfer performance, as stated before, is dependant on many different factors. Changing the mass flow of the working fluid inside the evaporator affects (some of) these factors. To gain some insight on what might occur in the evaporator due to a changing working fluid mass flow, some insight is created on available knowledge in literature.
In the existing literature, many researchers have studied plate heat exchanger boiling characteristics and created flow boiling models. These models result in the two phase heat transfer correlations that have been shown in Section 2.1.1.

Arima et al. [8] conducted experiments with a vertical plate evaporator to determine the local heat transfer coefficient of ammonia under different conditions. An analysis of the influence of the mass flux on the local heat transfer coefficient was also made. In Figure 2.4 the resulting data from these experiments can be seen.

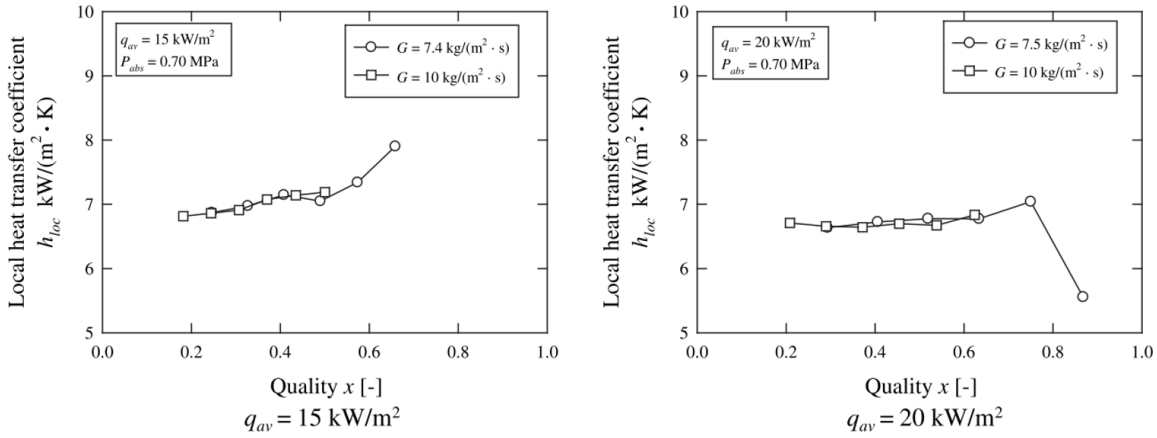

Figure 2.4: Local boiling heat transfer coefficient versus the vapor quality at various mass fluxes. Source [8].

For these experiments, an average heat flux of 15 [kW/m^2] and 20 [kW/m^2] were used, respectively. The saturation pressure for both experiments was maintained at 0.70 [MPa]. An interesting conclusion that can be drawn from these results is that the influence of the mass flux through the evaporator seems to only slightly affect the local heat transfer coefficient. The vapor quality has a larger effect. For vapor qualities lower than 0.3 it appears that the local heat transfer coefficient remains relatively constant. For vapor qualities between 0.3 and 0.7, it appears that the local heat transfer coefficient increases when the vapor quality increases. For

vapor qualities higher than 0.7, the local heat transfer coefficient declines rapidly with increasing vapor quality.

The resulting local heat transfer coefficient depending on the vapor quality appears to be in line with the expectations resulting from Figure 2.3. At first, the increase in vapor quality increases the nucleate boiling wall heat flux, by increasing the turbulence in the working fluid. After a certain point, apparently at a vapor quality of 0.7, the CHF is reached and transition boiling/ film boiling starts to occur, rapidly decreasing the local heat transfer coefficient.
The mass flux itself appears to have no or a very small influence on the resulting local heat transfer coefficient.

Djordjevic and Kabelac [63] investigated the evaporation heat transfer of ammonia in two different types of plate heat exchangers. Measurements were executed at different mass fluxes. The results of these experiments can be seen in Figure 2.5. The experiments shown in Figure 2.5 were executed in parallel 63 °chevron angle plate heat exchangers with mass flows ranging from 10-20 [kg/m^{2}s] and heat flux ranging between 10-20 [kW/m^2].

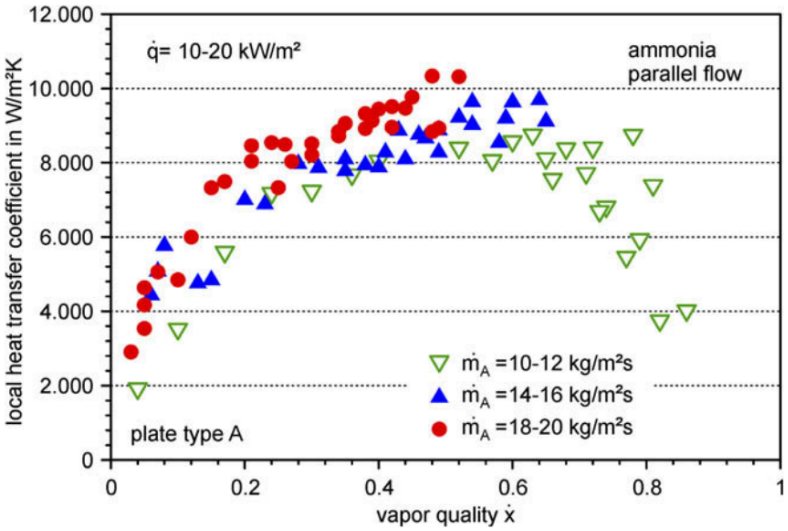

Figure 2.5: Local heat transfer coefficient versus vapor quality at different mass fluxes for ammonia in a plate heat exchanger. Source [63]

Looking at Figure 2.5 it can be seen that for the low mass flux data set, the vapor quality at the evaporator outlet is at around 0.8. For the intermediate max flux data set, the vapor quality at the evaporator outlet is at around 0.6. For the high max flux data set, the vapor quality at the evaporator outlet is at around 0.5.

As can be seen in Figure 2.5, the local heat transfer coefficient of ammonia in these experiments follows a different trend as noted in the previously explained results presented by Arima et al. For vapor qualities below 0.3, the local heat transfer coefficient increases drastically with increasing vapor quality. For vapor qualities between 0.3 and 0.7, the local heat transfer coefficient increases slightly with increasing vapor quality. For vapor qualities above 0.7, the local heat transfer coefficient declines rapidly with increasing vapor quality. The highest local heat transfer can be identified at around 0.5-0.6 vapor quality.

From Figure 2.5 it can be concluded that the mass flux has a small influence on the local heat transfer coefficient. Increasing mass flux through the evaporator slightly increases the local heat transfer coefficient, but this is less of an influence than the vapor quality.

Koyama et al. [64] studied the effect of mass flux on the heat transfer coefficient for flat non-corrugated plate heat exchangers using ammonia, at relatively low mass flux. The results of these experiments can be seen in Figure 2.6. The experiments shown in Figure 2.6 were executed with a channel width of 1 [mm], heat flux of 10 [kW/m^2] and at a saturation pressure of 0.7 [MPa].

These experiments show similar results to those executed by Djordjevic and Kabelac. For vapor qualities below 0.3, the local heat transfer coefficient increases drastically with increasing vapor quality. For vapor qualities between 0.3 and 0.7, the local heat transfer coefficient increases slightly with increasing vapor quality. High vapor qualities were not reached in these experiments, so film boiling doesn't occur.

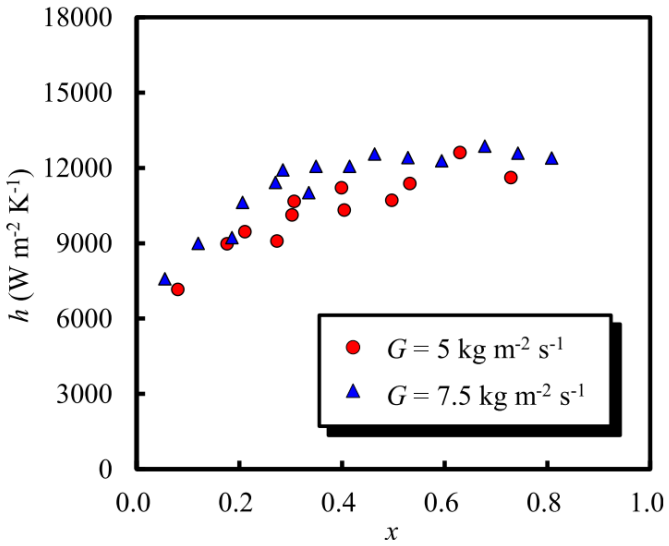

Figure 2.6: Local heat transfer coefficient versus vapor quality at different mass fluxes for ammonia in a non-corrugated plate heat exchanger. Source [64]

2.5.3. CONCLUSIONS ON PERFORMANCE

Concluding from the information gathered above, it can be stated that the heat transfer coefficient for pure ammonia is higher than the heat transfer coefficient for an ammonia-water mixture. Heat transfer degradation in working fluid mixtures is the cause of this phenomenon.

It can also be concluded that mass flux on its own has a minor effect on the heat transfer coefficient. Increasing the mass flux slightly increases the heat transfer coefficient, but vapor quality has a much greater effect on the resulting heat transfer coefficient. Logical reasoning would lead to conclude that for an evaporative process inside a heat exchanger, vapor quality is dependant on mass flux. If all other variables remain constant, increasing the mass flux of the working fluid through the evaporator would cause a lower vapor quality at the outlet of the evaporator. This can be explained by the fact that the heat available to a higher amount of working fluid mass would remain the same, therefore evaporating a lower fraction of the working fluid stream.

Figure 2.5 displays the local heat transfer coefficient inside the evaporator heat exchanger versus the vapor quality. No direct conclusion can be made on the difference in total heat transfer between different mass fluxes. To make any claims about the effect of mass flux through the evaporator on the total heat transferred in the evaporator, it is required to calculate an overall heat transfer coefficient for each mass flux domain. In Table 2.5 some information that is deducted from Figure 2.5 can be seen.

Table 2.5: Deducted data from Figure 2.5

Mass flux domain [kg/m^{2}s]	Number of data points	vapor quality at evaporator outlet	average local heat transfer coefficient [W/m^{2}K]
10-12	24	0.8-0.85	6800
14-16	28	0.6-0.6	7900
18-20	32	0.5-0.55	7800

As can be seen in Table 2.5, for the low mass flux with high consequential vapor quality at the evaporator outlet, the average local heat transfer coefficient is relatively low. For the medium and high mass fluxes in the data set obtained by Djordjevic and Kabelac, the average local heat transfer coefficient appears to have the highest point for a vapor quality at the evaporator outlet between 0.5 and 0.7. Unfortunately higher mass fluxes with even lower vapor qualities at the evaporator outlet were not used in this experiment. This quick estimation of the average local heat transfer coefficient is far from conclusive, but gives some insight resulting in a hypothesis.

The hypothesis will be based on the re-circulation rate, r. The re-circulation rate is calculated as the inverse of the vapor quality at the evaporator outlet.

The dependency of vapor quality on mass flux, together with the results from the experiments described above lead to the following hypothesis that can be used in the optimization of the ORC evaporator re-circulation rate:

- The mass flux of ammonia through the evaporator should not be low up to a degree where the vapor quality at the outlet exceeds 70%. A vapor quality higher than 70 percent means a re-circulation rate lower than 1.43. A re-circulation rate lower than 1.43 can cause dry-out of the heat exchanger surface area, decreasing the overall heat transfer coefficient.
- The mass flux of ammonia through the evaporator should not be high up to a degree where the vapor quality at the outlet is below 30%. A vapor quality lower than 30 percent means a re-circulation rate higher than 3.33. A re-circulation rate higher than 3.33 causes a significant drop in the heat transfer coefficient caused by deteriorated nucleate boiling.
- The mass flux of ammonia can be optimized between a vapor quality outlet of 30-70%, where the maximum heat transfer coefficient is probably reached between 50-70% vapor quality at the evaporator outlet. This means the heat transfer coefficient will be highest at a re-circulation rate between 1.43-2.00

3

OTEC Demo Adjustments

This chapter will describe and give an overview of the working principle of the current OTEC system Kalina cycle configuration and how to change this to a working ORC configuration.

3.1. Kalina Cycle

In Figure 3.1 a PFD of the OTEC system Kalina cycle as designed by Bluerise B.V. can be seen. The streams are numbered from 1 to 8 and the components (that are used in the model) have been assigned letters.

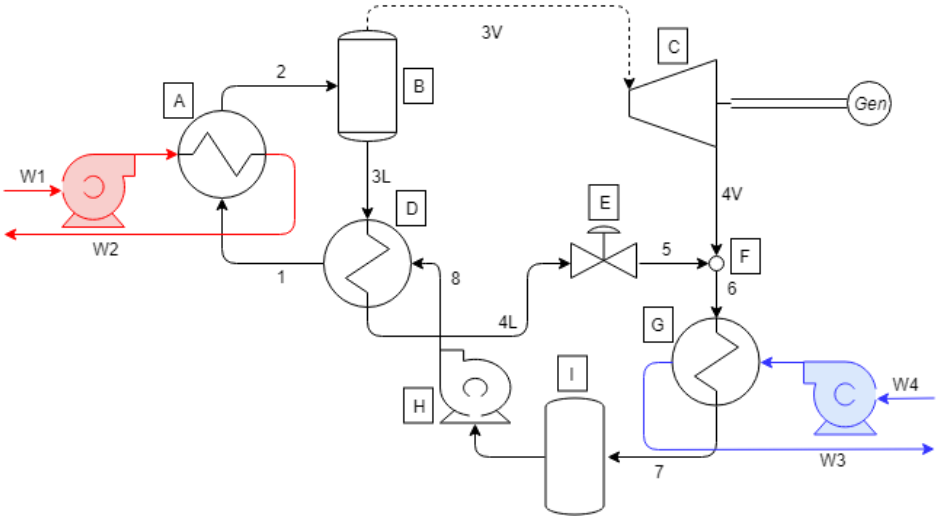

Figure 3.1: The system overview for the Kalina cycle designed and used by Bluerise B.V. in their OTEC system

The letters that can be seen in Figure 3.1 stand for:

A Evaporator	D Recuperator	G Condenser
B Separator	E Valve	H Working Fluid Pump
C Turbine	F Mixing point	I Buffer Tank

An OTEC Kalina cycle laboratory setup has been created at the Mechanical Engineering faculty, Process & Energy department, to verify software/ numerical models that simulate the OTEC cycle process. This laboratory setup is called "the OTEC Demo". Over the past years, some additions to the OTEC Demo have been made, like the addition of a gasketed plate heat exchanger as a condenser. This gasketed plate heat exchanger is implemented to test the behaviour of different plate materials in the condenser and to further study condensing phenomena inside a plate heat exchanger. The addition to the current cycle to create an ORC for

the OTEC Demo will not concern the gasketed plate heat exchanger, however. In Appendix E an overview of how the OTEC Demo Kalina cycle was constructed in the beginning can be seen, including a P&ID for this configuration.

3.2. ORC ADJUSTMENTS

To accommodate the ORC configuration within the OTEC Demo, some adjustments to the current OTEC Demo will have to be made. These adjustments will need to abide by certain criteria:

- The setup needs to be able to switch easily between an ORC and a Kalina cycle configuration once adjustments have been made.
- The alterations to the OTEC Demo setup need to be easily implemented, to make sure the required work in the setup can be done quickly.
- The ORC configuration needs to utilize as much of the sensors that are used in the Kalina cycle configuration as possible. This will reduce the need to purchase or relocate any sensors in the setup.

Another issue concerning the adaptation to an ORC configuration concerns the pressure levels between the separator and the evaporator. As stated in Section 2.2, for a thermosiphon re-boiler to function, the pressure head of the liquid column inside the separator must be high enough to overcome all pressure losses between the separator liquid outlet and separator inlet. A graphical depiction of this can be seen in Figure 3.2.

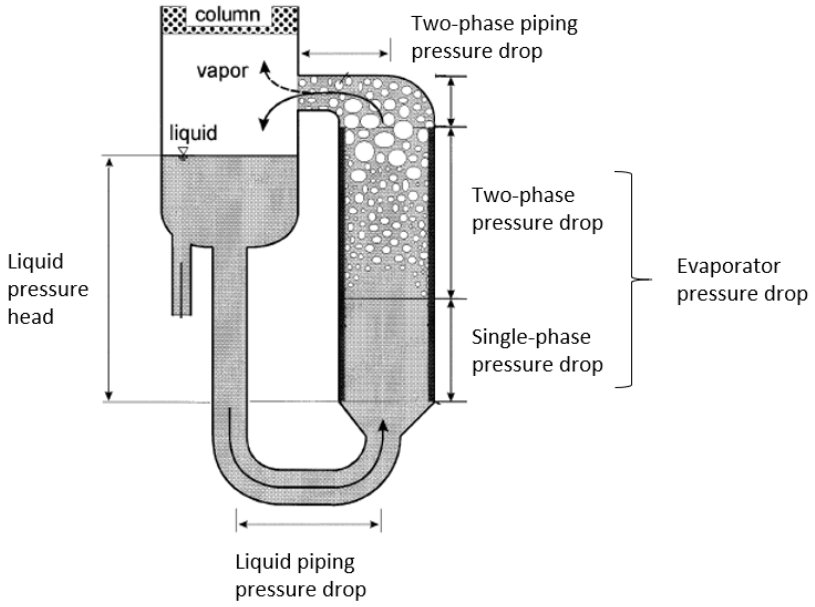

Figure 3.2: Schematic overview of the pressure build up around the thermosiphon evaporator

The vertical distance between the separator inlet and the evaporator inlet is the maximum height over which a liquid pressure head can be created. For the OTEC Demo, this vertical distance is only 0.97 [m]. The liquid pressure head can be calculated as follows:

$$\Delta p_{head} = \rho g y_{liq} \tag{3.1}$$

Where ρ is the density of ammonia in [kg/m^3], g is the gravitational acceleration in [m/s^2] and y_{liq} is the vertical length over which the pressure head is build up. With the known ammonia density, vertical length within the OTEC Demo and the gravitational constant, it is calculated that the maximum liquid pressure head in the OTEC Demo amounts to only 0.07 [bar]. Whether this pressure head is enough to overcome the evaporator and piping pressure losses is unknown at this point, but for the OTEC Demo there's another factor that needs to be taken into consideration. The working fluid pump, which pumps the working fluid through the recuperator to the evaporator, is a reciprocating pump. This type of pump causes a lot of oscillations in the

pressure level of its outlet. When the separator liquid outlet is connected to the piping coming from the working fluid pump to the evaporator, these oscillations will also cause the liquid inside the separator column to oscillate heavily. As a consequence, the liquid working fluid could be forced out of the top of the separator to the turbine and it will also be hard to determine when a steady state is reached. To prevent working fluid oscillations from running up the re-circulation line coming from the separator, a one-way valve will be installed.

Additionally, the decision is made to install a gear pump in the OTEC Demo to facilitate the ORC configuration. This gear pump will be placed between the separator and the mixing point, parallel to the one-way valve. Natural re-circulation using the liquid level in the separator column in combination with the one-way valve might have a limited re-circulation domain. This is caused by the limited height of the liquid column as explained before. The gear pump will be implemented to test the effect of a broader range of working fluid re-circulation rates.

A resulting PFD of the ORC configuration for the OTEC Demo can be seen in Figure 3.3.

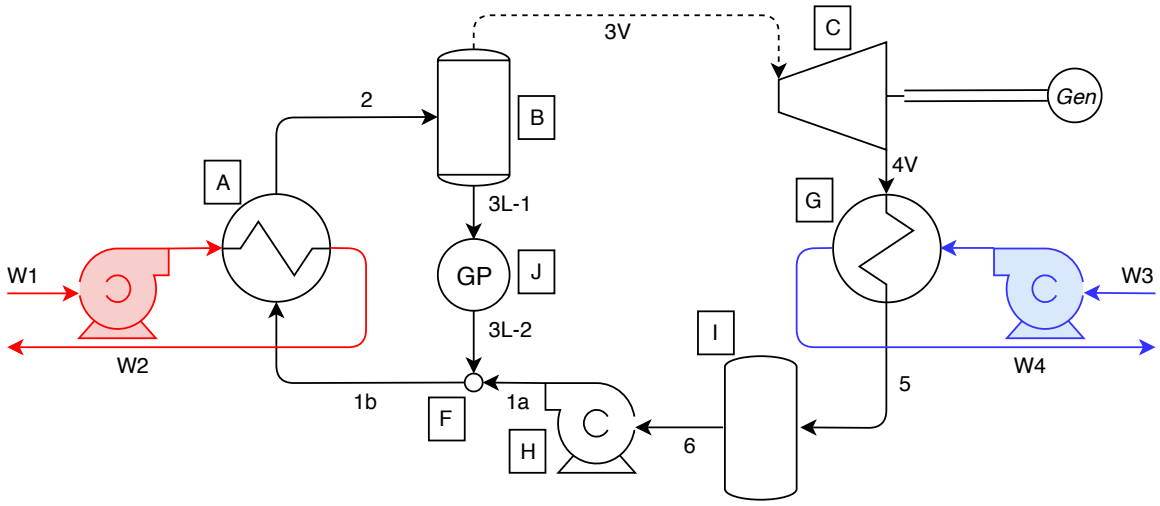

Figure 3.3: The system overview for the ORC configuration of the OTEC Demo

The letters that can be seen in Figure 3.3 stand for:

A Evaporator
B Separator
C Turbine
F Mixing point
G Condenser
H Working Fluid Pump
I Buffer Tank
J Gear Pump/ One-way Valve

A new P&ID for the OTEC Demo setup can be seen in Figure 3.4. This P&ID includes the option to run the working fluid stream over the gasketed plate heat exchanger, but this option will not be used in this thesis research. In Appendix F a short list of components labeling for the P&ID can be seen. Two other instances of the P&ID shown in Figure 3.4 can also be seen. These P&ID's show the working fluid paths in the ORC configuration or the Kalina Cycle configuration in green, respectively.

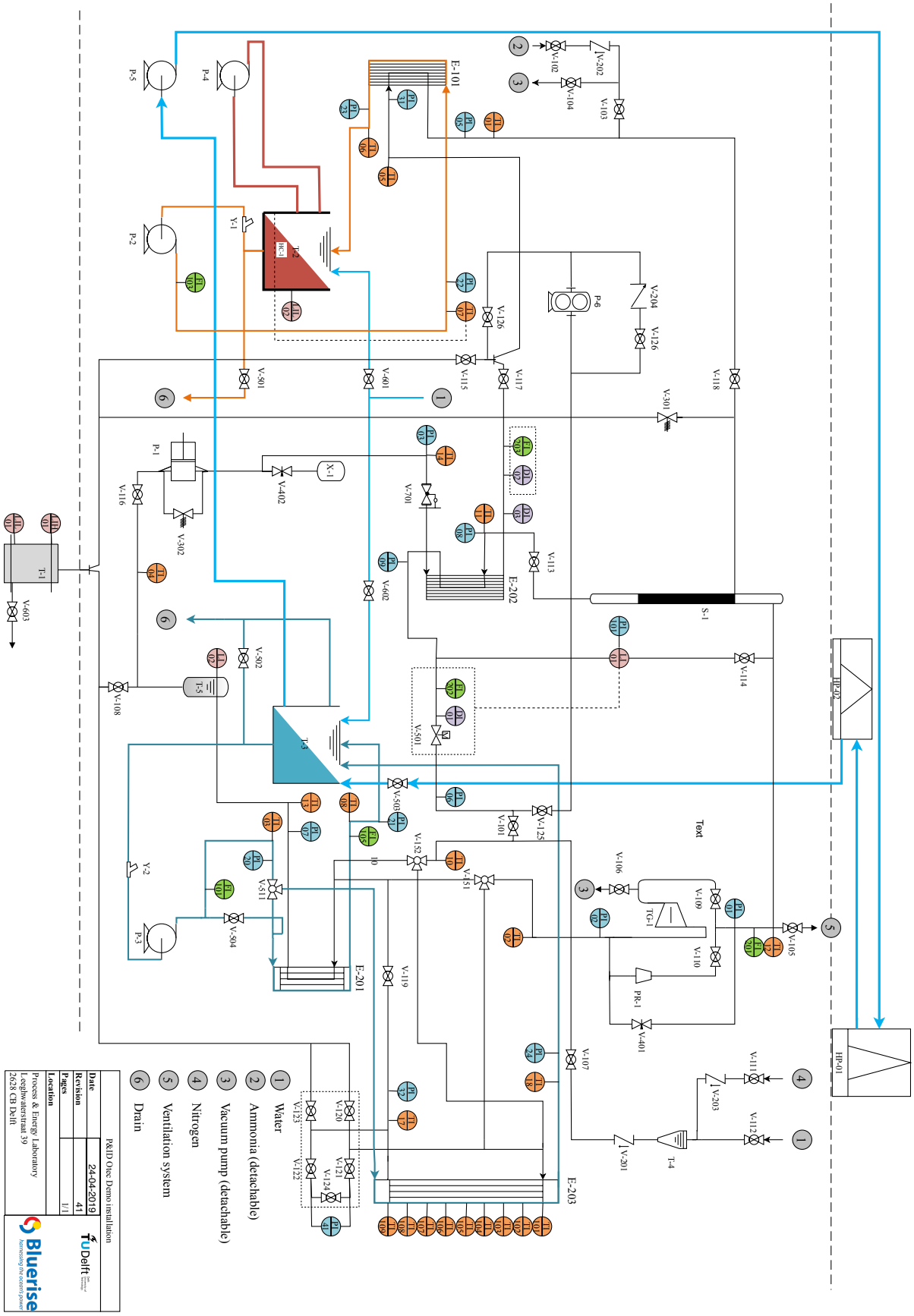

Figure 3.4: Piping & Instrumentation Diagram (P&ID) of the OTEC experimental setup including ORC liquid re-circulation line

As can be seen in Figure 3.4, the addition to the OTEC Demo setup is a line going from valve V-101, joining the feed towards the evaporator. In this line, two additional ball valves (V-125, V-127) and a gear pump (P-6) are placed, together with a bypass containing a ball-valve (V-126) and one-way valve (V-204). By controlling the new valves V-125, V-127 and valve V-101, the OTEC Demo can now switch between an ORC and a Kalina cycle. The by-pass including a one-way valve can be controlled with ball-valve V-126.

The decision to adjust the OTEC Demo this way abides by the criteria proposed earlier. The setup can switch between a Kalina cycle configuration and an ORC configuration quickly by controlling the valves. The setup alterations require only one additional piping segment, so are relatively easy to implement. The flow sensor FI-202 can still be used to measure the flow going through the bottom of the separator, without the need to relocate it. An additional advantage is that the recuperator will slightly subcool the liquid coming from the separator. This will decrease the chance of cavitation bubbles to occur in the gear pump, which would be detrimental to the pump lifetime. Using the recuperator won't energetically change the cycle, since exchanging heat between the flows and then mixing them or mixing them straight away would lead to the same working fluid output state.

In Figure 3.5 some pictures can be seen on the implemented ORC re-circulation line in the OTEC Demo.

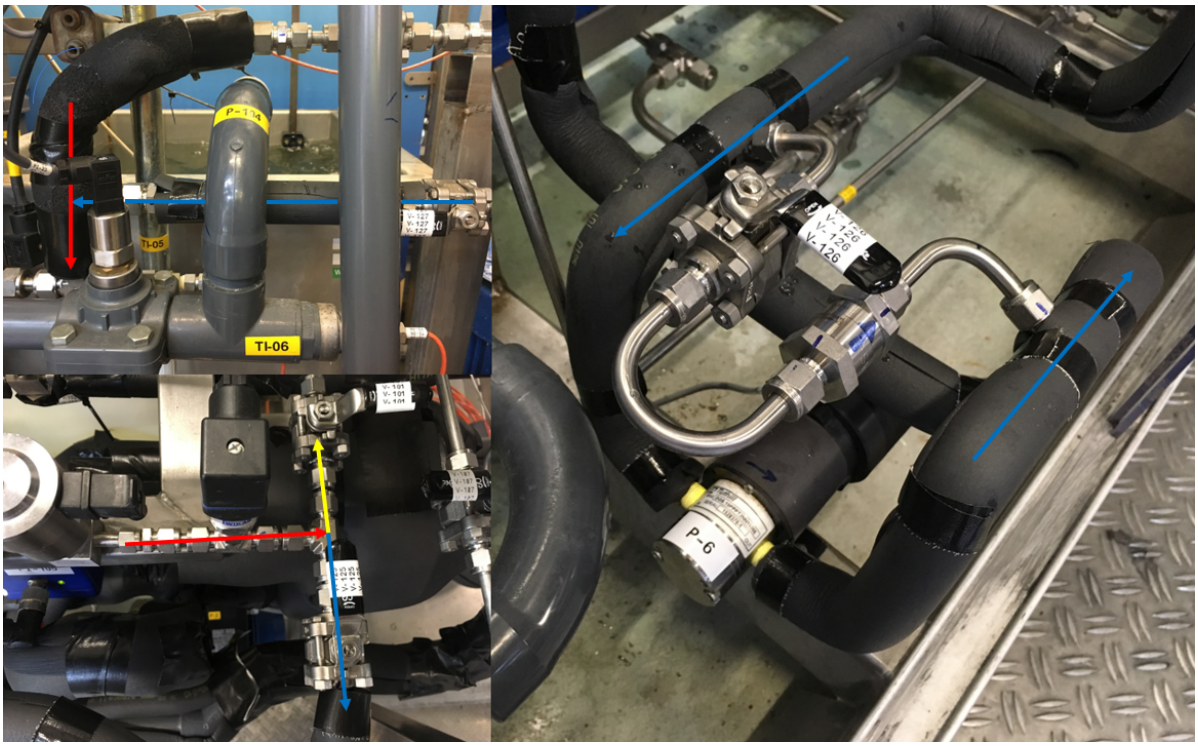

Figure 3.5: Some pictures of the additions made to the OTEC Demo to facilitate an ORC configuration. All red arrows indicate streams that are relevant for both ORC and Kalina cycle configuration. All blue arrows indicate streams that are only relevant for ORC configuration. All yellow arrows indicate streams that are only relevant for Kalina cycle configuration.
Top left: the connection from the ORC re-circulation line (blue) to the evaporator inlet line (red). Valve V-127 can be closed/ opened to switch between Kalina cycle and ORC configuration.
Bottom left: the separator outlet line (red) which can be directed towards the condenser (yellow) for Kalina cycle configuration or towards the gear pump (blue) for ORC configuration. This switch can be made be closing/ opening valve V-101 and V-125.
Right: The gear pump (P-6) and the by-pass consisting of ball-valve V-126 and one-way valve V-204

4

MODEL ADJUSTMENTS

At Bluerise B.V., a Python(c) model is created to simulate the characteristics and performance of the system. The off-design model determines the operating conditions of the OTEC cycle with respect to the working fluid, the geometries of the components and the mass flow in the system. Additional to the off-design model, van Strijp [5] created an on-design model to determine the right geometries dependant on the scaling of the system. The geometries resulting from the on-design model could then be used in the off-design model to calculate the actual working fluid states and system performance. A visual representation of this method can be seen in Figure 4.1.

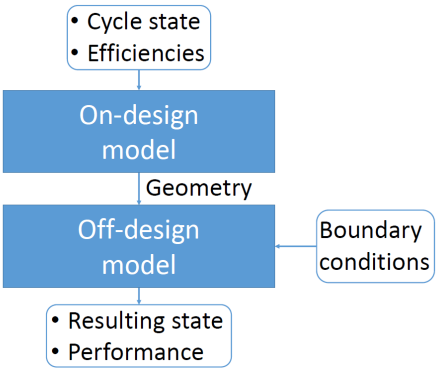

Figure 4.1: collaboration of the on-design model with the off-design model. Source [34]

The work in this research will focus on the off-design model, adding a methodology to calculate the operating conditions for an ORC OTEC system with system properties equivalent to the OTEC demo.
In the work done by Dickes et al. [65] it is mentioned that for any model describing an ORC or Kalina cycle, there is a trade-off between modeling complexity and simulation accuracy. Models that use complicated physical equations and phenomena usually have long computational time, but higher accuracy. Whereas models using several assumptions and simplifications have shorter computational time, but (in general) lower accuracy. Implementing a smart and high-quality computational method, where complexity and simulation accuracy are well balanced with the computational time needed for the model, is the major challenge in creating the model.
The model as created by Bluerise can be considered a semi-empirical model. The model is based on both empirical heat transfer-/ pressure drop correlations and physics-based equations.

4.1. PURPOSE

The model is designed as an off-design tool to visualize the flows of the working fluid through the system. The calculated states can be used to predict the operating characteristics and performance of a real-life system. All cycle components will be modeled and validated individually. This way all components can be adjusted according to new design wishes or the desire to scale up the system.

4.2. SYSTEM BOUNDARIES AND INPUT/OUTPUT VARIABLES

The system boundaries are set where the input and output values are known. This means the system boundaries are set over the cold and warm water in- and outlet. The inlet states (temperature, pressure, and mass flow rate) of the water streams are inputs to the system. The outlet states of the water are an output of the system. Furthermore, the working fluid mass flow rate to the evaporator and the pressure drop over the turbine, represented as an orifice, are inputs to the system. The power required by the pump is an output of the system.
In Figure 4.2 a schematic drawing for the OTEC Demo and its boundary can be seen. The red and blue arrows of the water streams represent the water input and output states. The green arrows represent the other two inputs and one output of the system. On a side note, in this notation, one can be forgiven to mistake the pump to generate power and deliver that to outside the system. This is incorrect. The green arrow pointing towards the outside of the system only indicates that the power required by the pump is a system output. In Table 4.1 the different input and output values for the whole system can be seen.

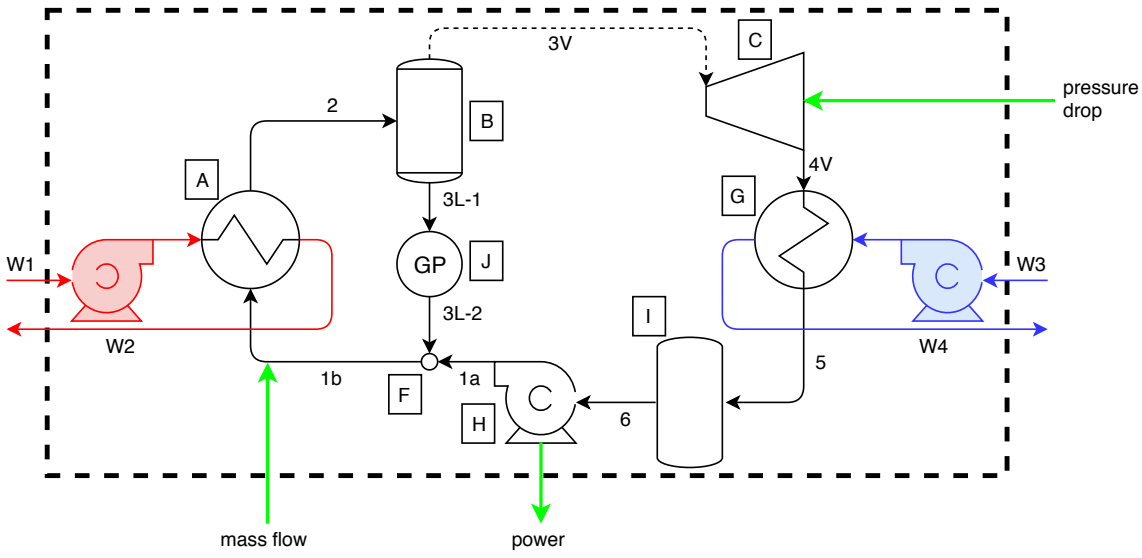

Figure 4.2: Process flow diagram of the OTEC Demo ORC configuration, including the system boundary.

Table 4.1: Inputs and outputs over the system boundary of the model. Based on Source [11]

Inputs	Outputs
Flow rate of the working fluid entering the evaporator	Power input to the working fluid pump
Pressure of the water entering the evaporator	Pressure of the water leaving the evaporator
Pressure of the water entering the condenser	Pressure of the water leaving the condenser
Temperature of the water entering the evaporator	Temperature of the water leaving the evaporator
Temperature of the water entering the the condenser	Temperature of the water leaving the condenser
Flow rate of the water entering the evaporator	
Flow rate of the water entering the condenser	
Pressure drop over the orifice (adjustable valve)	

4.3. MODEL DECOMPOSITION

Each of the components of the cycle is modeled as a separate module. Each module can be decomposed into sub-modules where necessary. For each module, the in- and outputs can be specified, where the model equations link the inputs to the outputs. Note that for the mixing point the outputs are generated against the flow direction of the working fluid, as the mixing point inlet from the reciprocating working fluid pump is determined from the separator liquid outlet and the evaporator inlet streams.

The goal of the model is to calculate the thermodynamic state of the working fluid at all points in the OTEC cycle. To successfully determine all state properties of the working fluid using CoolProp, two of the state parameters are needed at each point to determine all other state properties. For single phase streams, the temperature and pressure of the working fluid will suffice to determine all other state properties. For two phase streams, the vapor quality and pressure of the working fluid will suffice to determine all other state properties.

4.4. ASSUMPTIONS

For such a complex system, some assumptions have been made to create a working thermodynamic model. The assumptions are given for the whole of the system and also some assumptions per component are defined.

4.4.1. FULL CYCLE ASSUMPTIONS

- The system is assumed to be well insulated, so no heat is lost to the surroundings.
- A lumped parameter method is used at in- and outlets of process units, meaning that the working fluid at in- and outlet state is averaged for a certain amount of working fluid and no spatial distribution over the radial space inside piping can be obtained.
- The model calculates a steady state solution and cannot determine start-up or shut-down conditions.
- The height differences between all components are assumed to be negligible. An exception is made for the liquid column height calculation in the module of the gear pump. This will be explained later.
- All three fluid flows (ammonia, cold and warm water) are assumed to be steady state, inviscid and fully developed. Kinetic energy differences within the flows are negligible.

4.4.2. HEAT EXCHANGER ASSUMPTIONS

- The fluid flows inside the heat exchangers are assumed to be one-dimensional.
- The water flows are always single phase liquid.
- When there is two phase flow on the working fluid side of the heat exchangers, the vapor and liquid fractions are assumed to be perfectly mixed.
- Radiation is considered negligible, considering the low temperatures of the streams.
- Full condensation is assumed at the condenser outlet (saturated or sub-cooled).
- Heat accumulation in the heat exchanger walls and plates is assumed negligible.

4.4.3. SEPARATOR

- Perfect separation of the liquid and vapor phase is assumed.
- The separator is assumed to be perfectly insulated, so no heat is lost to the surroundings.

4.4.4. PUMPS

- Single phase liquid flow through the pumps is assumed.
- The pumps are assumed to generate a constant mass flow.

4.4.5. TURBINE (ORIFICE)

- The Orifice is assumed to be ideal, meaning that the inlet enthalpy is equal to the outlet enthalpy.

4.5. COMPONENT NUMERICAL MODELS

Goudriaan [11] and Kuikhoven [25] developed a numerical model to calculate the working fluid states within the OTEC cycle. For each component, the mass, momentum, and energy conservation equations, as well as the assumptions, are used to derive the model equations.

This section will explain the current ORC configuration numerical methods used in the OTEC cycle. These methods are extensions based on work done in previous research assignments.

4.5.1. HEAT EXCHANGERS NUMERICAL METHOD

The heat exchangers are modeled according to energy and mass conservation. Energy conservation is checked by comparing:

$$\dot{Q}_{load} = \dot{Q}_{duty} \tag{4.1}$$

Where $\dot{Q}_{load}$ and Q_{duty} can be calculated according to equations 2.1a and 2.2 respectively.

The LMTD method is often used to evaluate the performance of heat exchangers. Morisaki and Ikegami [66] concluded that the GMTD approach was better suited than the LMTD method as it accounts for the changing fluid properties during heat transfer. The GMTD divides the heat exchanger length into smaller segments, such that the changing fluid properties can be evaluated during two phase flow. A similar approach is used in the numerical method for the heat exchanger model. The traditional LMTD method is used, but evaluated per segment instead of using the four in and outlet temperatures. This approach will also take the changing fluid properties through the heat exchanger into account.

To accurately calculate the heat transfer over a heat exchanger a discretization of the heat exchanger is executed. The heat exchanger is divided into smaller control volumes, to accurately calculate the heat transfer (and pressure drop) according to the correlations. A graphical depiction of the control volume method is displayed in Figure 4.3

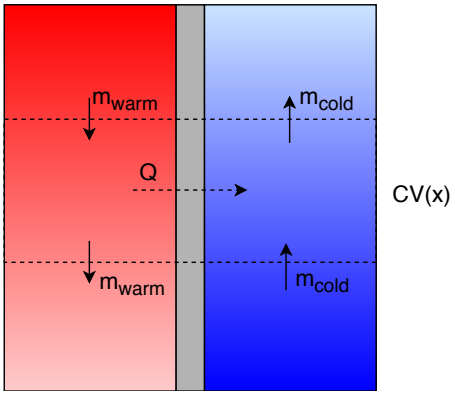

Figure 4.3: Control volume method for the heat exchangers

For each control volume in the heat exchanger, the heat transfer, flow characteristics, and pressure drop can be calculated. Once solved, the algorithm jumps to the next control volume to make the same calculations using the input from the previous control volume. Once all control volumes are solved, the resulting heat exchanger outlet states can be determined from the individual control volume results.

In the following section, the heat exchanger algorithms for the evaporator will be explained. This algorithm is based on the work done by Goudriaan [11], Kuikhoven [25] and van Strijp [34], but expanded upon to suit the ORC configuration.

EVAPORATOR

It is assumed that the water inlet state is known as well as the working fluid inlet state. The heat exchanger area imposed by geometry is known.

For the first iteration, a fixed heat exchanger pressure drop is used and divided linearly over the control volumes. This initial pressure drop is only used to calculate the first iteration over the heat exchanger and will be disregarded after, thus won't have any effect on the final result.

The heat exchanger algorithm starts by guessing the water outlet temperature. The next step is to divide the currently known total evaporator pressure drop over the control volumes. For the first iteration, this means dividing the initially given pressure drop over the control volumes. For any further iteration, this means dividing the previously calculated pressure drop over the control volumes.

The heat load available from the water side can now be determined using the guessed water outlet temperature. This heat is then divided by the number of control volumes to calculate the heat load per control volume. The heat load per control volume is used to determine the enthalpy difference per control volume:

$$\Delta h_{cv} = \frac{\dot{Q}_{cv}}{\dot{m}_{wf}} \tag{4.2}$$

The enthalpy difference per control volume can be used to determine the outlet enthalpy of the control volume, which is used as the inlet enthalpy of the next control volume. The pressure of each consecutive control volume is calculated by subtracting the control volume pressure drop from the control volume pressure

$$h_{cv+1} = \frac{\dot{Q}_{cv}}{\dot{m}} + \Delta h_{cv} \tag{4.3a}$$

$$p_{cv+1} = p_{cv} - \Delta p_{cv} \tag{4.3b}$$

With the calculated enthalpy and pressure of the next control volume, other working fluid state properties (like temperature, vapor quality and concentration of ammonia) can be determined using CoolProp. With the outlet temperature of the current control volume now calculated, the LMTD for the control volume can be determined.

$$\Delta T_{LMTD,cv} = \frac{(T_{warm,in} - T_{cold,out}) - (T_{warm,out} - T_{cold,in})}{ln(\frac{T_{warm,in} - T_{cold,out}}{T_{warm,out} - T_{cold,in}})} \tag{4.4}$$

For the current control volume, all the working fluid state properties at inlet and outlet, the LMTD and the heat duty for this control volume are now known. Using one of the single or two phase heat transfer correlations proposed in Section 2.1.1, the heat transfer coefficients of the control volume for the working fluid and water side can be calculated. With the heat transfer coefficients and the LMTD, the overall heat transfer coefficient (fouling is assumed to be negligible) and the resulting control volume heat transfer area can be calculated.

$$\frac{1}{U_{cv}} = \frac{1}{\alpha_{conv,water,cv}} + \frac{1}{\alpha_{conv,wf,cv}} + \frac{t}{k_{wall}} \tag{4.5}$$

$$A_{cv} = \frac{\dot{Q}_{cv}}{U_{cv}\Delta T_{LMTD,cv}} \tag{4.6}$$

Now that the control volume heat transfer area is known, the control volume vertical length can be calculated.

$$L_{cv} = \frac{A_{cv}}{L_w \Phi N_e} \tag{4.7}$$

Where L_w is the effective plate width in [m], Φ is the surface enhancement factor and N_e is the effective number of channels. Using this control volume vertical length and the pressure drop correlations described in Section 2.3, the pressure drop over the control volume can be calculated and updated.

This process is repeated for each control volume. Once each control volume has been evaluated the calculated control volume pressure drops are added up to give an updated total heat exchanger pressure drop. The area of each control volume is summed to give the total calculated heat transfer area, which is then compared to the actual heat exchanger area. If the calculated sum of the heat transfer area is smaller or larger than the actual heat transfer area, then the energy balance criterion is not met and a new water outlet temperature needs to be guessed. This loop continues until the calculated area equals the actual area of the heat exchanger within the given convergence criterion boundary.

This control volume approach as described is the basis for the ORC evaporator model. It is an extension made on the heat exchanger algorithm created by Kuikhoven [25] and Goudriaan [11]. A graphical depiction of their evaporator heat exchanger algorithm is displayed in Appendix J.

The algorithm as described above is depicted graphically in Figure 4.4, where the stream numbers are matched with those seen in Figure 4.2

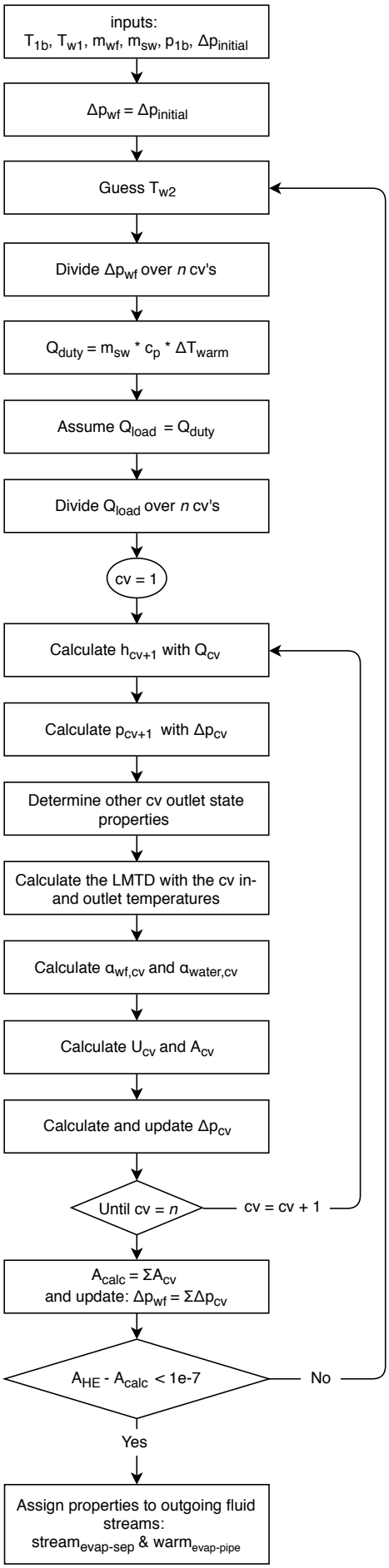

Figure 4.4: Evaporator heat exchanger algorithm for the ORC.

CONDENSER

The condenser heat exchanger algorithm is very similar to the evaporator algorithm and is based on the same control volume approach. The difference in the condenser is that the enthalpy difference over each control volume is subtracted on the working fluid side and added on the cold water side. The model is also able to use pressure drop correlations to calculate and update the pressure drop per control volume for the condenser. Since there is no direct necessity to accurately calculate the pressure drop over the condenser a fixed pressure drop will be used.

4.5.2. SEPARATOR

The off-design OTEC model models the separator as a black box where the method of separation is not specified. Knowing that the separator fully separates the vapor fraction from the liquid fraction, mass balance over the separator can be used to calculate the mass flow rates of the two outgoing streams.

$$\dot{m}_{wf} = \dot{m}_{vap} + \dot{m}_{liq} = q_{in}\dot{m}_{wf} + (1 - q_{in})\dot{m}_{wf} \tag{4.8}$$

Considering a perfectly insulated separator, energy conservation over the separator can be used to calculate the enthalpies of the outgoing streams.

$$\dot{m}_{wf} h_{in} = \dot{m}_v h_v + \dot{m}_l h_l \tag{4.9}$$

The pressure drop over the separator is caused by the inlet and two outlets ports. The pressure drop at the inlet port can be estimated by one velocity head and the pressure drop at the outlet ports can be estimated by a half velocity head [67].

$$\Delta p_{in} = \frac{\dot{m}_{in}^2}{2\rho_{in} A_{in}^2} \tag{4.10a}$$

$$\Delta p_{out} = \frac{\dot{m}_{out}^2}{4\rho_{out} A_{out}^2} \tag{4.10b}$$

4.5.3. PUMPS

The pumps modeled in the OTEC cycle make use of a fixed isentropic efficiency to calculate the work done by the pump and the effect on the working fluid. The energy conservation equation for the pumps will then follow.

$$W_{pump} = \frac{\dot{m}_{in}(h_{in} - h_{out,is})}{\eta_{is}} \tag{4.11}$$

Where W_{pump} is the work done by the pump on the working fluid in [W], $h_{out,is}$ is the enthalpy of the working fluid coming out of the pump as if the pump had an efficiency of 100% and η_{is} is the isentropic efficiency of the pump.

OSCILLATING WORKING FLUID PUMP

The working fluid pump in the OTEC Demo is an oscillating displacement pump, so a damper is installed to decrease pressure oscillations in the setup. Such a damper causes a significant energy loss in the system and since it is not modeled separately, the energy loss needs to be accounted for in the working fluid pump. To model this correctly the working fluid pump is given a relatively low isentropic efficiency, which is fitted from experimental data.

In the updated model the working fluid pump is calculated forwards, meaning that the working fluid inlet condition is known and the working fluid outlet condition needs to be calculated. The required outlet pressure is known, following the result from the mixing point. Using the outlet pressure and inlet entropy, the outlet isentropic enthalpy can be determined using CoolProp. With the isentropic outlet enthalpy and the isentropic efficiency, the actual outlet enthalpy can be calculated.

$$\eta_{is} = \frac{h_{out,is} - h_{in}}{h_{out} - h_{in}} \tag{4.12}$$

$$h_{out} = h_{in} + \frac{h_{out,is} - h_{in}}{\eta_{is}} \tag{4.13}$$

GEAR PUMP

The gear pump has a much higher isentropic efficiency than the working fluid pump, since it isn't oscillating and has a more continuous flow output, so no damper is required.

In the model the gear pump is calculated forwards, meaning that the working fluid inlet condition is known and the working fluid outlet condition needs to be calculated. The required outlet pressure is also known since it has to be equal to the evaporator inlet pressure plus a fixed pressure drop over the mixing point. The inlet entropy is used to determine the outlet isentropic enthalpy using CoolProp. With the isentropic enthalpy and the isentropic efficiency, the outlet enthalpy can be calculated, according to equation 4.13.

In the module of the gear pump, the liquid column height required to overcome the pressure drop is also calculated. This is a relatively simple calculation based on Equation 3.1. This calculation is done to give insight on the liquid column height required to build up enough pressure, so there would be no need for a gear pump. The liquid column height in the separator while using the gear pump is not taken into account as an additional driving force reducing the work required by the pump. The effect of the actual liquid column is neglected for several reasons:

- The off-design model does not make use of the actual mass of ammonia present in the system. Working fluid mass flows are used to calculate the required states, heat transfers and pumping work. No buffer tank is present in the model and thus no actual total amount of ammonia in the system is used. Because of this, the model can't calculate where the ammonia is situated in the system. In calculating the liquid column height while also using a gear pump it is required to know how much liquid is present in all parts of the system, as this is closely inter-related. If the system is filled with a high amount of ammonia, logically the liquid level in the separator and buffer tank will be higher. If the system is filled with a lower amount of ammonia, vice versa. If the vapor quality at the evaporator outlet is relatively low, more liquid will be present in the evaporator, reducing the liquid level height in the separator. All these inter-related factors make calculating the liquid level height in the separator while using a gear pump quite complex.
- The piping infrastructure of the system is also not taken into account for the off-design model. This is because the piping layout is very specific and will most likely never be the same for different OTEC systems, while the off-design model is intended to be used for any system. Not knowing how much ammonia is situated in which segment of the piping infrastructure adds to the difficulty of determining the liquid column height in the separator.
- The work done by the gear pump is assumed to be relatively small, compared to the other energy streams in the system. The ultimate effect of the liquid column on the net power output of the cycle will thus also be very small.

The combination of the three factors described above make calculating the exact separator liquid column height while using the gear pump redundant. The effect of this liquid level will be a reduction of the required power needed by the gear pump. Determining this liquid column height is very complex and system specific, while the work done by the gear pump is very small and this reduction in pump power needed can thus be neglected

4.5.4. MIXING POINT

The mixing point in the ORC setup is situated between the working fluid pump, the gear pump, and the evaporator. The mixer calculates the state properties of the working fluid stream coming from the working fluid pump depending on the working fluid state coming from the gear pump and the working fluid state going to the evaporator. Mass conservation determines the mass flow rate coming from the working fluid pump.

$$\dot{m}_{wfpump} = \dot{m}_{evap} - \dot{m}_{gpump} \tag{4.14}$$

The enthalpy of the stream coming from the working fluid pump is determined using the energy balance over the mixing point.

$$h_{wfpump} = \frac{h_{evap}\dot{m}_{evap} - h_{gpump}\dot{m}_{gpump}}{\dot{m}_{wfpump}} \tag{4.15}$$

The pressure of the stream coming from the working fluid pump is determined using a fixed pressure drop over the mixing point, adding this to the pressure of the stream going to the evaporator. Using the enthalpy and pressure, the other working fluid state properties for the stream coming from the working fluid pump are calculated.

4.5.5. ORIFICE

The turbine in the OTEC Demo is simplified to an orifice with a fixed pressure drop. This orifice is assumed to be ideal, so no heat loss will occur over the orifice. Using mass and energy balances it is determined that the orifice outlet mass flow and enthalpy are equal to the inlet mass flow and enthalpy. A fixed pressure drop determines the outlet pressure. Using the pressure and enthalpy of the outgoing flow, the other working fluid state properties can be determined

4.6. SYSTEM NUMERICAL METHOD

The main cycle numerical method solves a unique steady state condition at some initial conditions. The solver converges to a steady state solution, which (at the set operating conditions) should be close to reality in the OTEC Demo if the used correlations predict the heat transfer and pressure drop correctly. This section will discuss the inputs of the full system model, the inputs in the different components and the solving algorithm. The components in the off-design model need several different inputs to function and create realistic results. In Table 4.2 these inputs are shown. The inputs are based on work done by van Strijp [34], with several additions made.

Table 4.2: Additional inputs for the off-design model of the OTEC Demo

Component	**Required input/ initial guess**	**Value/ Name**
Evaporator	Geometry	See Appendix A
	Control volumes	100
	Heat transfer correlations	
	Two phase (wf-side)	From Section 2.1
	Single phase (wf-side)	Donowski & Kandlikar [24]
	Single phase (water-side)	GoudKuik [11] [25]
	Pressure drop correlation	
	Single phase (wf-side)	From Section 2.3
	Two phase (wf-side)	From Section 2.3
	Single phase (water-side)	VDI [54]
Condenser	Geometry	See Appendix A
	control volumes	100
	Heat transfer correlations	
	Two phase (wf-side)	Geschiere [4]
	Single phase (wf-side)	Donowski & Kandlikar [24]
	Single phase (water-side)	GoudKuik [11] [25]
	Pressure drop correlation	
	Single phase (water-side)	VDI [54]
Separator	Radius of the inlet port	$3.96e^{-3}$ [m]
	Radius of the vapor outlet port	$3.96e^{-3}$ [m]
	Radius of the liquid outlet port	$1.88e^{-3}$ [m]
Turbine (orifice)	Fixed pressure drop	Taken from experimental data

The main cycle numerical method uses an optimization algorithm based on the Scipy [68] implementation of a differential evolution algorithm. A differential evolution algorithm is a method that belongs to the genetic algorithms. These algorithms are widely used if system parameters are unknown or if multiple local minima exist [69]. Differential evolution is preferred over other solver methods since it is relatively fast converging, relatively simple to understand and to implement. A differential evolution algorithm searches for the local minimum of a function using a "population" of guesses. The population of input values creates a set of output values, which are then judged based on some convergence criteria. In the selection step, the members of the population which gave the best result have a higher chance of being selected for the crossover step. In the crossover step, a certain crossover constant determines how much the values of the selected population members will be mixed to create a new population, equal to the size of the original population. After the crossover step, the new mixed selected population will be mutated with a certain mutation probability. This new population will run through the full iteration and the results are judged once again. If the convergence criteria for a single member of the population have been met, the iteration is finished and the resulting member will be the result leading to the minimum of the function. This implementation of the genetic algorithm can be seen in Figure 4.5

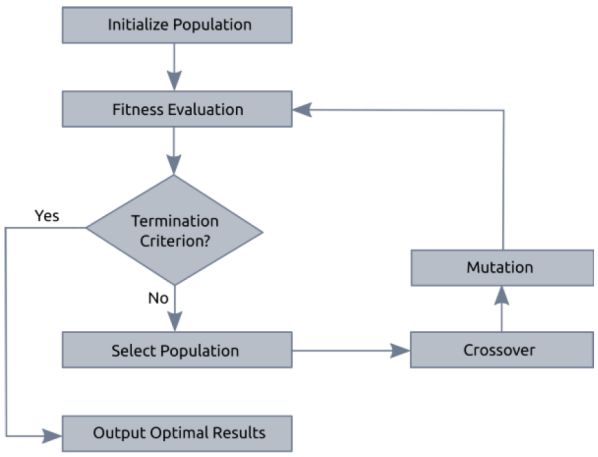

Figure 4.5: Basic structure of a genetic algorithm. Source [34]

The Scipy default settings are taken over in the differential evolution since the global minimum is found with these settings and the computational time is acceptable. The population size is a multiplier for setting the total population size. The solving strategy influences how the iteration guesses originate. The strategy, "best1bin", is the default setting of Scipy's differential evolution. In this strategy, two members of the population are randomly chosen. Their difference is used to mutate the best member. Table 4.3 shows an overview of the differential evolution settings.

Table 4.3: Differential evolution algorithm settings of the full cycle model. Source [34]

Setting		Value
Population size		20
Mutation		0.5 – 1
Recombination		0.9
Solving strategy		best1bin
Bounds	Pressure	7.0-11.0 [bar]
	Temperature	278.15-298.15 [K]
Convergence criteria	Enthalpy error	<1 [%] / <3 [%]
	Energy balance error	<1 [%] / <3 [%]

An objective function is a function to be maximized or minimized in optimization theory. In the full cycle objective function, the inputs are the guessed pressure and temperature of the working fluid inlet conditions of the evaporator. The parameters which are optimized are the enthalpy error of the working fluid state between the reciprocating working fluid pump and the mixing point and the total energy balance error over the cycle.

In the former off-design model for the Kalina cycle, there is a forward and backward loop. The forward loop, which follows the direction of the evaporator and a backward loop, which is going over the recuperator to the inlet of the working fluid pump. The inlet enthalpy of the working fluid pump from the backward loop can be compared with the inlet enthalpy of the cycle pump from the forward calculation. The resulting difference between the enthalpies is used as the enthalpy error and is fed back to the solver. The solver will evaluate the guessed input values of the evaporator based on the result for the enthalpy error.

The full cycle numerical method for the ORC setup follows a similar method. Starting at the evaporator inlet, the working fluid state is guessed. Then using forward calculations, the working fluid states going through the separator are calculated. The numerical method then follows two different paths. One path calculates the working fluid states over the orifice, the condenser and finally through the reciprocating working fluid pump to the mixing point. The other path calculates the working fluid states over the gear pump and backwards over the mixing point to the reciprocating working fluid pump. These two numerical paths then meet between the working fluid pump and the mixing point, where convergence based on the enthalpy error is checked. A graphical depiction of this numerical solving method can be seen in Figure 4.6, where the arrows point in the numerical solving direction through the components.

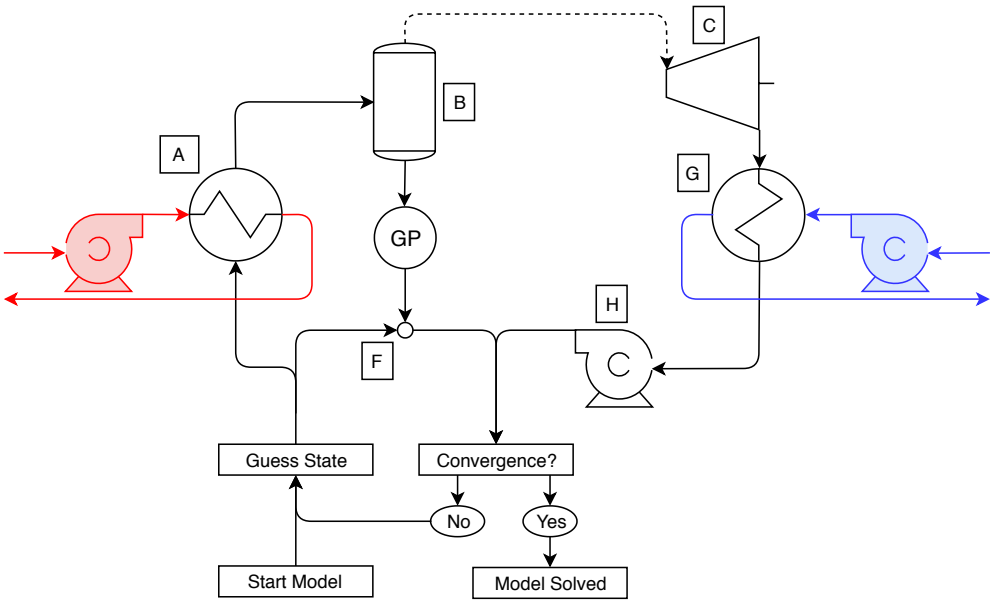

Figure 4.6: Numerical solving direction through the components of the off-design model.

The convergence criterion for the full cycle algorithm is twofold, namely the enthalpy error and energy balance over the system.

- The enthalpy difference between the forwards and backwards calculated stream between the reciprocating working fluid pump and the mixing point is calculated and then divided by the enthalpy of the forwards calculated stream. This enthalpy error has to be smaller than a certain imposed bound, usually 1%.
- The energy balance over the system is calculated. This is the heat added to the cycle in the evaporator plus the work done by the working fluid pumps, minus the heat subtracted from the cycle by the condenser. The value of the energy balance is divided by the condenser heat transfer rate and the absolute value of the result has to be smaller than a certain imposed bound, usually 1%.

If one of both the convergence criteria is not met, a new initial guess is made for the inlet of the evaporator. This iteration continues until the convergence criteria are met. In this situation, the inlet pressure and temperature are accepted as the solutions for the operating condition of the cycle. The mass and energy balance over the components are continuously monitored. In the model, several breakpoints are implemented, which are checks to ensure that the solver only converges to realistic solutions. Furthermore, the breakpoints speed up the convergence, since the iteration stops preemptively if an error occurs. Table 4.4 gives the errors, which can occur in the model. The sub-cooling and vapor fraction errors are dependent on how much sub-cooling or vapor fraction is present. The solver detects the different values of the iterations and evaluates the iterations so that this leads to convergence of the model. Some errors can be turned off since some errors can occur under certain conditions.

Table 4.4: Possible breakpoints in the model

Component	Error
Heat exchangers	No solution found
	Optimization not successfully finished
Evaporator	No vapor outlet
	Super heated vapor
Turbine	Pressure outlet not found
Condenser	Temperature inlet warm stream lower than inlet cold stream
	Outlet contains a vapor fraction
	Enthalpy out of range
Pump	Temperature inlet higher than outlet
	Pressure inlet higher than outlet
All components	Mass balance
	Energy balance

As stated before, the ORC numerical solution algorithm calculates the convergence of a steady state in the cycle using both the enthalpy error over two different calculated paths through the cycle and the total cycle energy balance. A step by step explanation of this solution algorithm looks as follows:

1. The warm and cold water inlet temperatures and mass flow rates are imported into the model. For the working fluid, the mass flow rate is also imported into the model.

2. The temperature and pressure of the working fluid going into the evaporator are guessed

3. The working fluid state coming out of the evaporator is calculated using the heat exchanger algorithm

4. If any breakpoint errors occur in the evaporator, the solution algorithm goes back to step 2.

5. The separator output working fluid state going to the turbine (orifice) is calculated.

6. The separator output working fluid state going to the gear pump is calculated.

7. The turbine (orifice) output working fluid state going to the condenser is calculated.

8. The gear pump output working fluid state going to the mixing point is calculated.

9. The condenser output working fluid state going to the working fluid pump is calculated with the heat exchanger algorithm.

10. If any breakpoint errors occur in the condenser, the solution algorithm goes back to step 2.

11. The mixing point inlet working fluid state coming from the working fluid pump is calculated backwards with the working fluid state going to the evaporator and the working fluid state coming from the gear pump.

12. The working fluid pump outlet working fluid state to the mixing point is calculated.

13. the backwards and forwards calculated state of the working fluid between the working fluid pump and the mixing point is checked on enthalpy error. If the convergence criteria are not met, the algorithm goes back to step 2. If the convergence criteria are met, a converged steady state is reached and all resulting working fluid states in the system are exported as results.

Figure 4.7 shows the ORC solution algorithm, where the state points in the algorithm are based on Figure 4.2:

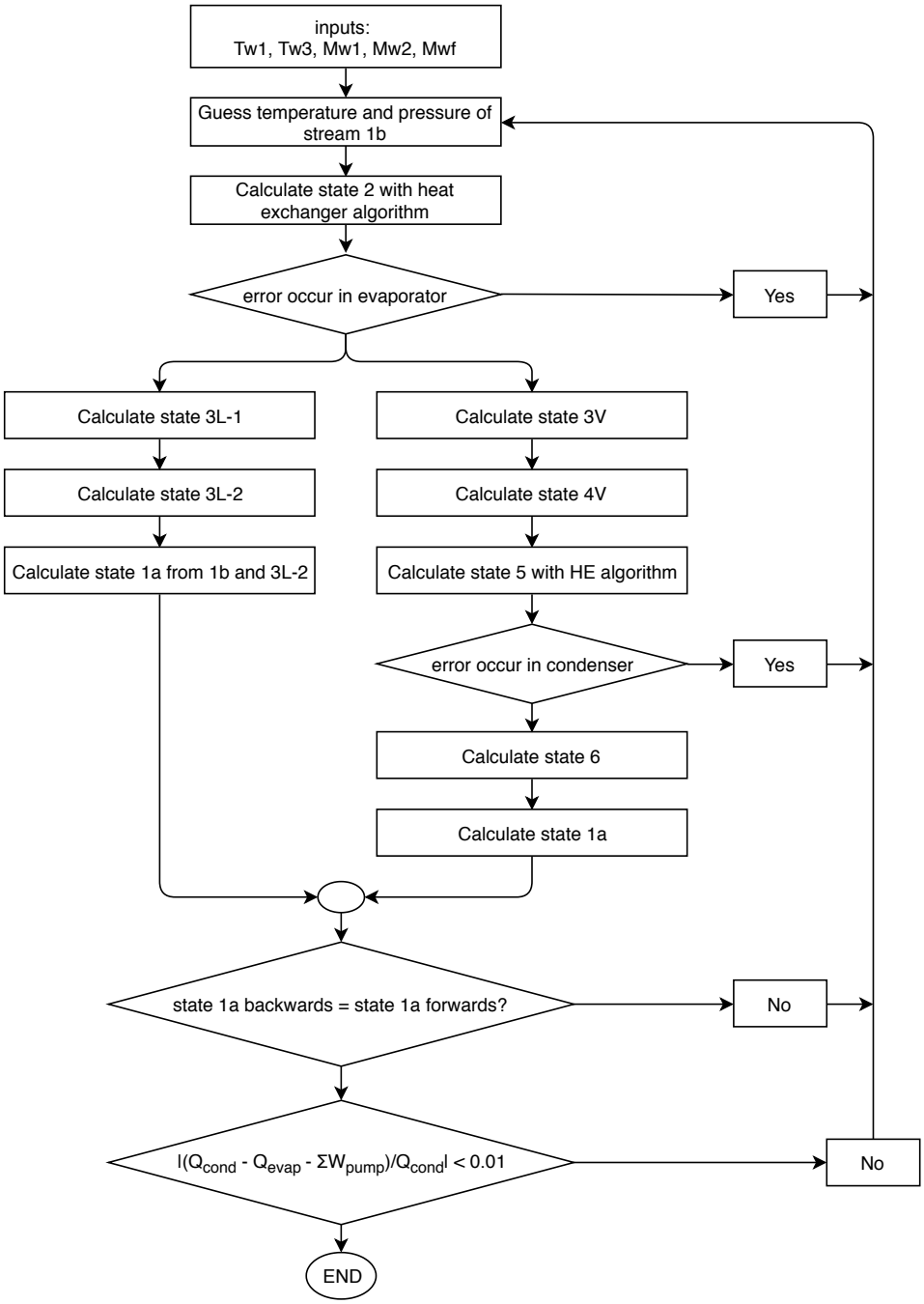

Figure 4.7: ORC solution algorithm

5

Validation, Verification & Experimental Procedure

5.1. Previous Component Validations

Before the full cycle model is validated and tested against the experimental setup of the OTEC Demo, the separate components need to be validated. This is done to make sure the best fitting correlations are selected and used in the full cycle model validation. In previous research done by Goudriaan [11] and Kuikhoven [25] the components were validated against differing ammonia/ water concentrations in a Kalina cycle configuration. These experimental data sets form the basis for the validations executed in this research assignment, but can't all be used in the ORC configuration. Firstly, the emphasis of validation is shifted from the ammonia - water concentration to a difference in evaporator mass flow i.e. re-circulation rate. In an ORC configuration, the ammonia - water concentration is constant, 100% ammonia, so correlations that might have the best fit for a difference in ammonia - water concentration over a certain domain might not have the best fit for pure ammonia. Secondly, the OTEC Demo has changed a lot over the past years. Executing a full cycle comparison between data obtained by Goudriaan [11] and Kuikhoven [25] and data obtained in the current setup might not be considered fair. Some validations of the OTEC Demo can still be used, however. The first sections below state all validations that have been done in the past which can be assumed to still apply in the current setup.

5.1.1. Water-water experiments

Goudriaan and Kuikhoven conducted three different types of water-water experiments to validate the single phase water side heat transfer correlation. These experiments contained a data set where the warm and cold water mass flow rates were varied and the working fluid (which is water in this case) mass flow rate was kept constant. The second data set contained data where the warm and cold water mass flow rates were kept constant and the working fluid mass flow rate was varied. The third data set contained combinations of varying cold, warm and working fluid mass flow rates to assess the validity of the previous results of the entire range of combinations.

The results of the water-water experiments were used to create a single phase heat transfer correlation for the water side of the heat exchangers, which is now known as the GoudKuik correlation. This correlation can still be used in the current ORC setup because nothing has changed on the water side of the experiments. The GoudKuik correlation can be seen in equation 5.1

$$Nu = 0.291 Re^{0.72} Pr^{0.33} \tag{5.1}$$

5.1.2. Single Phase Ammonia Validation (Recuperator)

In the previous Kalina cycle, see Figure 3.1, a single phase heat transfer correlation for the ammonia - water mixture has been selected by Goudriaan [11] and Kuikhoven [25]. The validation of the single phase heat transfer correlations was made over the recuperator, since the working fluid exchanges heat between the cold

and warm flow in liquid single phase only.

The validation over the recuperator was made at differing concentrations of ammonia ranging between 90 - 100%. The variables that were used as an input to the recuperator validation model were (see Figure 3.1):

- The temperature, pressure and mass flow of the working fluid stream going from the separator to the recuperator, stream 3L.
- The temperature, pressure and mass flow of the working fluid stream going from the recuperator to the evaporator, stream 1.
- the pressure of the working fluid stream going from the valve to the mixing point, stream 5.

The variables that were created as results from the model which were compared against the experimental data were (See Figure 3.1):

- The temperature of the working fluid stream going from the recuperator to the valve, stream 4L.
- The temperature of the working fluid stream going from the working fluid pump to the recuperator, stream 8.
- The temperature of the working fluid stream going from the valve to the mixing point, stream 5.
- The heat duty of the recuperator, component D.

An average deviation from experimental data was made for all correlations based on these four resulting variables. Based on the result of the average deviation, the single phase heat transfer correlation proposed by Donowski & Kandlikar [24] was picked as the one having the best fit to the measured data.

Looking at the outcomes of the analysis made by Goudriaan and Kuikhoven, it can be noticed that the correlations have a very consistent deviation from the measured data over the range of concentrations, thus indicating that the average deviation for the single phase heat transfer correlations is a good indicator for the deviation on any concentration level of ammonia.
Additionally, the heat transferred in the evaporator is transferred mostly in the two phase state of ammonia, since the degree of subcooling for the working fluid upon entering the evaporator is relatively small. Any errors that might occur in the calculation of the single phase heat transfer for the working fluid have very little effect on the consequential total evaporator heat transfer rate.
Combining these two insights with the resulting average deviation leads to the conclusion that Donowski & Kandlikar is the preferred single phase heat transfer correlation on the working fluid side for a concentration of 100% ammonia. The single phase heat transfer correlation proposed by Donowski & Kandlikar, which can be found in Appendix D, is also used in the current validation of the OTEC off-design model.

5.1.3. SEPARATOR AND ORIFICE VALIDATION

The separator and orifice were validated in a combined validation method by Goudriaan [11] and Kuikhoven [25] since the orifice is fed the vapor fraction of the working fluid stream coming from the evaporator. The variables that were used as inputs to the separator/ orifice validation model were (See Figure 3.1):

- The temperature, pressure and mass flow of the working fluid stream going from the evaporator to the separator, stream 2.
- the fixed pressure drop over the orifice, stream 4V - stream 3V.

The variables that were created as results from the model which were compared against the experimental data were (See Figure 3.1):

- The temperature, pressure and mass flow of the working fluid stream going from the separator to the orifice, stream 3V.
- The temperature, pressure and mass flow of the working fluid stream going from the separator to the recuperator, stream 3L.

- The temperature and pressure of the working fluid stream going from the orifice to the mixing point, stream 4V.

The pressure drop correlation used in the separator, stated by equation 4.10, accurately predicted the pressure drop, with an average deviation in the liquid stream of 1.15% and 1.20% in the vapor stream.

5.1.4. WORKING FLUID PUMP VALIDATION

Goudriaan [11] and Kuikhoven [25] also performed a validation of the model for the reciprocating pump. In the OTEC Demo, the power of the pump is not measured, so no direct comparison to the off-design model could be made. Instead, the enthalpy values over the working fluid pump were determined from experimental data using CoolProp. The pressure differential over the working fluid pump was measured with pressure sensors, and the specific volume was determined using a density sensor. Since the work done by the pump is equal to the enthalpy difference over the pump, equation 2.9 can be changed into:

$$\eta_{is} = \frac{v\Delta p}{h_{in} - h_{out}} \tag{5.2}$$

This equation is used to calculate and plot the isentropic efficiency of the working fluid pump over different ammonia concentrations and different mass flow rates. These results can be seen in Figure 5.1.

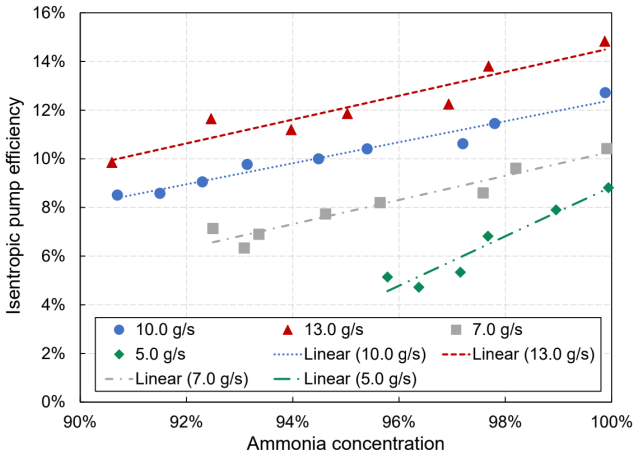

Figure 5.1: The isentropic efficiency of the working fluid pump versus the ammonia concentration. Source [25]

As can be seen in Figure 5.1, the isentropic efficiency for an ammonia concentration of 100% varies between 8-15%. Since the working fluid pump is still the same and no conditions concerning the pump have changed, this isentropic efficiency range can still be used for the working fluid reciprocating pump. In the following sections, if any calculations concerning the reciprocating working fluid pump are made, an isentropic efficiency of 8% is assumed.

5.2. MASS FLOW DIFFICULTIES

Originally, determining the experimental vapor quality at the evaporator outlet was thought to be relatively straight forward. As advised by a colleague working on the OTEC Demo, the mass flow sensor of the separator vapor stream (FI-201, see the P&ID in Figure 3.4) could be considered unreliable and the values it measured were disregarded from the start. But with the ammonia mass flow rate through the bottom of the separator and the ammonia mass flow rate through the reciprocating working fluid pump known, the total mass flow rate through the evaporator would just be the sum of these two. The vapor quality at the outlet would be the ammonia mass flow rate through the reciprocating working fluid pump, divided by the total mass flow rate through the evaporator. This is true in the ORC configuration because the working fluid mass flow rate through the reciprocating working fluid pump is equal to the vapor mass flow rate. When analyzing the experimental results in this manner, a strange discrepancy between the evaporator water side and ammonia side heat transfer rate was observed. Since energy balance can be applied to the evaporator, the water side heat transfer rate should be equal to the ammonia side heat transfer rate. When calculating the vapor quality in

the before mentioned manner, the ammonia side heat transfer rate would consistently be around 1.4 times the water side heat transfer rate. This would mean that the vapor quality calculated was roughly 1.4 times higher than the actual vapor quality created in the OTEC Demo.

The cause for this phenomenon was found in the measured values for the working fluid mass flow rate going through the reciprocating working fluid pump. An example of the output signal on mass flow sensor FI-203 and FI-202 (see the P&ID in Figure 3.4) can be seen in Figure 5.2.

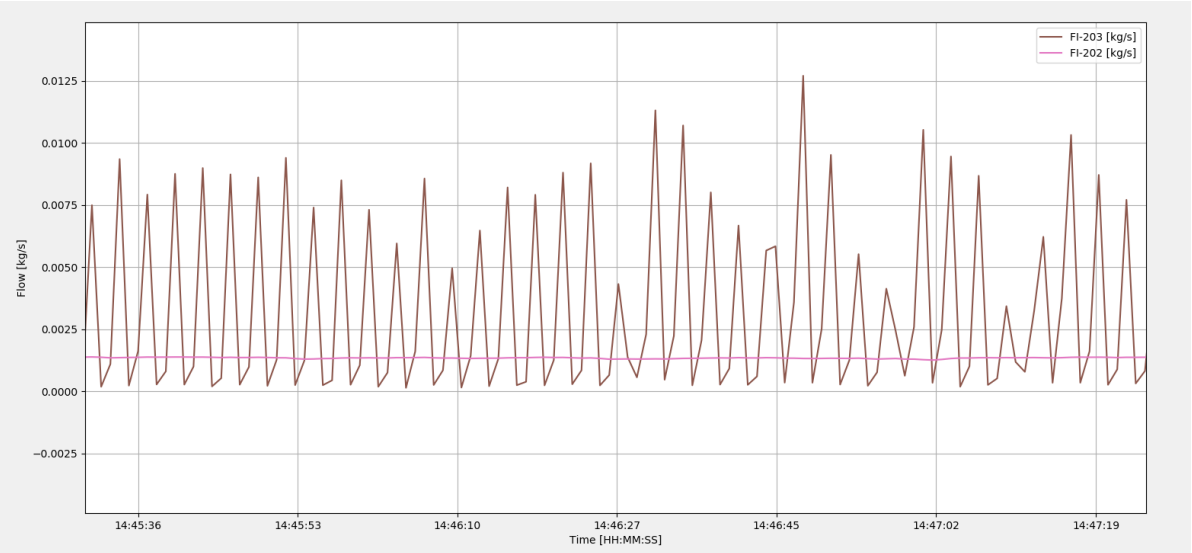

Figure 5.2: A typical read-out of mass flow sensor FI-203 and FI-202 for a 2 minute time span, showing how inconsistent the flow measured by sensor FI-203 is.

Since the reciprocating working fluid pump does not create a stable working fluid mass flow rate, the output for mass flow sensor FI-203 is not consistent either. When the changes in mass flow rate happen quicker than the sampling frequency of the sensor, the average of the sensor value can be different to what the actual average mass flow in the system would be.

After identifying this flaw, the decision was made to not use the mass flow rate measured by FI-203 in the calculations concerning the experiments anymore. The mass flow rate measured by FI-202 is considered accurate and stable, as can be seen in Figure 5.2.

A different methodology is needed to accurately calculate the mass flows throughout the OTEC Demo. A method using the evaporator water side heat transfer rate was created and tested as follows.

The experimental evaporator heat transfer rate is determined by subtracting the water side outlet enthalpy from the water side inlet enthalpy and multiplying this with the water side mass flow rate. The calculated water side heat transfer rate can be used to calculate the ammonia mass flow rates through the system.

Before the evaporator heat transfer rate can be used to calculate the mass flow rates through the system, the working fluid states in and around the evaporator need to be characterized. In Figure 5.3 an overview can be seen on three identified working fluid states inside the evaporator.

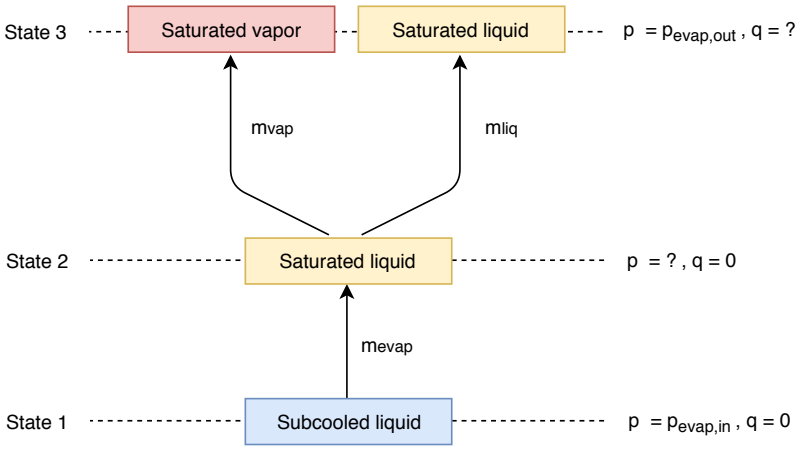

Figure 5.3: The identified working fluid states throughout the evaporator, starting with the evaporator inlet at the bottom and the evaporator outlet at the top.

As can be seen in Figure 5.3, the working fluid enters the evaporator in a (slightly) subcooled state, which is a single phase liquid at the evaporator measured inlet pressure. This state is labeled as state 1.
As heat is transferred to the working fluid going through the evaporator, the working fluid heats up until it reaches a saturated liquid state. The working fluid in this state will still be a single phase liquid. The pressure level at this point is unknown, but has a value anywhere between the evaporator inlet and outlet pressure. This state is labeled as state 2.
Once the working fluid has become fully saturated, evaporation starts to occur. a part of the working fluid stream is evaporated and leaves the evaporator in a saturated vapor phase. This part of the working fluid stream is the part that will leave the separator as the vapor fraction and will move through the orifice, condenser, and reciprocating working fluid pump.
The other part of the working fluid stream is assumed to stay at saturated liquid conditions, leaving the evaporator in a saturated liquid phase. This part of the working fluid stream is the part that will leave the separator as the liquid fraction and will move through the gear pump/ one-way valve back towards the evaporator.
The combined saturated liquid and saturated vapor at the evaporator outlet is labeled as state 3.
Using energy balance over the evaporator, it is known that the evaporator water side heat transfer rate has to be equal to the working fluid heat transfer rate. With the identified states in the evaporator as explained above, the energy balance over the evaporator becomes as follows:

$$\dot{Q}_{evap} = \dot{m}_{evap}(h_{out} - h_{in}) \tag{5.3}$$

$$\dot{Q}_{evap} = \dot{m}_{vap}(h_{3,vap} - h_{2,liq}) + \dot{m}_{liq}(h_{3,liq} - h_{2,liq}) + \dot{m}_{evap}(h_{2,liq} - h_{1,liq}) \tag{5.4}$$

The following assumptions are made to solve this equation with the known sensor values as stated in the previous section:

- The degree of subcooling of the working fluid at the evaporator inlet is assumed to be very small compared to the heat required to evaporate the vapor fraction in the working fluid stream. As a consequence, it is assumed that state 2 occurs relatively early within the evaporator, close the evaporator inlet. Under these assumptions, the pressure difference between state 1 and state 2 is assumed negligible.
- The enthalpy difference between the saturated liquid in state 3 and the saturated liquid in state 2 is assumed negligible since both states are saturated liquid. The only difference between them is the pressure, but the consequential enthalpy difference is considered very small compared to the heat required to evaporate the vapor fraction.

Using these assumptions, equation 5.4 can now be rewritten to:

$$\dot{Q}_{evap} = \dot{m}_{evap}\Delta h_{sl} + \dot{m}_{vap}\Delta h_{lv} \tag{5.5}$$

Where Δh_{sl} is the enthalpy difference between subcooled liquid and saturated liquid working fluid at the evaporator inlet pressure. Δh_{lv} is the enthalpy difference between saturated liquid working fluid at the evaporator inlet pressure and saturated vapor working fluid at the evaporator outlet pressure. The total evaporator mass flow rate is equal to the sum of the vapor and liquid fraction mass flow rates, so equation 5.5 can be rewritten to:

$$\dot{Q}_{evap} = \dot{m}_{vap}\Delta h_{sl} + \dot{m}_{liq}\Delta h_{sl} + \dot{m}_{vap}\Delta h_{lv} \tag{5.6}$$

Δh_{sl} and Δh_{lv} can both be determined using CoolProp. The liquid fraction mass flow rate is the same as the mass flow rate going through the bottom of the separator, which is measured by sensor FI-202, as explained in the previous section.

Now that all required values are known, equation 5.6 can be rewritten to calculate the vapor mass flow rate:

$$\dot{m}_{vap} = \frac{\dot{Q}_{evap} - \dot{m}_{liq}\Delta h_{sl}}{\Delta h_{sl} + \Delta h_{lv}} \tag{5.7}$$

The calculated vapor mass flow rate can be used to calculate the evaporator mass flow rate, which is the sum of the vapor and liquid mass flow rate, and the evaporator outlet vapor fraction, which the vapor mass flow rate divided by the evaporator mass flow rate.

To verify whether this method is feasible, the calculated evaporator mass flow rate and evaporator outlet vapor quality are used to calculate the working fluid side heat transfer rate. This value can then be compared to the water side heat transfer rate. In Appendix K a table can be seen with the deviations between the measured water side heat transfer rate and the working fluid side heat transfer rate, calculated with the method described above. The comparison is made using a data set of 53 measurement points created on the OTEC Demo. The result shows that the working fluid side heat transfer rate doesn't deviate from the water side heat transfer rate by more than 0.16%, which is acceptable.

The method described above is used in the following sections to determine the vapor mass flow rate, evaporator mass flow rate and vapor quality at the evaporator outlet for all experimental analyses.

5.3. NEW COMPONENT VALIDATIONS

In the sections below additional validations for several components are explained.

5.3.1. EVAPORATOR VALIDATIONS

The evaporator heat transfer and pressure drop correlations need to be validated to select the most accurate correlation. In this section, the evaporator heat transfer rate will first be validated to an experimental data set created with the OTEC Demo. The validated heat transfer correlation will then be implemented in the model and used to validate the pressure drop correlation. This pressure drop correlation will be used in the full cycle ORC off-design model validation.
In the following sections both the heat transfer and pressure drop correlation validations will be explained.

Experimental data of 53 different experiments are used to validate the two phase heat transfer and two phase pressure drop correlations. In all the experiments the concentration of ammonia is kept at 100%. The water mass flow rates, the water temperatures, and the working fluid mass flow rates are all varied throughout these experiments, so no conclusions on the evaporator performance under different working fluid mass flow rates can be made. This data set is solely used to validate the accuracy of different correlations used in the evaporator model.

To successfully validate the accuracy of the correlations for the evaporator, input values for the evaporator need to be selected. From the experimental data, the following sensors are used to generate input data for the evaporator model (See Figure 3.3):

- PI-22: The pressure of the warm water inlet stream, stream W1.
- PI-31: The pressure of the working fluid inlet stream, stream 1b.

- TI-07: The temperature of the warm water inlet stream, stream W1.
- TI-05: The temperature of the working fluid inlet stream, stream W1.
- FI-103: The mass flow rate of the water stream, stream W1.
- FI-202: The mass flow rate of the working fluid liquid stream coming from the separator, stream 3L-1.

From the experimental data, the following sensors are used to generate data to which the evaporator model outputs can be compared (See Figure 3.3):

- PI-23: The pressure of the warm water outlet stream, stream W2.
- PI-05: The pressure of the working fluid outlet stream, stream 2.
- TI-06: The temperature of the warm water outlet stream, stream W2.
- TI-01: The temperature of the working fluid outlet stream, stream 2.

The accuracy of the heat transfer correlations will be validated on their ability to successfully model the heat transfer rate in the evaporator. The accuracy of the pressure drop correlations will be validated on their ability to successfully model the evaporator working fluid pressure drop. The expectation is that the pressure drop correlations will have little to no effect on the calculated heat transfer rate in the evaporator, but this will also be tested to create certainty.
The results will be judged based on three different criteria:

- *The deviation from the required value.*
  A plot is made where for each experiment the deviation of the correlations compared to the experimental value will be displayed versus the vapor quality at the evaporator outlet.
- *The average deviation and standard deviation.*
  For each correlation, the average deviation over all experiments will be calculated. After this calculation, the standard deviation of each correlation to its average deviation will be given. E.g. if a correlation has an average deviation of +10% and a standard deviation of +- 5%, the results from this correlation will mostly deviate +5 to +15% from the experimental data.
- *A "box-and-whisker plot"*
  A box plot (in short) will be made for each correlation on the deviation for each experiment. A box plot displays a data-set through its quartiles and is particularly useful when trying to compare the variation of data points between different sets of data.

TWO PHASE HEAT TRANSFER CORRELATIONS RESULTS

For each experimental data-set used, the evaporator model is executed with a fixed working fluid and water side pressure drop. The water side pressure drop is calculated by subtracting the experimental water outlet pressure from the experimental water inlet pressure, which is then used as an input for the model. The same procedure is followed to calculate the working fluid pressure drop and use this as an input to the model.

From the measured values of temperature and pressure for the cold inlet and warm in- and outlet streams, knowing that they're all single phase liquids, the state of these streams can be determined using CoolProp. After determining all experimental stream properties, the water side volumetric flow rate is changed into a mass flow rate, using the water side density.

After the water side heat transfer rate is determined, the method described in Section 5.2 is used to determine the vapor mass flow rate, evaporator mass flow rate and the vapor quality at the evaporator outlet.

After all experimental working fluid states around the evaporator are calculated, the model runs the evaporator heat exchanger algorithm for all of the two phase heat transfer correlations. For the mentioned data-set of 53 measurements, the heat exchanger algorithm has thus solved a total of $11 \cdot 53 = 583$ times. The resulting numerical heat transfer rate of the evaporator for each correlation is compared to the experimental heat transfer rate as follows:

$$D_{\dot{Q}(Z)} = \frac{\dot{Q}(Z) - \dot{Q}_{experimental}}{\dot{Q}_{experimental}} \tag{5.8}$$

Where (Z) stands for the used two phase heat transfer correlations. The resulting deviation on the evaporator heat transfer rate is plotted against the experimental vapor quality at the evaporator outlet. In Appendix L these plots can be seen for each individual heat transfer correlation. In Figure 5.4 a plot of the results for all correlations can be seen between a deviation range of 50% to -300%, 50% to -50% and 20% to -20%.

Using the calculated deviation on the evaporator heat transfer rate, per experiment, the average deviation on the heat transfer rate per two phase heat transfer correlation is calculated. The standard deviation on the average deviation is calculated according to the following equation:

$$std = \sqrt{\frac{1}{N-1}\sum_{i=1}^{N}(D_{\dot{Q}(Z),i} - D_{\dot{Q}(Z),average})^2} \tag{5.9}$$

The average deviation on the evaporator heat transfer rate and standard deviation on the average deviation per correlation for all experimental data can be seen in Table K.2

Table 5.1: Average deviation on evaporator heat transfer rate and standard deviation on average deviation per two phase heat transfer correlation

Correlation	**Average deviation on $\dot{Q}$ (%)**	**Standard deviation (%)**
Amalfi	-164.05	57.25
Yan & Lin	14.77	12.49
Longo et al.	-37.02	8.89
Khan et al.	7.34	8.47
Palmer et al.	6.39	10.43
Huang et al.	-54.23	5.73
Arima et al.	-154.97	81.41
Han et al.	-14.36	7.33
Ayub (Thermosiphon)	10.20	11.88
Ayub (Flooded)	22.18	13.79
Taboas	-14.36	10.54

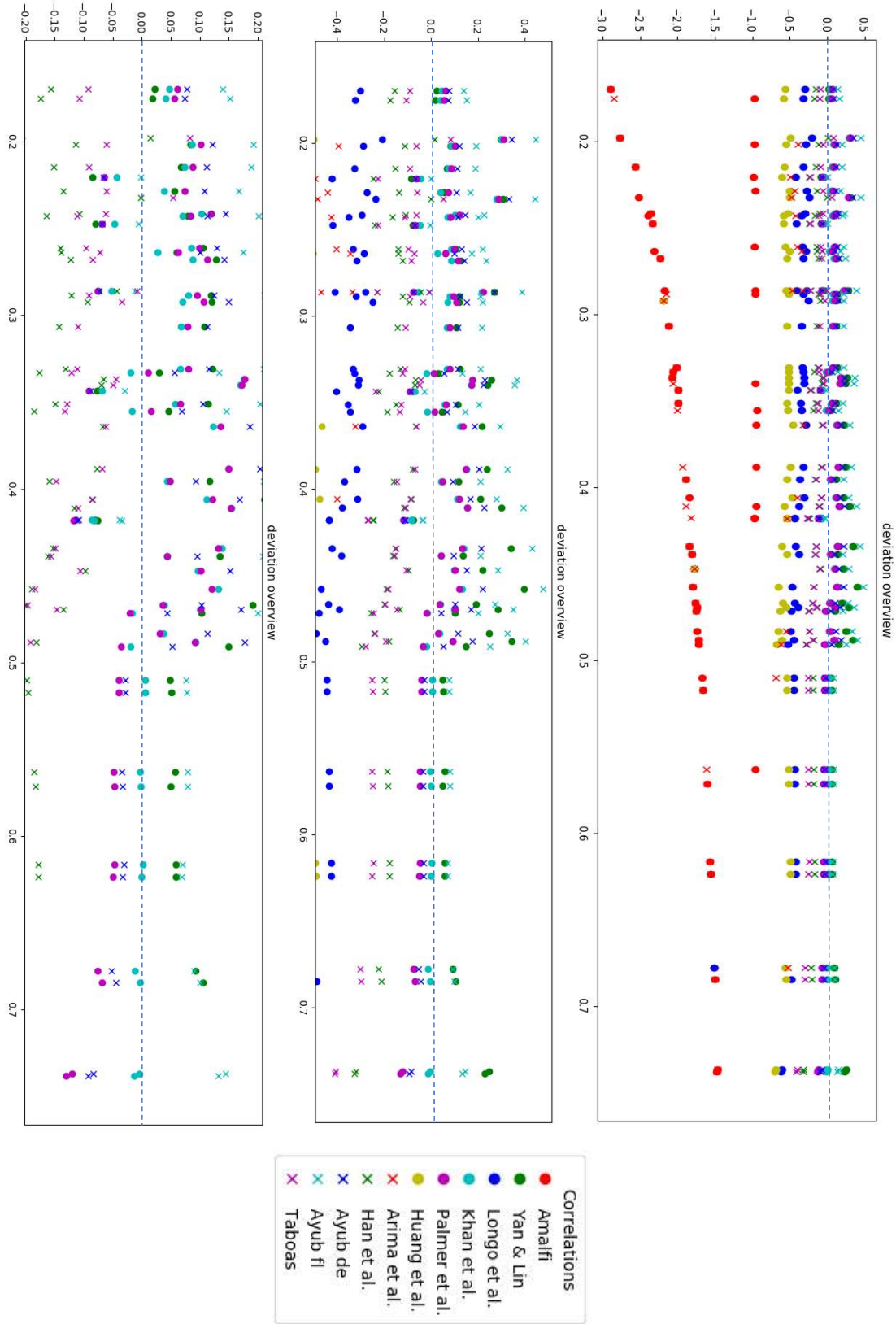

Figure 5.4: An overview of the deviation on evaporator heat transfer rate from experimental data per heat transfer correlation against the evaporator experimental vapor quality at the evaporator outlet.

In Figure 5.5 box plots on the deviation on experimental data for each two phase heat transfer correlation can be seen.

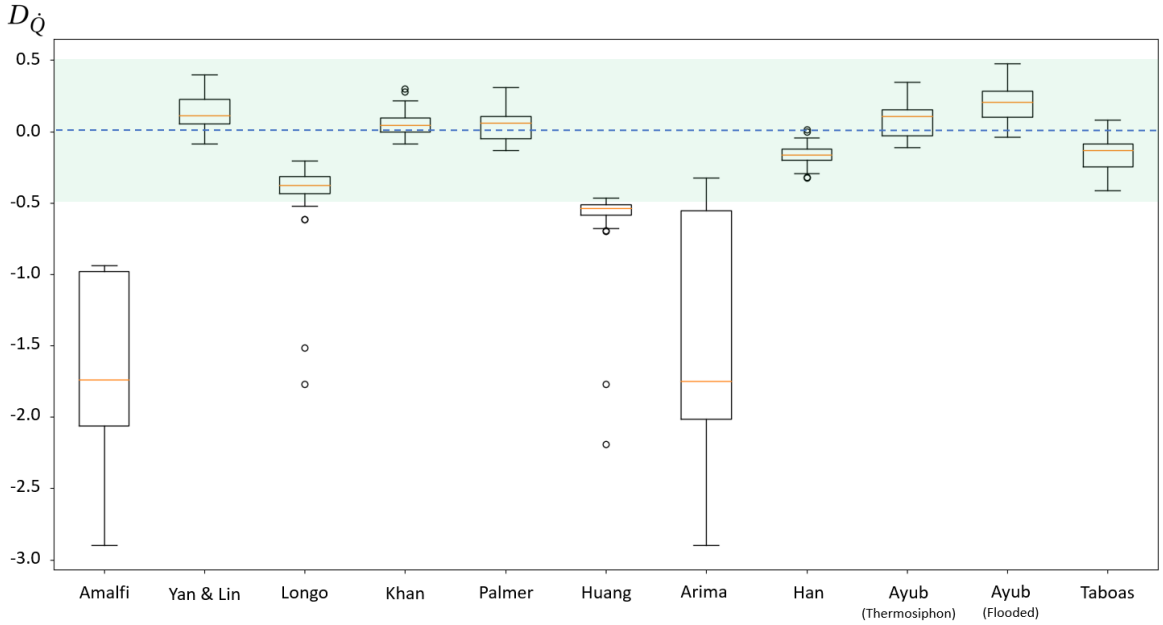

Figure 5.5: Box plots on the deviation on experimental data for each two phase heat transfer correlation.

TWO PHASE HEAT TRANSFER CORRELATIONS DISCUSSION

Looking at Figure 5.4, one can conclude that none of the heat transfer correlations has a perfect fit for the used experimental data set. This is to be expected considering the intricacies of boiling heat transfer as explained in Section 2.1.1. One thing that stands out from Figure 5.4 is the drop in the deviation that appears to occur for the heat transfer correlations when the evaporator outlet vapor quality is above 50%. The heat transfer correlations that were consistently over-estimating the evaporator heat transfer rate for vapor qualities of 50% and lower at the evaporator outlet, do not do so for vapor qualities of 50% and higher at the evaporator outlet.

Figure 5.4 on its own is not conclusive enough to decide on the heat transfer correlation to use in further work. But what can be concluded from this figure is that the heat transfer correlations proposed by Amalfi [26], Arima [8], Huang et al. [31], Longo et al. [28] and Han et al. [20] consistently under-predict the heat transfer rate in the evaporator. The deviation on the heat transfer rate between these correlations and the experiments is too big for these correlations to still be considered accurate on this data set.

The heat transfer correlation proposed by Taboas [33] slightly under-predicts the heat transfer rate for experiments with low vapor fraction at the evaporator outlet (up to 40%). Unfortunately, this under-prediction of the heat transfer rate grows bigger for higher vapor quality at evaporator outlet (above 40%) which also deems this heat transfer correlation inaccurate on this data set. This result seems logical since this correlation is specifically fitted against low vapor quality ammonia/ water mixture heat transfer.

The heat transfer correlation proposed by Ayub [32] with a C value for flooded evaporators over-predicts the heat transfer in the evaporator, for experiments with a vapor quality at the evaporator outlet of 50% or lower. Because of the drop in deviation like explained earlier, this correlation has a better fit for heat transfer on experiments with a vapor quality at the evaporator outlet above 50%. Since a correlation is required that has a good fit over the entire range of vapor qualities at the evaporator outlet, this correlation is also disregarded for this data set.

The four remaining heat transfer correlations are the ones proposed by Yan & Lin [27], Khan et al. [29], Palmer et al. [30] and the correlation proposed by Ayub [32] with a C value for thermosiphon evaporators.

Looking at Table 5.1, it can be seen that the average deviations on heat transfer rate for all four heat transfer correlations are very promising, with 14.77%, 7.34%, 6.39%, and 10.20% respectively. The standard deviations on the average deviations for these heat transfer correlations are also very close in their results, with respective values of 12.49%, 8.47%, 10.43%, and 11.88%.

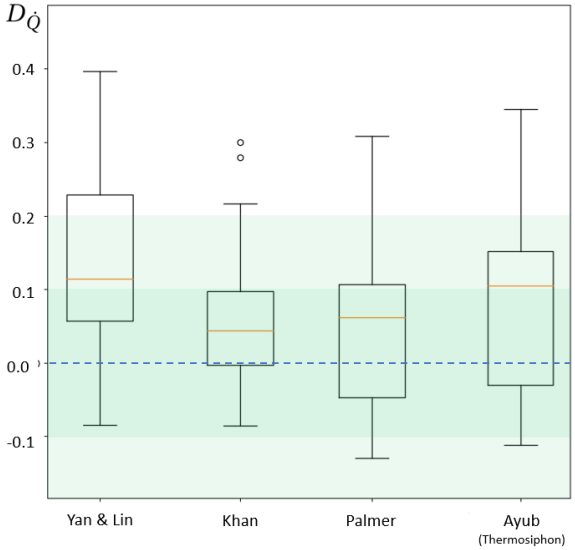

Figure 5.6: Box plots on the deviation on experimental data for four two phase heat transfer correlations.

When looking at the box plots for all four heat transfer correlations, as in Figure 5.6, we can see that the heat transfer correlation proposed by Khan et al. has the best fit for the executed experiments. The first and third quartile are within a +- 10% deviation domain and the whiskers are roughly located at -10% to +20% deviation. The heat transfer correlation proposed by Palmer has the second best fit, followed by the heat transfer correlation proposed by Ayub for thermosiphon evaporators. The heat transfer correlation proposed by Yan & Lin has the worst fit out of the remaining four heat transfer correlations, according to the box plot.

The performance of the heat transfer correlation by Khan et al., based on the average deviation, the standard deviation on the average deviation and the box plot, is considered to be the best fit for the used data set. This correlation is chosen to be used in the validation of the two phase pressure drop correlations in the next section.

TWO PHASE PRESSURE DROP CORRELATIONS RESULTS

Now that a two phase heat transfer correlation has been decided on, the same experimental data set can be used to validate the two phase pressure drop correlations for the evaporator model. For each of the experiments used, the evaporator model is executed with the two phase heat transfer correlation proposed by Khan et al., as proposed in the previous section. The experimental water inlet pressure and temperature, together with the experimental working fluid inlet pressure and temperature are used as inputs to the model. All the experimental working fluid states are calculated in the same manner as explained for the two phase heat transfer correlation validation method.

When the experimental working fluid states around the evaporator are calculated, the model runs the evaporator heat exchanger algorithm for each of the proposed two phase pressure drop correlations. The used two phase pressure drop correlations are the two phase fanning friction factor correlations mentioned in Section 2.3, the Lockhart and Martinelli method, and the Kinetic Energy Model. In total, this means the evaporator heat exchanger is again solved $11 \cdot 53 = 583$ times.

For each of the two phase pressure drop correlations the numerical evaporator outlet state will be compared to the experimental evaporator outlet state on two criteria.

- The model evaporator heat transfer rate will be compared to the experimental heat transfer rate, per two phase pressure drop correlation.

- The model evaporator pressure drop will be compared to the measured evaporator pressure drop, per two phase pressure drop correlation

The first comparison is made to check whether the pressure drop correlations do indeed not affect the calculated heat transfer rate, as can be expected. The second comparison is to see which two phase pressure drop correlation has the best fit to the experimental data used. Both comparisons will be made with equations similar to equation 5.8. The results are plotted against the experimental vapor quality at the evaporator outlet. In Appendix M these plots can be seen for each individual pressure drop correlation.

In Figure 5.7 a plot can be seen for the deviation on evaporator heat transfer rate per pressure drop correlation versus the experimental vapor quality at the evaporator outlet. The top graph shows the full range of deviation, from -250% to +30%. The middle graph shows a deviation range from -30% to +30%. The bottom left graph shows the pressure drop correlations performance on a specific data-point. The bottom right graph shows the identified outliers within the results.

In Figure 5.8 a plot can be seen for the deviation on the evaporator pressure drop per pressure drop correlation versus the experimental vapor quality at the evaporator outlet. The top graph shows the full range of deviation, from 0% to 100,000%. The middle graph shows the deviation range from -1000% to +2000% and the bottom graph shows a deviation range from -200% to +150%.

The average deviation on the evaporator pressure drop, together with the standard deviation on the average deviation per two phase pressure drop correlation can be seen in Table 5.2. The calculated standard deviation is calculated according to equation 5.9.

Table 5.2: Average deviation on evaporator pressure drop and standard deviation on the average deviation per two phase pressure drop correlation.

Correlation	**Average deviation on Δp_{evap} (%)**	**Standard deviation (%)**
Dahlgren	426.21	2960.52
Ayub	-97.40	3.54
Khan et al.	-94.23	7.83
Yan & Lin	2661.00	11935.83
Kuo et al.	18.72	177.49
Yan et al.	1728.38	13184.54
Hsieh & Lin	-17.15	121.79
Jokar et al.	-94.66	7.90
Tao	1.40	2504.11
Lockhart & Martinelli	323.67	2503.22
Kinetic Energy Model	1729.25	13184.42

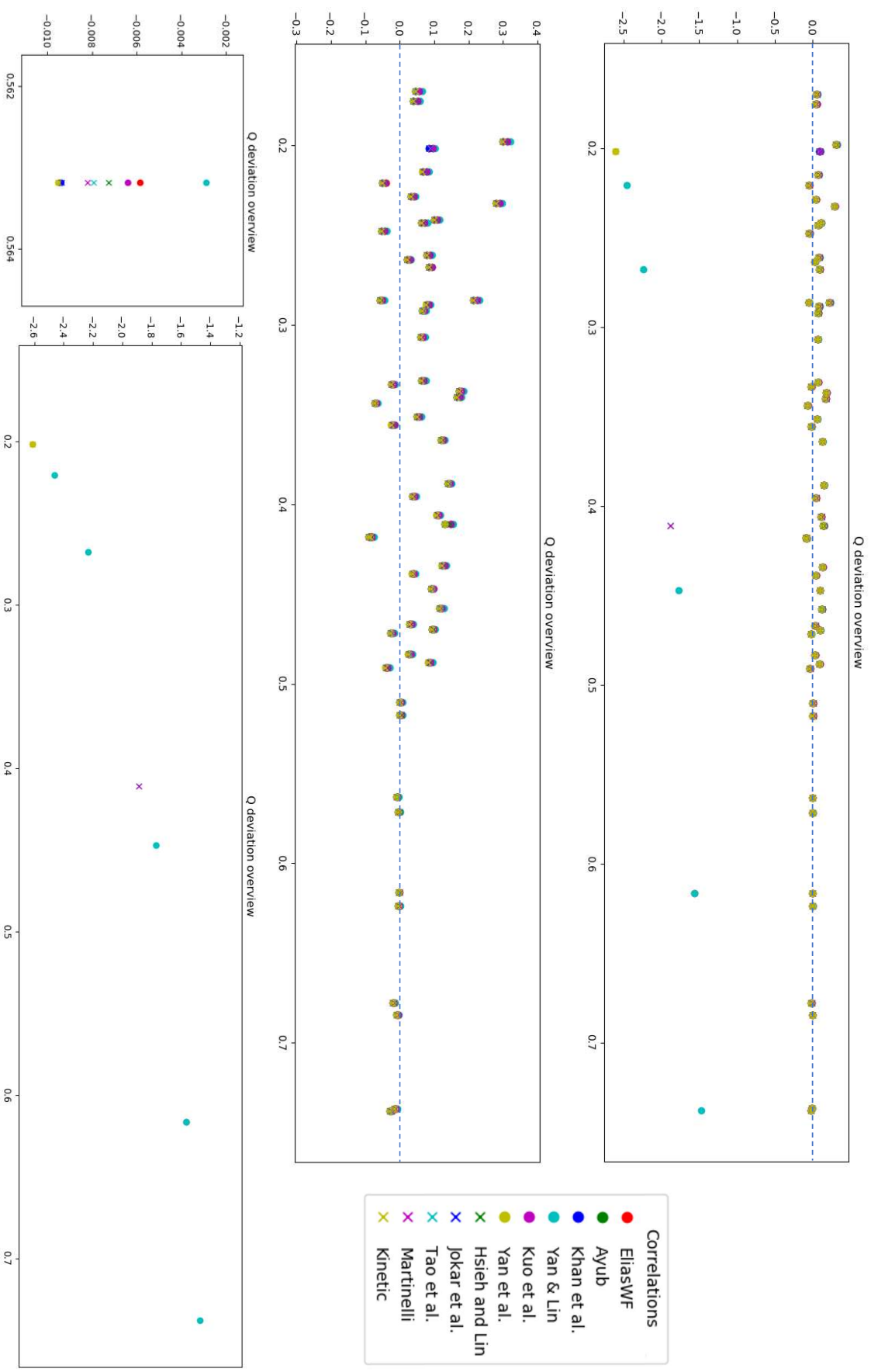

Figure 5.7: An overview of the deviation on evaporator heat transfer rate from experimental data per pressure drop correlation against the evaporator experimental vapor quality at the evaporator outlet.

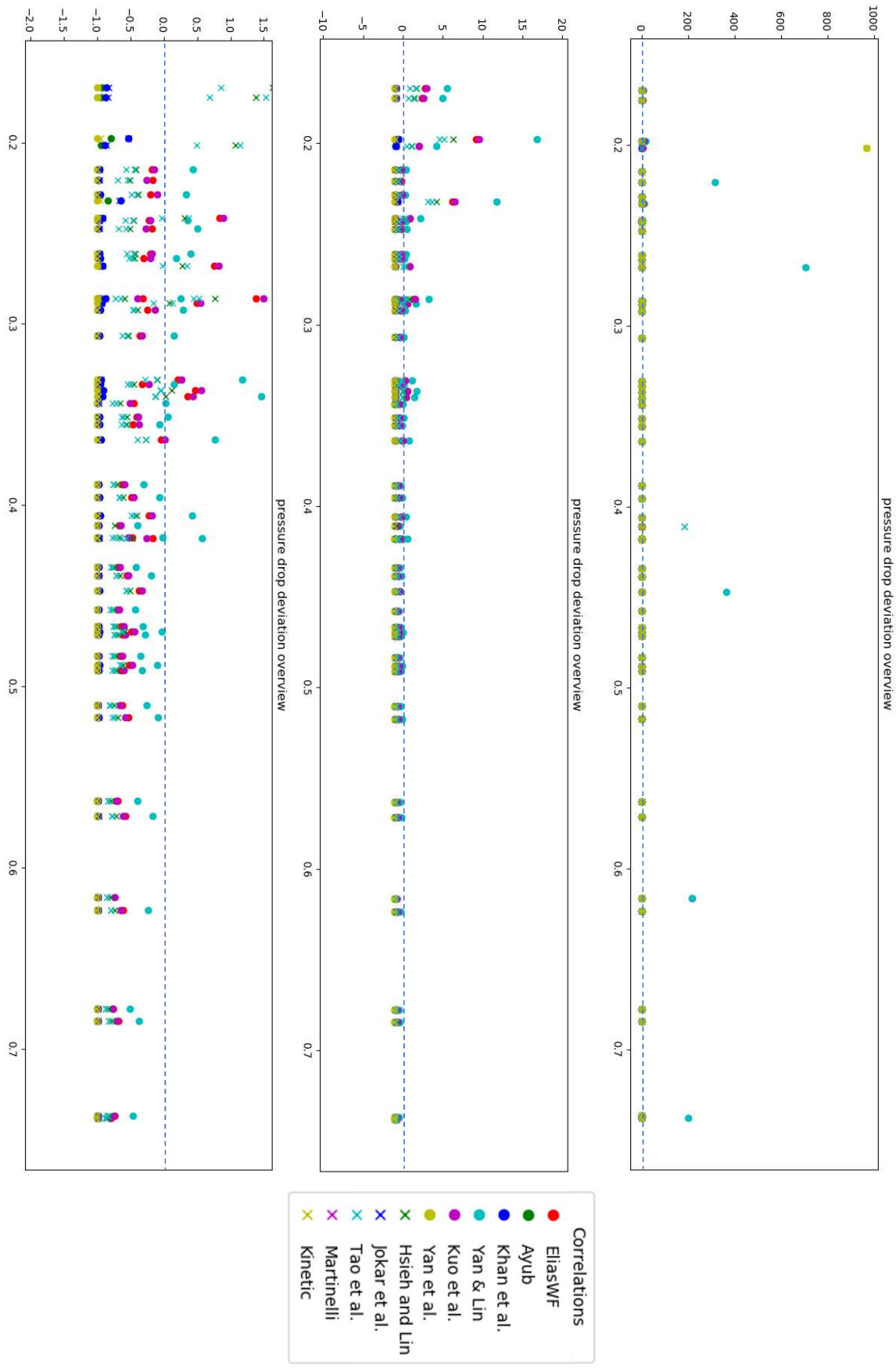

Figure 5.8: An overview of the deviation on evaporator pressure drop from experimental data per pressure drop correlation against the evaporator experimental vapor quality at the evaporator outlet.

In Figure 5.9 and Figure 5.10 the box plots for the deviation on evaporator pressure drop per pressure drop correlation can be seen, with or without the outliers respectively.

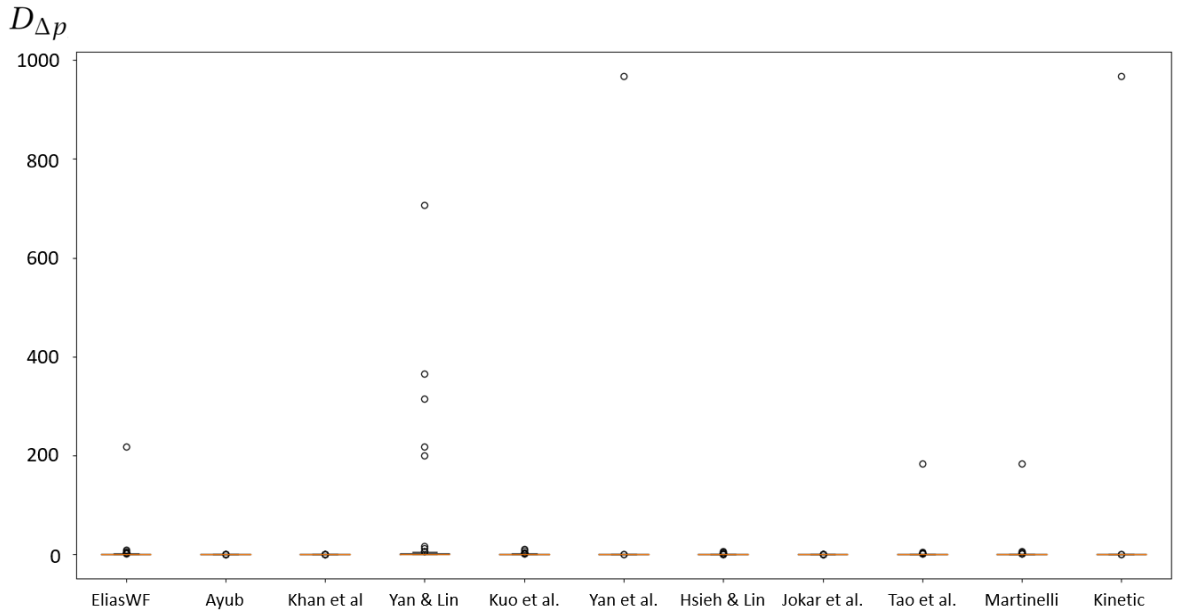

Figure 5.9: Box plots on the deviation on evaporator pressure drop per pressure drop correlation, without excluding the outliers.

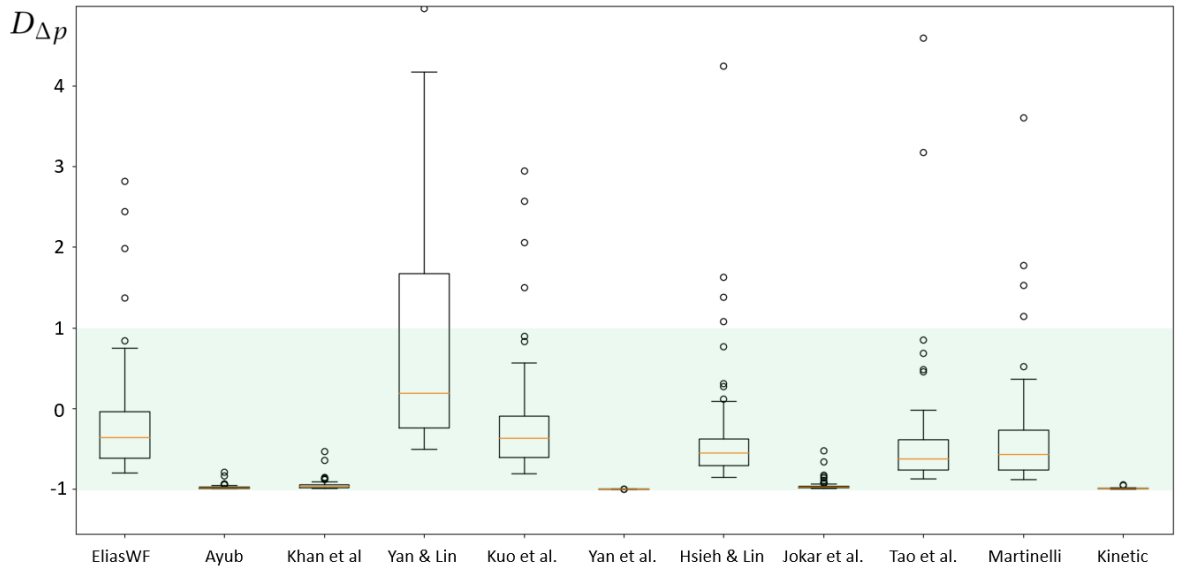

Figure 5.10: Box plots on the deviation on evaporator pressure drop per pressure drop correlation, while excluding the furthest outliers.

TWO PHASE PRESSURE DROP CORRELATIONS DISCUSSION

As can be seen in Figure 5.7, the heat transfer rate over the evaporator is hardly influenced by the chosen two phase pressure drop correlation. Apart from some outliers, which can be seen in the bottom right graph of the figure, the resulting heat transfer rates only divert a maximum of around 1% between two phase pressure drop correlations. This result can be expected since the pressure drop is low enough to hardly influence the evaporator outlet state, even when the calculated pressure drop is relatively far off the actual pressure drop.

Figure 5.8 shows that some results on the pressure drop calculation with two phase pressure drop correlations have a quite severe deviation from the experimental value, with the highest outlier at almost 100,000%. Ignoring the largest outlier deviations, some relatively large deviations on the experimental results remain, as can be seen in the middle graph of Figure 5.8. The cause for these large deviations is explained by the magnitude of the evaporator pressure drop. Since the pressure drop over the evaporator is so small, compared to the actual pressure in the evaporator, the resulting pressure drop deviation can be very large while the resulting evaporator outlet pressure can still be relatively accurate. E.g. for one of the experiments, the evaporator inlet pressure is 8.903 bar and the evaporator outlet pressure is 8.863 bar meaning the evaporator pressure drop is 0.04 bar. A deviation of +1000% on the pressure drop would mean the evaporator model calculates the outlet pressure to be 8.503 bar. This 8.503 bar outlet pressure only deviates by -4% from the actual evaporator outlet pressure. This shows that a relatively high evaporator pressure drop deviation could still be an acceptable result when looking at the evaporator outlet pressure. The reason why the emphasis is still kept on evaporator pressure drop is because the best fit for the pressure drop correlations has to be chosen. When looking at the deviation from the outlet pressure for each two phase pressure drop correlation, the results are accurate within such a small margin that it is hard to decide which correlation has the best performance and thus the best fit to the experimental data. The relatively large pressure drop deviations might give the feeling that the pressure drop at the evaporator outlet is calculated completely wrong, but they are just used to differentiate between worse and better performing two phase pressure drop correlations.

Again looking at the results for the pressure drop over the evaporator per two phase pressure drop correlation as in Figure 5.8, another interesting trend can be identified. For some correlations, most of the results deviate from the actual pressure drop over the evaporator by roughly -100%. Looking at equation 5.8, it can be concluded that if -100% is the deviation on the experimental result, the correlation calculated the pressure drop over the evaporator to be close to 0. This result is, of course, undesirable and correlations resulting in an average pressure drop deviation of around -100% will be disregarded. Looking at Table 5.2, it is concluded that the two phase pressure drop correlations proposed by Ayub, Khan et al., Yan et al., Jokar et al. and the Kinetic Energy Model can be disregarded, since they calculate the average pressure drop to be (close to) zero.

Looking at Figure 5.9, it can be seen that the remaining two phase pressure drop correlations include some outliers on the pressure drop calculations. Removing these outliers from the data set, the updated average deviation and standard deviation on the average deviation for the remaining two phase pressure drop correlations can be seen in Table 5.3.

Table 5.3: Average deviation on evaporator pressure drop and the standard deviation on the average deviation per two phase pressure drop correlation after removing the outliers.

Correlation	$D_{p_{evap,out},avg}$ (%)	Std. dev. on $D_{p_{evap,out},avg}$ (%)
Dahlgren	-36.31	35.10
Yan & Lin	33.76	97.02
Kuo et al.	-37.72	33.39
Hsieh & Lin	-57.18	21.20
Tao	-62.06	21.19
Lockhart & Martinelli	-57.96	26.88

The results from Table 5.3 show that only the two phase pressure drop correlation proposed by Yan & Lin overestimates the pressure drop in the evaporator. The other two phase pressure drop correlations all underestimate the pressure drop in the evaporator. Choosing a two phase pressure drop correlation with the best fit on the experimental data based on the described criteria is a hard decision. The remaining six two phase pressure drop correlation all have different flaws. E.g. The two phase pressure drop correlations proposed by Tao and Hsieh & Lin are quite consistent with a standard deviation of around 20%, but they consistently

underestimate the pressure drop by around 60%. The correlation proposed Yan & Lin is conservative because it will on average overestimate the pressure drop in the evaporator, but the standard deviation is quite large with 97.02%. Again looking at Figure 5.8, we can see that most of the deviation on the evaporator pressure drop is for vapor qualities at the evaporator outlet of 30% or lower. Since the expectation is that the optimal re-circulation rate will result in a vapor quality at the evaporator outlet of 50-70%, this region of vapor qualities at the evaporator outlet of 30% or less is not as significant. Looking at the resulting pressure drop deviation in Figure 5.8 in a range of 40-80% vapor quality at the evaporator outlet, it can be seen that all pressure drop correlations tend to under-estimate the resulting evaporator pressure drop. The two phase pressure drop correlation proposed by Yan & Lin has the smallest deviation on the actual pressure drop in this range. Since this range is of most interest to this research, the two phase pressure drop correlation proposed by Yan & Lin is chosen to be used in further work.

5.4. FULL CYCLE EXPERIMENTS

With the component validations completed, full cycle experiments can now be conducted. The goal of these experiments is to give insight on the evaporator performance depending on the re-circulation rate and orifice pressure drop, to compare the ORC configuration performance to the Kalina cycle configuration performance and to validate the OTEC off-design ORC model. Validating the OTEC off-design model will allow for a scaling analysis to be made in Chapter 6.

In this section, the experimental methodology will be explained, after which several assessments will be made.

The experiments are executed on the OTEC Demo setup, as stated in Chapter 3. For a certain set of experiments, the parameters that can be changed in the OTEC Demo are kept constant apart from one parameter which is the subject of the specific experiment. The parameters that can be adjusted in the OTEC Demo are:

- The power supplied to the reciprocating working fluid pump.
- The power supplied to the gear pump.
- The mass flow rate and inlet temperature of the warm water stream to the evaporator.
- The mass flow rate and inlet temperature of the cold water stream to the condenser.
- The pressure drop over the orifice, which represents the turbine.

For each experiment, it is important that a steady state within the system is reached. This is done by looking at the liquid levels in both the separator and the buffer tank. If the buffer tank liquid level is stable, it means that the amount of ammonia vapor created in the evaporator is equal to the amount of ammonia pumped by the reciprocating working fluid pump. If the liquid level in the separator is stable, it means that the amount of liquid ammonia re-circulated through the evaporator is equal to the amount of ammonia pumped by the gear pump.

Reaching a steady state when using the gear pump in the ORC configuration is done as follows:

1. Set the temperatures and mass flows of the cold and warm water flows going into the condenser/ evaporator.
2. Wait until the temperatures of the water flows going into the heat exchangers are stable around the set temperature level.
3. Send a certain power level to the reciprocating working fluid pump.
4. Send a certain power level to the gear pump.
5. With small steps, increase or decrease the power send to the reciprocating working fluid pump until the liquid levels in the separator and buffer tank remain constant for a timespan of 10 minutes.
6. If the slope of any of the sensor values remains within a +- 0.1% domain for ten minutes, the system is assumed to be in steady state.

7. The sensor values are averaged over a 10-minute timespan to obtain the steady state values for these sensors.

When using the ORC configuration with natural re-circulation around the evaporator, the gear pump is switched off and the working fluid is re-circulated over the one-way valve. The steady state procedure remains the same, apart from step 4, which is removed.

When using the Kalina cycle configuration, the reciprocating working fluid pump can be set to any value. The valve between the separator liquid outlet and the condenser can be set to a control value. The control value used is the liquid level in the buffer tank. The control algorithm finds how far open (in percentage) the control valve needs to be for a steady state to occur.

Using any of these steady state methodologies, the full cycle experiments can be conducted.

5.4.1. EVAPORATOR RE-CIRCULATION PERFORMANCE

The OTEC Demo installation is used to conduct several experiments with varying re-circulation rates from the separator, resulting in different vapor qualities at the evaporator outlet. The gear pump is only able to create a liquid ammonia flow at the bottom of the separator of a maximum 0.006 kg/s. The amount of ammonia pumped by the reciprocating working fluid needs to be of similar proportions, to create a range of vapor qualities at the evaporator outlet.

As explained in the previous section, a steady state within the system is created for 10 minutes to determine the steady state values of the parameters of interest. For the experiments executed, the power fed to the gear pump is increased from 0% to 40% in increments of 1, 5% or 10%. Increasing the power fed to the gear pump by more than 40% will not increase the ammonia mass flow, so 40% power is considered as the upper boundary.

The input conditions imposed on the executed experiments can be seen in Table 5.4

Table 5.4: Input conditions for the executed experiments

Number of data points	$dp_{orifice}$ [bar]	T_{warm} [°C]	$\dot{V}_{warm}$ [l/s]	T_{cold} [°C]	$\dot{V}_{cold}$ [l/s]
8	2.67	25.00	0.30	5.0	0.40

To successfully create a steady state within the system, the mass flow rate coming from the gear pump and reciprocating working fluid pump need to be balanced such that the liquid levels in the separator and the buffer tank remain constant. In Table 5.5 the supplied power to the gear pump and the resulting mass flows through the system for the experimental data set can be seen. The vapor quality at the evaporator outlet and the re-circulation rate, r, can also be seen. The re-circulation rate, r, is calculated as the inverse of the vapor quality at the evaporator outlet. The resulting mass flow from the bottom of the separator is measured through a sensor. The vapor mass flow (which also goes through the reciprocating working fluid pump) is calculated using the methodology explained in Section 5.2.

Table 5.5: Power supplied to the gear pump and the resulting mass flows

	p_{evap} = 8.58 [bar]			
P_{gp}[%]	$\dot{m}_{vap}$ [kg/s]	$\dot{m}_{liq}$ [kg/s]	$q_{evap,out}$	r
0	0.00293	0.00052	0.85	1.18
1	0.00288	0.00194	0.60	1.67
2	0.00288	0.00219	0.57	1.75
5	0.00288	0.00240	0.55	1.82
10	0.00288	0.00293	0.49	2.04
20	0.00287	0.00405	0.41	2.44
30	0.00286	0.00517	0.36	2.78
40	0.00287	0.00544	0.34	2.94

The resulting evaporator heat transfer rate, the evaporator in- and outlet temperatures and the evaporator

overall heat transfer coefficient are plotted against the vapor quality at the evaporator outlet in Figure 5.11. The individual temperature profiles for each experiment can be seen in Appendix N.

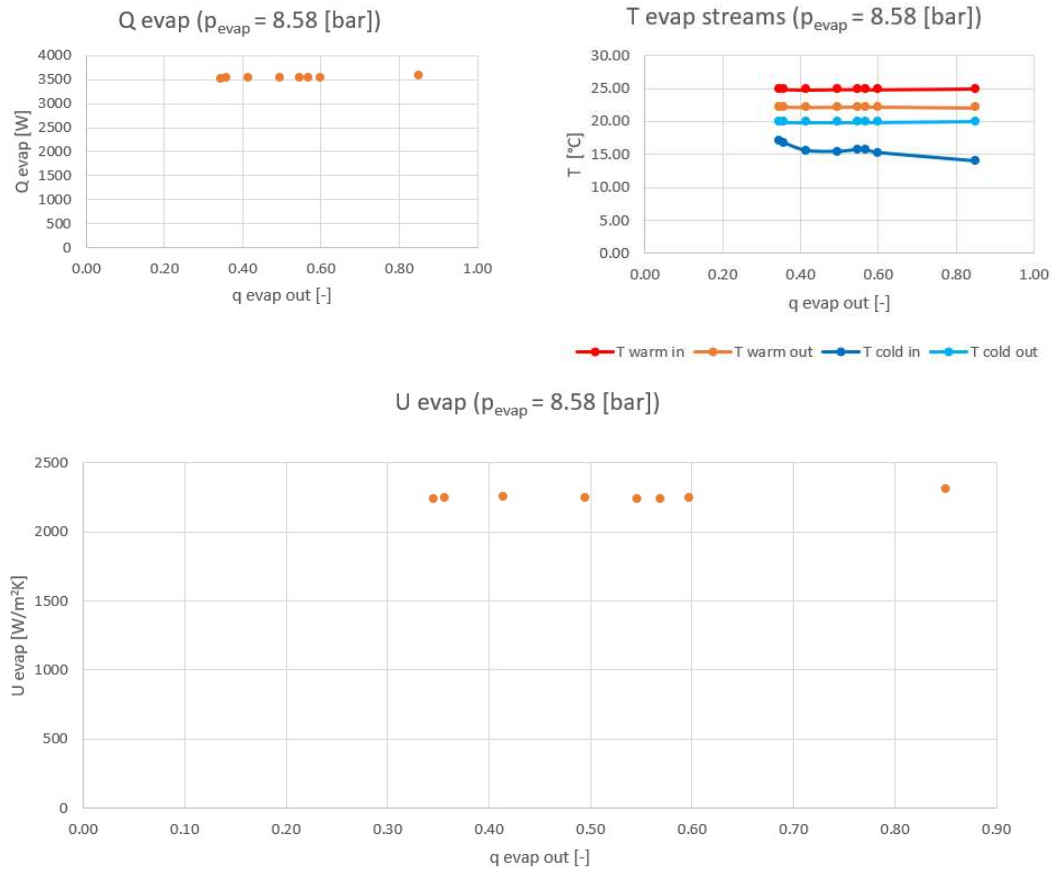

Figure 5.11: Evaporator heat transfer rate versus the vapor quality at the evaporator outlet caused by different re-circulation rates.

The evaporator heat transfer rate displayed in Figure 5.11 is calculated using the temperature difference between the water side in- and outlet temperature. The evaporator overall heat transfer coefficient displayed in Figure 5.11 is calculated by dividing the evaporator heat transfer rate by the evaporator heat exchanger surface area, as found in Appendix A, and the LMTD of the cold and warm stream. For the warm outlet and cold inlet temperature difference in the LMTD calculation, the cold inlet temperature is set to be the saturated liquid temperature of the working fluid. This assumption is based on the fact that the heat transfer required to heat the working fluid from its subcooled to a saturated liquid state is very low compared to the heat required to evaporate the working fluid. The difference in heat required between these two phenomena can also be seen in Table N.1 in Appendix N.

INTERPRETATION & DISCUSSION

First of all, looking at the implementation of the gear pump and the difficulties that arose, the situation concerning the OTEC Demo experiments will be explained. After an intensive search for a gear pump that was both suitable for the application and affordable, a stroke of luck presented itself. From another setup at the 3mE faculty, two gear pumps were not being used anymore and were free to be implemented in the OTEC Demo. After installation and commissioning, the first gear pump implemented broke down after a single day of test runs. After removing and inspecting the gear pump (in consultation with the supplier) the conclusion was that the magnetic drive of the gear pump had broken down either by wear or by not being able to withstand pure ammonia. The encapsulating material for the magnetic drive is a plastic called PPS, which supposedly is very well resistant to chemical strains up to 200 °C. Taking the age and many previous applications of the gear pumps in consideration, together with the material properties of PPS, the hypothesis was made that the gear pump had broken down because of wear. After installing the second gear pump two successful days of experiments could be conducted, resulting in the presented data set. Unfortunately, the second gear pump also broke down after

these two days and wasn't able to generate a flow anymore. Whether this is indeed caused by wear, which is unlikely for 2 gear pumps in a row, or chemical strain caused by pure ammonia is still unknown.
This unfortunate result means a very limited data set was made available about the effect of re-circulation on the evaporator heat transfer rate. Luckily, the OTEC Demo can run on natural circulation through the one-way valve. This allows conducting different experiments, which will be discussed in the coming sections.

A phenomenon worth mentioning about the results presented in Table 5.5 and Figure 5.11 is the fact that a vapor quality of 100% at the evaporator outlet is never reached. This is caused by the fact that the gear pump is not completely sealed when set to a 0% power input, meaning ammonia is leaking through it in small amounts. This causes a natural re-circulation to occur with a re-circulation rate of about 1.18.

Another interesting phenomenon is the fact that even for only 1% power supplied to the gear pump, the consequential re-circulation rate is roughly 1.67, meaning a vapor quality at the evaporator outlet of 60% is obtained.

Looking at Table 5.5 and Figure 5.11 it is very clear that the evaporator heat transfer rate and overall heat transfer coefficient are independent on the re-circulation rate (or the vapor quality at the evaporator outlet) between 1.18-2.94 re-circulation rate. This is a very interesting result and not what was expected when a hypothesis was made in Section 2.5.2. The hypothesis made stated three things, namely:

1. That a re-circulation rate lower than 1.43 would cause dry-out and thus a lower overall heat transfer coefficient.
2. That a re-circulation rate higher than 3.33 would cause deteriorated nucleate boiling and thus a lower overall heat transfer coefficient.
3. That a re-circulation rate between 1.43-2.00 would cause the highest overall heat transfer coefficient.

Even for a re-circulation rate of 1.18 the overall heat transfer coefficient is the same as for a higher re-circulation rate, so the first hypothesis is determined to be not true.
Unfortunately, the OTEC Demo wasn't able to reach re-circulation rates higher than 3.33 so the second hypothesis could not be tested.
The re-circulation rate on a domain of 1.18-2.94 had no significant effect on the evaporator overall heat transfer coefficient, so the third hypothesis is also determined to be not true.

A possible explanation for these phenomena can be found looking at the velocities of the working fluid flow in the evaporator. Knowing the total evaporator mass flow rate, the working fluid mass flux through the evaporator can be calculated. Using the ammonia liquid density, ammonia vapor density and the average vapor quality in the evaporator for each experimental data set, the average vapor and liquid velocities in the evaporator can be calculated. The results of these calculations can be seen in Table 5.6

Table 5.6: Working fluid flow velocities in the evaporator for the conducted re-circulation experiments.

	p_{evap} = 8.58 [bar]		
r	G_{evap} [kg/m^{2}s]	$u_{liq,avg}$ [m/s]	$u_{vap,avg}$ [m/s]
1.18	1.94	0.0018	0.123
1.67	2.71	0.0031	0.121
1.75	2.85	0.0033	0.121
1.82	2.97	0.0035	0.121
2.04	3.27	0.0040	0.121
2.44	3.89	0.0051	0.120
2.78	4.52	0.0061	0.120
2.94	4.67	0.0063	0.120

The average liquid flow velocities that are calculated are quite low. When the liquid inside the evaporator is moving at this velocity, it raises the question whether flow boiling phenomena or pool boiling phenomena dominate the heat transfer rate. If pool boiling were to be the dominant heat transfer mechanism for the entire re-circulation domain, the heat transfer rate would not be influenced by the mass flow rate of the working

fluid through the evaporator. Looking at the relatively low liquid velocities in the evaporator, the consequential overall heat transfer coefficient will probably be determined by pool boiling heat transfer mechanisms, causing the overall heat transfer coefficient to be independent on the re-circulation rate.

Since the heat transfer rate of the evaporator is independent on the re-circulation rate, a second conclusion can be drawn. This result also means that forced circulation in the plate heat exchanger evaporator for this mass flow domain has no benefit over natural circulation since the heat transfer rate in the evaporator will not be influenced by increasing or decreasing the re-circulation rate.

5.4.2. KALINA CYCLE VS ORC CONFIGURATION

During the previous experiments, it has been noted that the re-circulation rate has little to no effect on the performance of the evaporator heat exchanger. Forced circulation utilizing a gear pump is thus not needed to optimize the evaporator heat transfer rate. The following experiments are conducted utilizing natural re-circulation over the one-way valve installed parallel to the gear pump, as can be seen in Figure 3.5.

In the coming sections, a comparison between the performance of the ORC configuration and the Kalina cycle configuration for the OTEC Demo will be made. Before the comparison can be made, an optimization of the ORC configuration and Kalina cycle configuration has to be executed, such that the comparison can be made on equal terms. Since the ORC configuration performance is independent of the re-circulation rate, as discussed in the previous section, a new optimization parameter has to be picked. As noted in the previous work by Goudriaan [11] and Kuikhoven [25], the pressure drop over the orifice has a large impact on the heat transfer rate in the evaporator in Kalina cycle configuration, since it causes a different operating pressure in the evaporator.
To make a fair comparison between the ORC and Kalina cycle configurations, it is imperative to understand how the ORC configuration and Kalina cycle configuration act under different orifice pressure drops, which cause a different evaporator operating pressure.

Before any claims can be made on the performance of the ORC configuration versus the Kalina cycle configuration, a fair comparison methodology has to be created to ensure that correct conclusions will be formed. The comparison methodology will be explained in the next section.

COMPARISON METHODOLOGY

The comparison between the Kalina cycle and ORC configuration in the OTEC Demo will need to be executed in such a way that it can be considered a fair comparison and in such a way that the comparison relates to what an OTEC system has to achieve.

First, a comparison between the temperature profiles in the evaporator heat exchanger will be made for both configurations. The Kalina cycle temperature profiles used will be for different ammonia concentrations, and the data used will be taken from the work done by Goudriaan [11] and Kuikhoven [25]. The results between these (relatively old) Kalina cycle experiments and ORC experiments are not conclusive on the difference in performance. Since the OTEC Demo test setup has changed so much over the years, it is not possible to claim that similar operating conditions still apply. The piping and sensor infrastructure has changed too much for a direct comparison to still be considered fair. The ORC configuration and Kalina cycle configuration data can be compared amongst themselves however, which will give some insights on the evaporator performance for both configurations under different operating pressures.

The full cycle comparison is based on the fundamental objective of the work done by Bluerise B.V. Looking back at the relevance of this research, Chapter 1 states that the main driver for OTEC developments is cost-effective means of power production. For an OTEC plant, the operational costs (maintenance, operators, etc.) plus the capital investment costs have to be outweighed by the profits of the energy it produces. The difference between the produced energy profits and the operational costs plus the capital investment costs divided over the system lifetime is the net earnings that can be made.

When trying to assess the differences between different cycle configurations, one should thus look for differences in the net power output of the cycle, under the same boundary conditions. For the OTEC system that

would mean:

How much net power can the cycle produce with a certain set warm and cold water side temperature?

The power produced by the cycle is the work produced by the generator, which converts the mechanical turbine work to electricity, minus the work done by all the pumps in the cycle. In the complete OTEC system, these pumps would be the (reciprocating) working fluid pump, (possibly but not necessarily) a gear pump for liquid re-circulation and the cold and warm water side pumps.

To simplify this analysis, the water side mass flow rates on the warm and cold sides will be kept constant for all data used. This means that the water side pumps require the same amount of work for all data sets, and (for comparison purposes) can be neglected in this analysis.

To further simplify the analysis, the assumption is made that the re-circulation in the ORC configuration happens through natural re-circulation. As is explained in Section 5.4.1, the re-circulation rate of ammonia through the evaporator has no significant effect on the heat transfer rate of the evaporator, therefore it is not possible to optimize the re-circulation rate. If it's not possible to optimize the re-circulation rate through the evaporator, it is not required to use a gear pump to achieve the highest performance, and natural re-circulation will suffice.

Goudriaan [11] and Kuikhoven [25] conducted experiments to test the full cycle performance. They found that the Kalina cycle configuration of the OTEC Demo at that time performed best when pure ammonia was used as the working fluid. Table 5.7 shows the full cycle results for the experiments conducted by Goudriaan [11] and Kuikhoven [25].

Table 5.7: Full Kalina cycle configuration performance analysis created by Goudriaan [11] and Kuikhoven [25]

NH3 conc. [%]	$\dot{Q}_{evap}$ [W]	$\dot{W}_{pump}$ [W]	$dp_{orifice}$	$\dot{W}_{turb}$ [W]
90.7	4991	32	1.37	90
92.3	5071	31.56	1.49	97
94.5	4988	33.26	1.82	116
95.4	5089	30.33	1.77	113
100	5329	31.76	2.2	135

Concluding from the work done by Goudriaan and Kuikhoven, the full cycle performance of the Kalina cycle configuration is highest when pure ammonia is used. Since the current OTEC Demo can be used in both the ORC configuration and the Kalina cycle configuration, the full cycle comparison will be made for pure ammonia in both configurations.

Each configuration can be optimized through the orifice pressure drop. Increasing the orifice pressure drop will increase the turbine power output, but it will decrease the evaporator heat transfer rate and thus the vapor mass flow through the turbine. The combination of these mechanisms causes an optimum in the net power output of the cycle for a certain turbine pressure drop. In the Kalina cycle experiments executed by Goudriaan and Kuikhoven, the orifice (turbine) pressure drop was selected in such a way that the evaporator heat duty was roughly 5 [kW]. This value is not the optimum turbine pressure drop for these cycle configurations, but picked as a point of reference. To create an equal level playing ground, both the ORC configuration and the Kalina cycle configuration will be tested for different orifice pressure drops. The resulting net power output of each cycle over the domain of orifice pressure drops will be compared.

The result of this methodology is that for the same cold and warm water temperatures and mass flow rates, the net power output of the Kalina cycle configuration and ORC configuration will be compared at a range of orifice pressure drops, using pure ammonia as a working fluid. The net power output is equal to the turbine work, following equation 2.8, minus the reciprocating pump work. This is the case for both the Kalina cycle configuration and the ORC configuration since liquid re-circulation in the ORC configuration happens naturally, no work is done by an additional gear pump.

In the next section, the temperature profiles of the Kalina cycle evaporator for different ammonia concentrations will be compared to the temperature profiles of the ORC evaporator for different orifice pressure drops. In the section after that, the full cycle comparison will be made.

EVAPORATOR PERFORMANCE ORC AND KALINA CYCLE

Figure 5.12 shows how the temperature of the warm water and working fluid changes throughout the evaporator heat exchanger for the ORC configuration experiments. The warm water enters the evaporator at 27 [°C] and is cooled down in the opposite direction as the working fluid is warmed up.

Figure 5.13 shows how the temperature of the warm water and the working fluid changes throughout the evaporator heat exchanger for the Kalina cycle configuration experiments executed by Goudriaan and Kuikhoven.

For each of the experimental data sets used, the overall heat transfer coefficient for the evaporator has also been calculated.
Looking at these results, a noticeable phenomenon is the reversed relationship between evaporator operating pressure and evaporator performance in ORC configuration. The LMTD for the evaporator reduces with higher operating pressure, since the saturated liquid temperature increases. Consequentially, the temperature difference between the warm and cold stream becomes lower. This causes the evaporator heat transfer rate to decline with increasing operating pressure.
Looking at the evaporator overall heat transfer coefficient, a decline with increasing operating pressure can also be seen. This means that the heat transfer for the evaporator decreases with increased pressure, even when the temperature profiles of the warm and cold stream are not considered.

The combination of the decline in LMTD and decline in evaporator overall heat transfer coefficient with increasing operating pressure causes the evaporator heat transfer rate to decline rapidly with increasing operating pressure. From 5492.6 [W] at 8.39 [bar] operating pressure to 2450.8 [W] at 9.24 [bar] operating pressure.

When comparing the evaporator performance between the ORC and Kalina cycle configuration, it can be concluded that the evaporator performance is significantly higher for the Kalina cycle configuration.
Looking at an evaporator operating pressure of 8.39 [bar], it can be seen that the evaporator overall heat transfer coefficient is 2277.36 [W/m^{2}K] for the ORC configuration. For the same operating pressure, the evaporator in the Kalina cycle configuration has an overall heat transfer coefficient of 4830.57 [W/m^{2}K]. Even when the ammonia concentration is 100% in the Kalina cycle configuration, the evaporator performance is higher than in the ORC configuration. Looking at an operating pressure of 8.96 [bar], the evaporator in the Kalina cycle configuration has an overall heat transfer coefficient of 3390.84 [W/m^{2}K]. At the same operating pressure, the ORC configuration has an overall heat transfer coefficient of only 1809.34 [W/m^{2}K].

However, as stated before, caution must be taken when comparing the results of the experimental data obtained by Goudriaan [11] and Kuikhoven [25] and the new ORC configuration experimental data. As stated before, since the OTEC Demo has changed a lot in the past two years, it is impossible to guarantee that the same operating conditions still apply. The piping infrastructure and the sensor layout within the system has changed so much that any conclusive statement on the difference in evaporator performance between the ORC configuration and Kalina cycle configuration cannot be made solely based on these results. The only statements that can be made with certainty are:

- For the ORC configuration, the evaporator performance decreases with increasing evaporator operating pressure.
- For the Kalina cycle configuration, the evaporator performance for pure ammonia is lower than the evaporator performance for a mixture of ammonia/ water. Of the tested concentrations, an ammonia/ water concentration of 95.4 % resulted in the highest evaporator performance.

Using these statements, another statement on the difference in the evaporator performance can be deduced:

If the evaporator performance for pure ammonia is higher in the Kalina cycle configuration than in the ORC configuration, the evaporator performance of an ammonia/water mixture of 90.7-95.4% in the Kalina cycle configuration will also be higher than the evaporator performance of the ORC configuration.

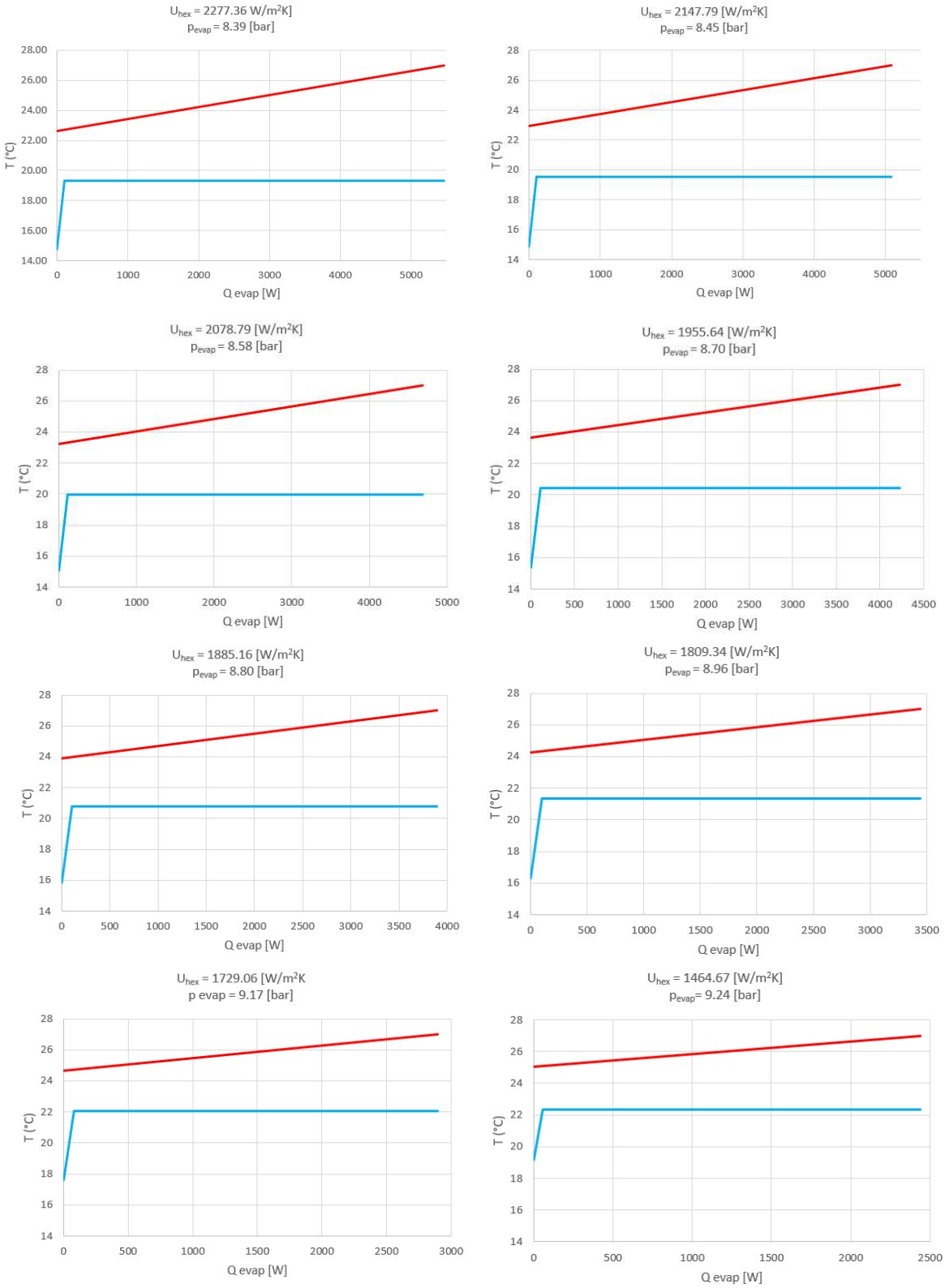

Figure 5.12: The temperature profiles of the water and working fluid through the evaporator for the executed ORC experiments.

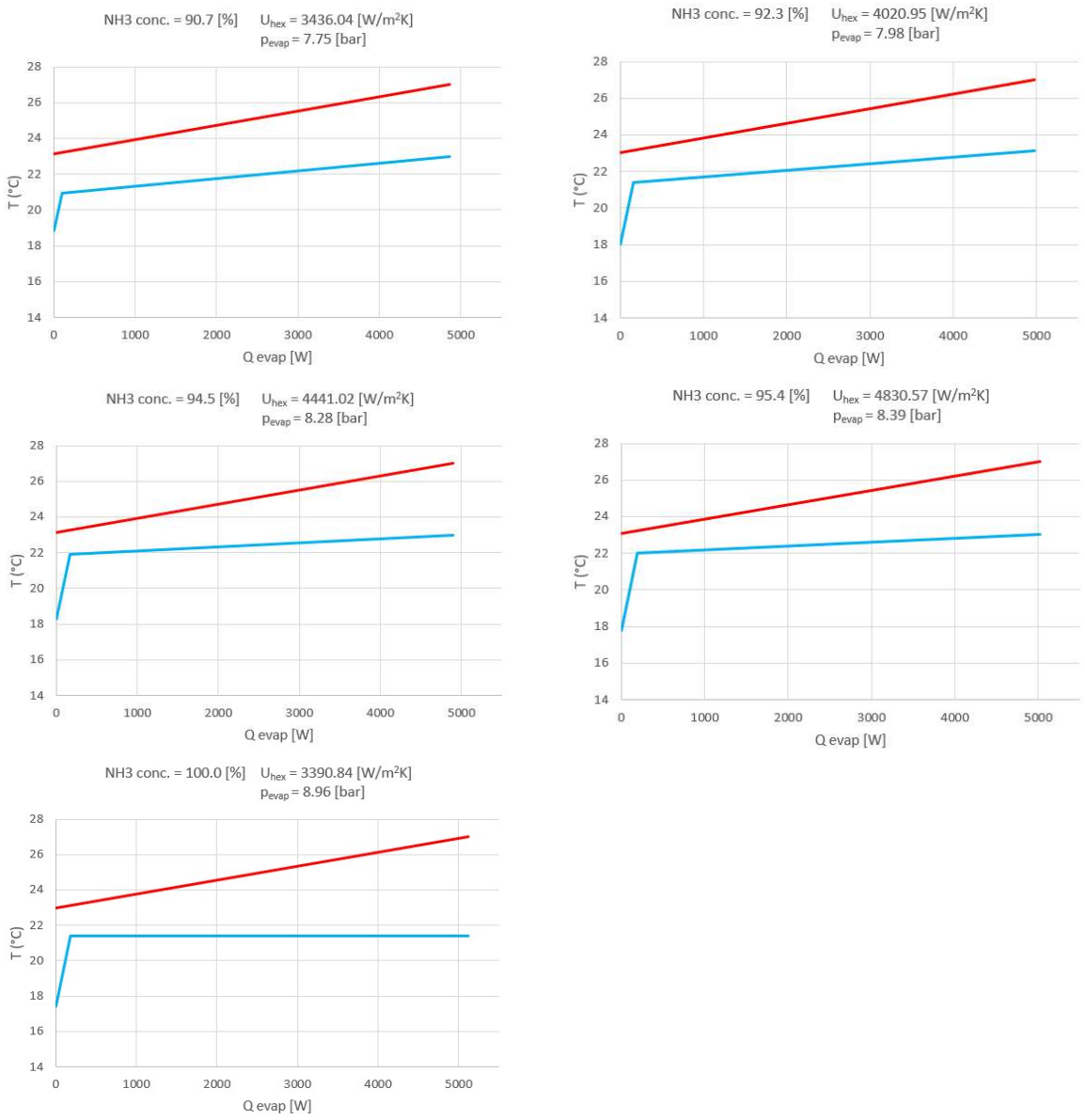

Figure 5.13: The temperature profiles of the water and working fluid through the evaporator for the Kalina cycle data from Goudriaan [11] and Kuikhoven [25].

Now that some insight on the evaporator performance for the ORC configuration and Kalina cycle configuration has been created, a comparison between the Kalina cycle and ORC evaporator performance can be made. The evaporator performance will be determined under different evaporator operating pressures for both the ORC configuration and Kalina cycle configuration of the current OTEC Demo setup, both operating with pure ammonia.
The experiments that were conducted to see what the effect of the evaporator operating pressure on the evaporator heat transfer rate is, were conducted under the following input conditions:

Table 5.8: Input conditions for the executed experiments

	Number of data points	$dp_{orifice}$ [bar]	T_{warm} [°C]	$\dot{V}_{warm}$ [l/s]	T_{cold} [°C]	$\dot{V}_{cold}$ [l/s]
ORC	8	1.48-3.32	27.00	0.30	5.0	0.225
Kalina cycle	8	1.48-3.41	27.00	0.30	5.0	0.225

The resulting evaporator outlet vapor quality, heat transfer rate and overall heat transfer coefficient versus the evaporator operating pressure can be seen in Figure 5.14.

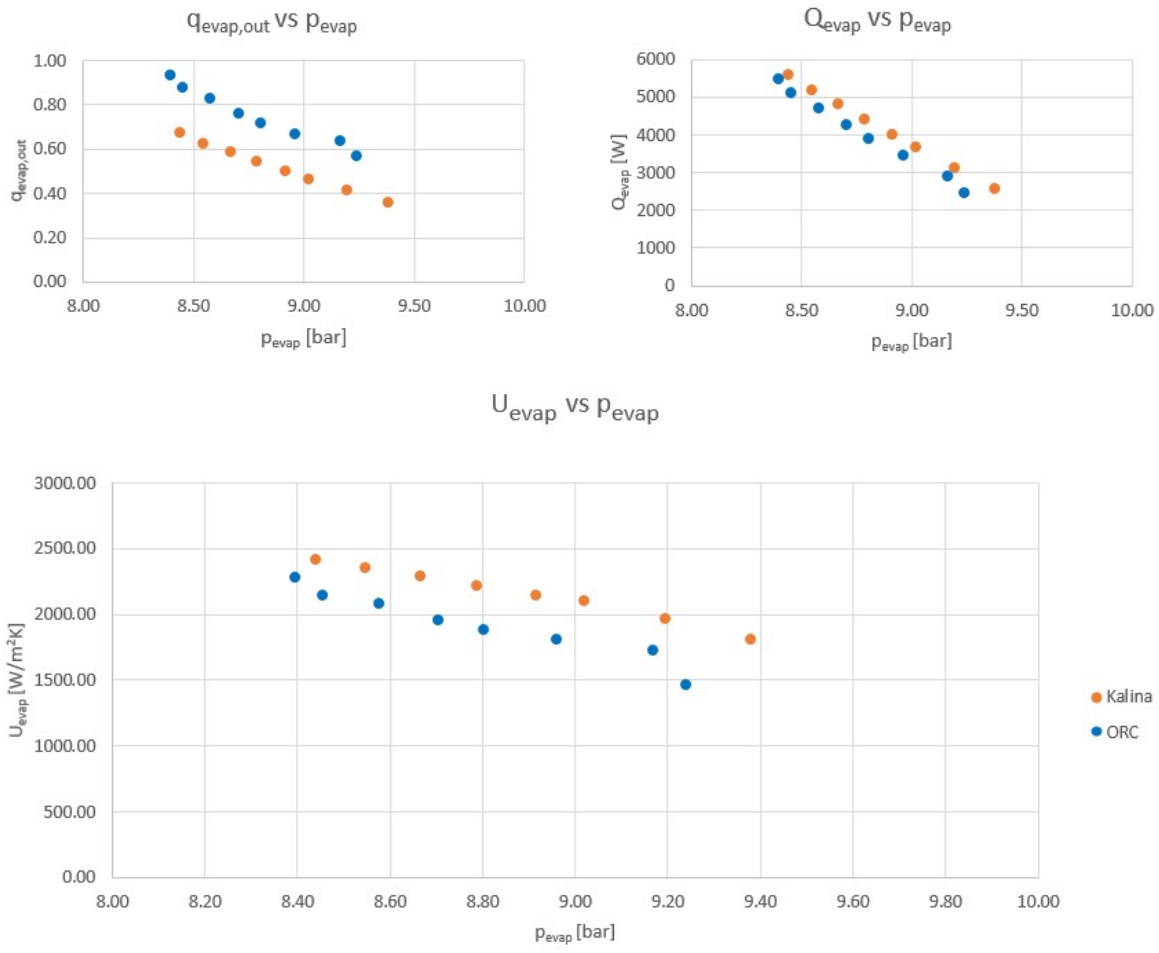

Figure 5.14: Evaporator outlet vapor quality, evaporator heat transfer rate and the evaporator overall heat transfer coefficient versus the evaporator operating pressure, for both the ORC and Kalina cycle configuration.

Looking at Figure 5.14, the phenomenon that stands out is the decreasing evaporator performance with increasing evaporator operating pressure. Similar to the results in the previous section, the evaporator overall heat transfer coefficient decreases with increasing operating pressure, in both the ORC configuration and the Kalina cycle configuration. Since the LMTD also decreases with increasing evaporator operating pressure, the evaporator heat transfer rate decreases even more with increasing evaporator operating pressure.

Looking at the resulting overall heat transfer coefficients for the ORC configuration versus the Kalina cycle configuration, it is quite clear that the Kalina cycle configuration results in higher evaporator performance. Using the deduced statement from the previous section, it can be concluded that the ORC configuration evaporator performance is indeed lower than the evaporator performance for the Kalina cycle configuration, whether or not an ammonia/ water mixture of 90.7-95.4% or pure ammonia is used.

FULL CYCLE PERFORMANCE

When looking at the evaporator performance, the ORC configuration is outperformed by the Kalina cycle configuration. The full OTEC cycle performance is dependant on this evaporator performance, but not solely. Like explained in Section 5.4.2, the net power output of the OTEC system is the final benchmark upon which systems are graded. Using the same input conditions for both cycles, the highest net power output will determine which cycle configuration outperforms the other.

In this section, the net power outputs of the ORC configuration and Kalina cycle configuration operating with pure ammonia are compared. First, the ORC configuration net power output versus the orifice pressure drop is determined, to show where the optimum in this balance is situated. The same is done for the Kalina cycle configuration for pure ammonia, after which the results will be compared.

Table 5.9 shows the measured values used to calculate the net power output for the ORC experiments under different orifice pressure drops.

Table 5.9: Measured experimental values used to calculate the net power output for the ORC configuration

Parameter	$dp = 1.48$ [bar]	$dp = 1.74$ [bar]	$dp = 2.00$ [bar]	$dp = 2.26$ [bar]
p_{evap} [bar]	8.39	8.45	8.58	8.70
$p_{turb,in}$ [bar]	8.28	8.35	8.47	8.61
$p_{turb,out}$ [bar]	6.80	6.60	6.48	6.35
$T_{turb,in}$ [°C]	19.42	19.65	20.09	20.54
c_p [kJ/kgK]	2931.22	2936.49	2946.42	2956.66
$\dot{m}_{vap}$ [kg/s]	0.00452	0.00420	0.00387	0.00350
$\eta_{turb,is}$	0.9	0.9	0.9	0.9
γ	1.44	1.44	1.44	1.44
$\dot{W}_T$ [W]	232.94	257.18	272.28	279.55
$\Delta h_{rec.pump}$ [kJ/kg]	2.97	4.11	4.91	5.25
$\dot{W}_p$ [W]	13.43	17.28	19.01	18.35
$\dot{Q}_{evap}$ [W]	5492.6	5105.5	4701.3	4241.9
U_{evap} [W/m^{2}K]	2277.36	2147.79	2078.79	1955.64
$\dot{W}_T - \dot{W}_p$ [W]	219.52	239.90	253.28	261.20

Parameter	$dp = 2.46$ [bar]	$dp = 2.75$ [bar]	$dp = 3.11$ [bar]	$dp = 3.32$ [bar]
p_{evap} [bar]	8.80	8.96	9.17	9.24
$p_{turb,in}$ [bar]	8.71	8.88	9.09	9.17
$p_{turb,out}$ [bar]	6.25	6.12	5.98	5.85
$T_{turb,in}$ [°C]	20.90	21.40	22.24	22.35
c_p [kJ/kgK]	2964.84	2977.17	2993.45	2999.18
$\dot{m}_{vap}$ [kg/s]	0.00323	0.00286	0.00241	0.00205
$\eta_{turb,is}$	0.9	0.9	0.9	0.9
γ	1.44	1.44	1.45	1.45
$\dot{W}_T$ [W]	281.66	279.81	267.54	243.28
$\Delta h_{rec.pump}$ [kJ/kg]	5.82	7.51	9.98	12.03
$\dot{W}_p$ [W]	18.77	21.49	24.10	24.63
$\dot{Q}_{evap}$ [W]	3907.61	3459.8	2905.9	2450.8
U_{evap} [W/m^{2}K]	1885.16	1809.34	1729.06	1464.67
$\dot{W}_T - \dot{W}_p$ [W]	262.88	258.32	243.44	218.65

In Figure 5.15 a graph can be seen that shows the turbine work, the work done by the reciprocating working fluid pump and the consequential net work produced by the ORC configuration versus the pressure drop over the orifice.

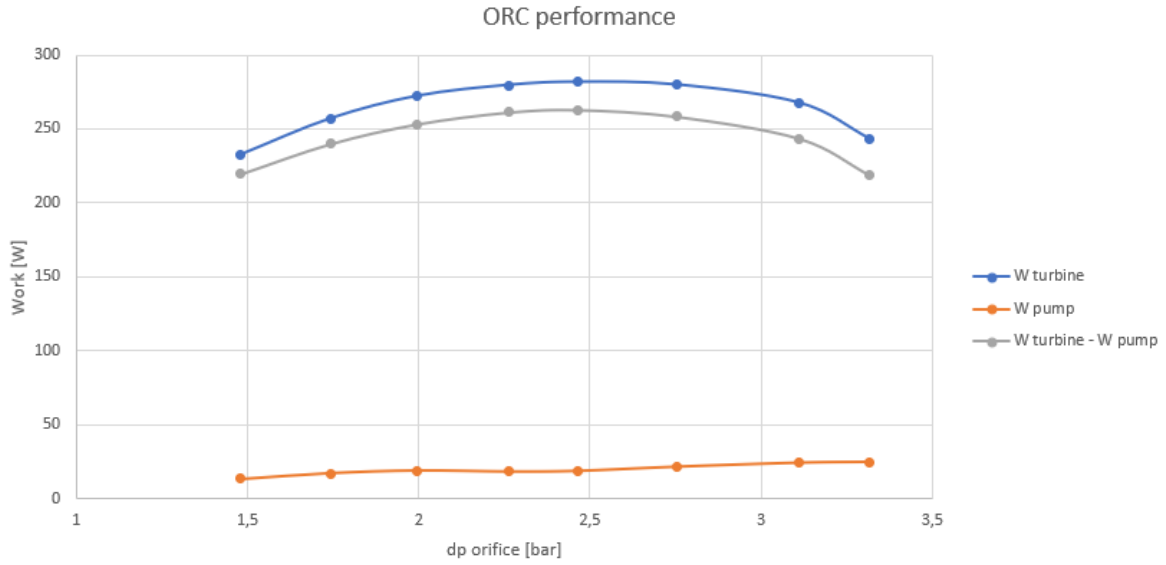

Figure 5.15: Turbine work, work done by the reciprocating working fluid pump and l net work produced by the ORC configuration versus the pressure drop over the orifice.

The same experiments were performed for the Kalina cycle configuration using pure ammonia. A note must be made, however, since the working fluid mass flow rate through the reciprocating pump in ORC configuration and Kalina cycle configuration is not the same. In ORC configuration, the working fluid mass flow rate through the reciprocating working fluid pump is equal to the vapor mass flow rate coming from the separator. In Kalina cycle configuration, this is equal to the sum of the vapor and liquid mass flow rates coming from the separator.

Table 5.10 shows the measured values used to calculate the net power output for the Kalina cycle experiments under different orifice pressure drops.

Table 5.10: Measured experimental values used to calculate the net power output for the Kalina cycle configuration

Parameter	$dp = 1.48$ [bar]	$dp = 1.75$ [bar]	$dp = 2.01$ [bar]	$dp = 2.26$ [bar]
p_{evap} [bar]	8.44	8.55	8.67	8.79
$p_{turb,in}$ [bar]	8.30	8.42	8.55	8.68
$p_{turb,out}$ [bar]	6.82	6.67	6.54	6.42
$T_{turb,in}$ [°C]	19.45	19.86	20.29	20.73
c_p [J/kgK]	2933.25	2942.09	2952.10	2962.12
$\dot{m}_{vap}$ [kg/s]	0.00457	0.00426	0.00392	0.00359
$\eta_{turb,is}$	0.9	0.9	0.9	0.9
γ	1.44	1.44	1.44	1.44
$\dot{W}_T$ [W]	235.20	260.57	275.41	284.37
$\Delta h_{rec.pump}$ [kJ/kg]	3.26	3.53	4.01	4.31
$\dot{W}_p$ [W]	22.22	24.03	26.92	28.65
$\dot{Q}_{evap}$ [W]	5567.63	5196.44	4793.13	4393.96
U_{evap} [W/m^{2}K]	2414.49	2352.66	2288.24	2221.65
$\dot{W}_T - \dot{W}_p$ [W]	212.98	236.54	248.50	255.72

Parameter	$dp = 2.51$ [bar]	$dp = 2.71$ [bar]	$dp = 3.05$ [bar]	$dp = 3.41$ [bar]
p_{evap} [bar]	8.92	9.02	9.20	9.38
$p_{turb,in}$ [bar]	8.81	8.92	9.10	9.29
$p_{turb,out}$ [bar]	6.30	6.22	6.05	5.88
$T_{turb,in}$ [°C]	21.16	21.53	22.09	22.75
c_p [J/kgK]	2972.40	2980.86	2994.38	3008.40
$\dot{m}_{vap}$ [kg/s]	0.00325	0.00299	0.00254	0.00208
$\eta_{turb,is}$	0.9	0.9	0.9	0.9
γ	1.44	1.44	1.45	1.45
$\dot{W}_T$ [W]	287.74	285.56	274.33	251.62
$\Delta h_{rec.pump}$ [kJ/kg]	4.81	4.94	5.94	6.64
$\dot{W}_p$ [W]	31.32	31.98	36.72	38.40
$\dot{Q}_{evap}$ [W]	3989.76	3660.65	3123.99	2559.64
U_{evap} [W/m^{2}K]	2147.04	2096.64	1967.57	1807.92
$\dot{W}_T - \dot{W}_p$ [W]	256.42	253.58	237.61	213.22

In Figure 5.16 a graph can be seen that shows the turbine work, the work done by the reciprocating working fluid pump and the consequential net work produced by the Kalina cycle configuration versus the orifice pressure drop using pure ammonia.

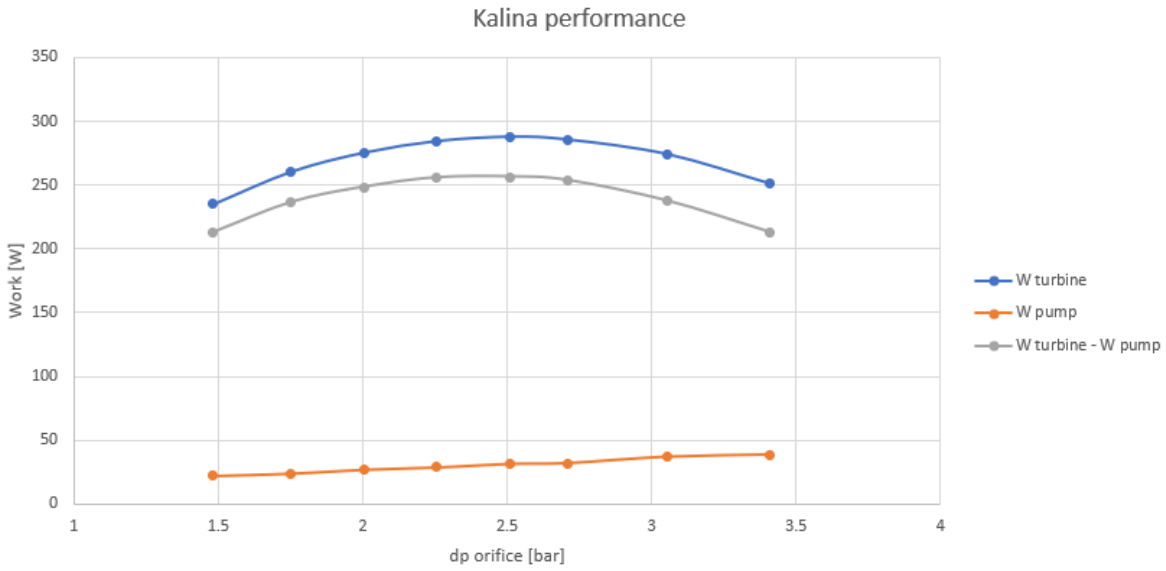

Figure 5.16: Turbine work, work done by the reciprocating working fluid pump and net work produced by the Kalina cycle configuration versus the orifice pressure drop for pure ammonia.

INTERPRETATION & DISCUSSION

When looking at both Figure 5.15 and Figure 5.16, a peak in the net power output can be seen for an orifice pressure drop of around 2.5 [bar]. The net power output of the cycle at this point is 263 [W] for the ORC configuration and 256 [W] for the Kalina cycle configuration.

Figure 5.17 shows the net power output of both the ORC configuration and the Kalina cycle configuration versus the orifice pressure drop.

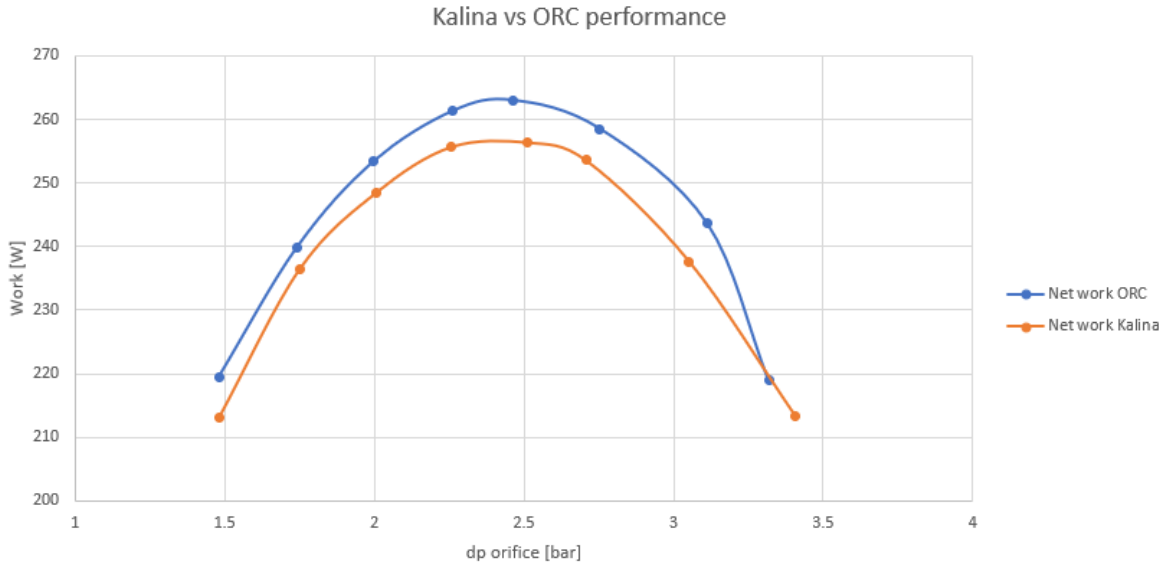

Figure 5.17: The net power output of the ORC configuration and the Kalina cycle configuration versus the orifice pressure drop.

As can be seen in Figure 5.17, the ORC configuration just slightly outperforms the Kalina cycle configuration for pure ammonia. The reason for this is the fact that in the ORC configuration, the reciprocating working fluid pump only has to pump the vapor mass flow rate. In the Kalina cycle configuration, the reciprocating working fluid pump has to pump the total evaporator mass flow. The net turbine work is greater for the Kalina cycle configuration, but the difference in pump work required between the two configurations is larger, causing the Kalina cycle net power output to be lower than the ORC net power output.

5.4.3. VALIDATION OF THE MODEL

Now that the ORC configuration has been successfully tested in the OTEC Demo, the goal is to validate the functionality of the OTEC ORC off-design model to the experimental results. Once the model has been validated, a scaling analysis towards a 3 [MW] OTEC power plant can be made in the next chapter.

This section will first re-evaluate the performance of the two phase heat transfer correlations in the evaporator model. After that, the full cycle outcomes of the off-design model in ORC configuration will be compared to the experimental data.

RE-EVALUATE HEAT TRANSFER CORRELATIONS

Since the heat transfer correlations were validated on an experimental data set that is quite different from the data collected in the current ORC configuration, it is necessary to re-evaluate the two phase heat transfer correlations performance. The main reason for this is found in the different ammonia mass flow rate going through the evaporator. In the data set used before, the ammonia mass flow rate through the evaporator varied between 0.007-0.013 [kg/s]. In the newly acquired data set, the ammonia mass flow rate going into the evaporator varies between 0.0035-0.0049 [kg/s]. This is a consequence of the geometry of the system. Since the driving force for re-circulation is the liquid level in the separator column, the liquid mass flow rate going through the bottom of the separator is limited by the size of the separator column. To create a ratio between the liquid mass flow rate through the bottom of the separator and the liquid mass flow rate coming from the reciprocating working fluid pump that enables the system to operate in steady state, the liquid mass flow rate coming from the reciprocating pump must be kept relatively low. The resulting mass flow rates of ammonia going through the evaporator are thus quite low, and different from the ones used in the previous data set.

In Section 5.4.1, it was found that the re-circulation rate had little to no effect on the evaporator heat transfer rate, for a re-circulation rate ranging from 1.18-2.94. The ammonia mass flow rates, for the tested re-circulation range, ranged from 0.00345-0.00831 [kg/s].
The reason why the heat transfer was independent of the re-circulation rate was thought to originate from the heat transfer mechanism that was dominant in this mass flow domain. Considering the liquid flow velocity was quite low, pool boiling was probably the dominant heat transfer mechanism, causing the heat transfer rate to be independent on the working fluid mass flow rate through the evaporator.

For the two phase heat transfer correlations to be correct, they need to show the same independent character for the calculated heat transfer rate over the same mass flow domain.

The input conditions used in the re-evaluation of the two phase heat transfer coefficients are taken from experimental values. The validation procedure used is similar to the methodology explained in Section 5.3.1.

The experimental data used for this validation comes from the same experiments that are presented in Table 5.9. When using these experimental data sets as inputs to the evaporator model, the resulting deviation on the heat transfer rate per heat transfer correlation can be seen in Figure 5.18. In this figure, the deviation on the heat transfer rate compared to the experimental heat transfer rate per two phase heat transfer correlation versus the evaporator outlet vapor quality is displayed. The deviation on the evaporator heat transfer rate is calculated according to equation 5.8. In the top graph, the full domain of deviation on heat transfer rate can be seen, from -170% to +80%. In the bottom graph, the deviation domain between -50% and +50% deviation can be seen.

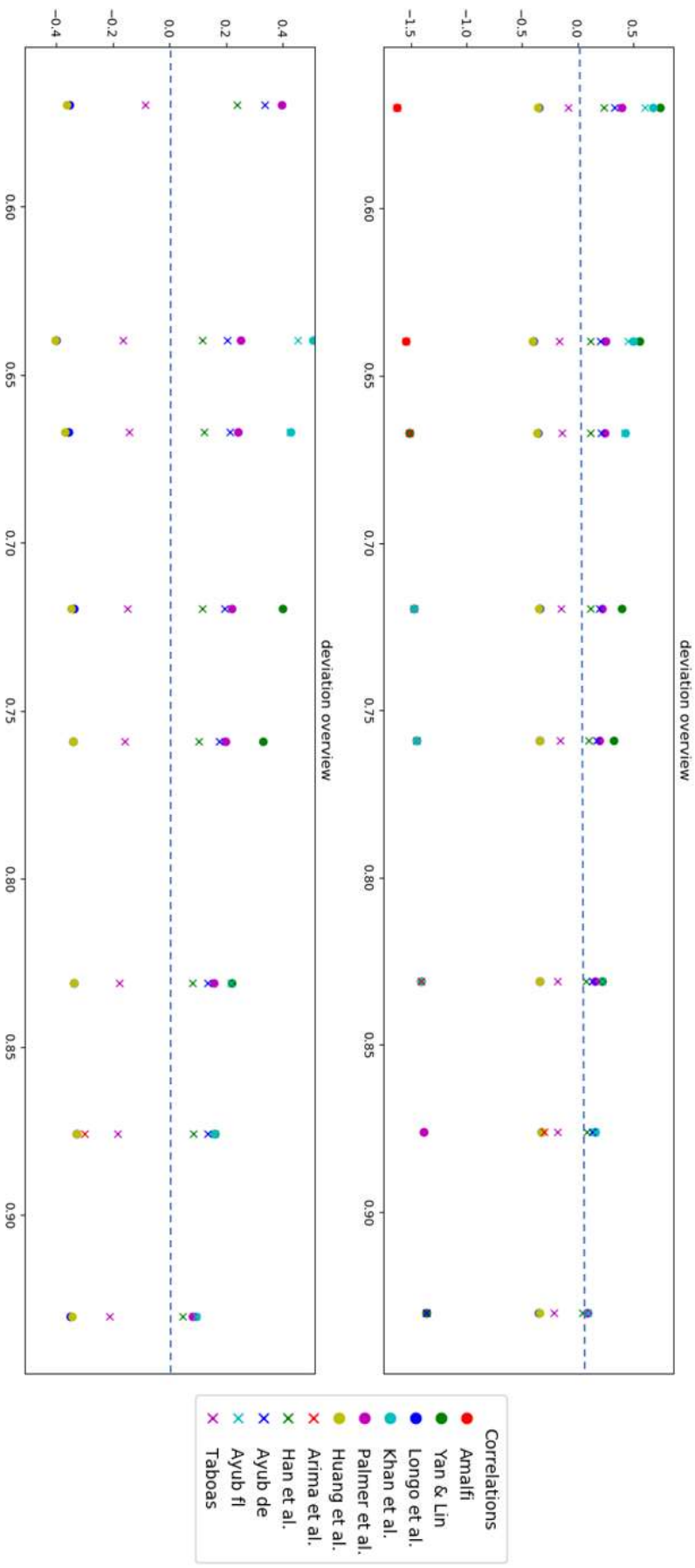

Figure 5.18: An overview of the deviation on evaporator heat transfer rate from ORC experimental data per two phase heat transfer correlation against the evaporator experimental vapor quality at the evaporator outlet.

It is clear that with these new mass flow rates in the evaporator, the two phase heat transfer correlations do not perform as they did with the mass flow rates from the previous data set. The heat transfer correlation proposed by Khan et al. [29] now performs poorly. The heat transfer prediction by the correlations proposed by Taboas [33] and Han et al. [20] deviate similarly as they did before, which is in accordance to the requirement of mass flow independent heat transfer.

To explain why the heat transfer correlations do not perform as expected, some non-dimensional numbers considering the measured flows in the evaporator have to be calculated. Table 5.11 shows the Reynolds numbers calculated for the experimental flows through the evaporator.

Table 5.11: Relevant non dimensional numbers for the experimental mass flow rates.

$dp_{orifice}$ [bar]	$\dot{m}_{evap}$ [kg/s]	G_{evap} [kg/m^{2}s]	$Re_{liq,o}$	$Re_{vap,o}$	$Re_{eq,avg}$
1.48	0.00486	2.73	59.12	841.1	203.09
1.74	0.00480	2.70	62.09	883.3	231.84
2.00	0.00466	2.62	70.65	1005.2	272.88
2.26	0.00461	2.59	73.78	1049.7	300.72
2.46	0.00448	2.52	75.92	1080.1	322.42
2.75	0.00429	2.41	76.74	1091.8	348.87
3.11	0.00377	2.12	79.05	1124.6	376.24
3.22	0.00359	2.02	80.04	1138.7	398.04

Looking at the liquid only, vapor only and equivalent Reynolds numbers calculated for the experimental working fluid flow in the evaporator, it can be noted that they are outside the domain of the heat transfer correlations.
The correlation proposed by Amalfi [26], which is based on a very extensive database of 1903 heat transfer data points, could be expected to predict the evaporator heat transfer rate quite accurately. Unfortunately, the evaporator flow measured in the OTEC Demo ORC configuration has a vapor only Reynolds number which is not higher than 1138.7. The correlation proposed by Amalfi was fitted to a vapor only Reynolds number domain between 1580-42200.
The correlation proposed by Khan et al. [48], which performed well in the previous heat transfer correlation validation is fitted to an equivalent Reynolds number range of 1225-3000. Looking at Table 5.11, this is also outside the current equivalent Reynolds number domain.

Looking at the two phase heat transfer correlation proposed in Section 2.1.1, the heat transfer correlations that are mentioned are all fitted to working fluid flows which are higher than the ones encountered in the current OTEC Demo ORC experiments. Consequentially, these two phase heat transfer correlations are not well suited to predict the heat transfer rate in the evaporator when pool boiling heat transfer mechanisms are dominant over flow boiling heat transfer mechanisms. Only the correlations proposed by Taboas and Han et al. still predict the heat transfer rate with a reasonable deviation.

For the following full cycle validations, the two phase heat transfer correlation proposed by Taboas will be used. It is preferred over the two phase heat transfer correlation proposed by Han et al. for two reasons.

The first reason being the fact that for the data used, the two phase heat transfer correlation by Taboas underpredicts the evaporator heat transfer rate. Using this correlation, the evaporator performance calculation will more likely be conservative. When assessing the system performance of a 3 [MW] plant in the scaling analysis, it is preferred to under-estimate the heat transfer rate in the evaporator rather than to over-estimate it.

The second reason is the fact that the two phase heat transfer correlation proposed by Taboas was specifically fitted to evaporating ammonia. The two phase heat transfer correlation proposed by Han et al. was fitted to experiments for which R410A was evaporated, and is thus judged to not be as consistent in the prediction of the heat transfer rate for ammonia as the two phase heat transfer correlation proposed by Taboas when the geometry of the heat exchanger changes.

FULL CYCLE VALIDATION

After re-evaluating the two phase heat transfer correlations to a data set with a lower mass flux in the evaporator, the full ORC off-design model can be validated to the experimental results. The experimental results used for the validation will be taken from the experiments that are also displayed in Table 5.9.

In the validation of the full cycle model, the input conditions as can be seen in Table 5.12 have been applied.

Table 5.12: input conditions for the validation of the ORC off-design model

	Number of data sets	$dp_{orifice}$ [bar]	T_{warm} [°C]	$\dot{V}_{warm}$ [l/s]	T_{cold} [°C]	$\dot{V}_{cold}$ [l/s]
ORC	8	1.48-3.32	27.00	0.30	5.0	0.22

For each of the experimental data sets used, the ORC off-design model is executed with the water side input temperatures and mass flows, the ammonia mass flow rate through the evaporator and the orifice pressure drop taken from the experimental data. The ORC off-design model iterates the cycle until it has found an evaporator inlet state that makes the iteration convert. The converging criteria are:

- The forwards and backwards calculated stream enthalpy of the stream going from the reciprocating working fluid pump to the mixer must not differ more than 1%.
- The energy balance over the system (the heat transfer rate over the condenser minus the heat transfer rate over the evaporator minus the work done by the reciprocating working fluid pump) must not be more than 1% of the condenser heat transfer rate.

The resulting working fluid states after each component is compared to the experimental data in Tables 5.13 to 5.14.

Table 5.13: Full model outputs compared to the experimental outputs for a singly iteration run over the ORC model, where the pressure drop in the orifice is equal to 1.48 [bar].

		Experimental		**Off-design Model**		
Component	Variable	Measured	Unit	Output	Unit	Deviation [%]
Evaporator	$\dot{m}_{evap}$	0.00486	kg/s	0.00486	kg/s	-
	T_{in}	14.77	°C	13.27	°C	-10.16
	p_{in}	8.40	bar	8.18	bar	-2.62
	T_{out}	19.39	°C	18.48	°C	-4.69
	p_{out}	8.38	bar	8.17	bar	-2.51
	$T_{sw,out}$	22.63	°C	23.17	°C	3.62
	$p_{sw,out}$	1.00	bar	0.98	bar	-2.00
	$q_{evap,out}$	0.93	-	0.81	-	-12.90
	$\dot{Q}_{evap}$	5493	W	4799	W	-12.63
Separator	$T_{liq,out}$	17.87	°C	18.47	°C	3.36
	$p_{liq,out}$	8.38	bar	8.16	bar	-2.63
	$T_{vap,out}$	19.42	°C	18.47	°C	-4.89
	$p_{vap,out}$	8.28	bar	8.16	bar	-1.45
Gear Pump/	T_{out}	-	°C	18.48	°C	-
One Way Valve	p_{out}	-	bar	8.18	bar	-
	y_{liq}	-	m	0.262	m	-
Orifice	T_{out}	15.33	°C	14.11	°C	-7.96
	p_{out}	6.80	bar	6.68	bar	-1.76
Condenser	T_{out}	12.41	°C	12.08	°C	-2.66
	p_{out}	6.75	bar	6.63	bar	-1.78
	$T_{sw,out}$	11.52	°C	10.08	°C	-12.50
	$p_{sw,out}$	0.97	bar	0.96	bar	-1.03
	$\dot{Q}_{cond}$	5765	W	4798	W	-16.77
Rec. WF Pump	T_{out}	13.34	°C	12.73	°C	-4.57
	p_{out}	8.55	bar	8.18	bar	-4.33
	$\dot{W}_{pump}$	13.43	W	12	W	-10.65
				Average Deviation [%]		**-4.58**

Table 5.14: Full model outputs compared to the experimental outputs for a singly iteration run over the ORC model, where the pressure drop in the orifice is equal to 1.74 [bar].

		Experimental		**Off-design Model**		
Component	Variable	Measured	Unit	Output	Unit	Deviation [%]
Evaporator	$\dot{m}_{evap}$	0.00480	kg/s	0.00480	kg/s	-
	T_{in}	14.85	°C	10.28	°C	-30.77
	p_{in}	8.46	bar	8.58	bar	1.42
	T_{out}	19.66	°C	19.94	°C	1.42
	p_{out}	8.44	bar	8.56	bar	1.42
	$T_{sw,out}$	22.93	°C	23.81	°C	3.84
	$p_{sw,out}$	1.00	bar	0.98	bar	-2.00
	$q_{evap,out}$	0.88	-	0.66	-	-25.00
	$\dot{Q}_{evap}$	5106	W	4002	W	-21.62
Separator	$T_{liq,out}$	18.98	°C	19.94	°C	5.06
	$p_{liq,out}$	8.45	bar	8.58	bar	1.30
	$T_{vap,out}$	19.65	°C	19.94	°C	1.48
	$p_{vap,out}$	8.35	bar	8.56	bar	2.51
Gear Pump/	T_{out}	-	°C	19.94	°C	-
One Way Valve	p_{out}	-	bar	8.58	bar	-
	y_{liq}	-	m	0.294	m	-
Orifice	T_{out}	14.83	°C	14.89	°C	0.40
	p_{out}	6.60	bar	6.82	bar	3.33
Condenser	T_{out}	11.16	°C	5.01	°C	-55.11
	p_{out}	6.56	bar	6.77	bar	3.20
	$T_{sw,out}$	10.74	°C	9.24	°C	-13.97
	$p_{sw,out}$	0.97	bar	0.96	bar	-1.03
	$\dot{Q}_{cond}$	5399	W	4007	W	-25.78
Rec. WF Pump	T_{out}	12.73	°C	5.76	°C	-54.75
	p_{out}	8.60	bar	8.58	bar	-0.23
	$\dot{W}_{pump}$	17.28	W	11	W	-36.34
				Average Deviation [%]		**-9.63**

Table 5.15: Full model outputs compared to the experimental outputs for a singly iteration run over the ORC model, where the pressure drop in the orifice is equal to 2.00 [bar].

		Experimental		**Off-design Model**		
Component	Variable	Measured	Unit	Output	Unit	Deviation [%]
Evaporator	$\dot{m}_{evap}$	0.00466	kg/s	0.00466	kg/s	-
	T_{in}	15.05	°C	10.97	°C	-27.11
	p_{in}	8.59	bar	8.70	bar	1.28
	T_{out}	20.09	°C	20.39	°C	1.49
	p_{out}	8.57	bar	8.68	bar	1.28
	$T_{sw,out}$	23.25	°C	24.10	°C	3.44
	$p_{sw,out}$	1.00	bar	0.98	bar	-2.00
	$q_{evap,out}$	0.83	-	0.63	-	-24.10
	$\dot{Q}_{evap}$	4701	W	3701	W	-21.27
Separator	$T_{liq,out}$	19.64	°C	20.39	°C	3.82
	$p_{liq,out}$	8.57	bar	8.68	bar	1.28
	$T_{vap,out}$	20.09	°C	20.39	°C	1.49
	$p_{vap,out}$	8.47	bar	8.68	bar	2.48
Gear Pump/	T_{out}	-	°C	20.39	°C	-
One Way Valve	p_{out}	-	bar	8.70	bar	-
	y_{liq}	-	m	0.303	m	-
Orifice	T_{out}	14.56	°C	14.58	°C	0.14
	p_{out}	6.48	bar	6.68	bar	3.09
Condenser	T_{out}	10.54	°C	5.02	°C	-52.37
	p_{out}	6.44	bar	6.63	bar	2.95
	$T_{sw,out}$	10.28	°C	8.92	°C	-13.23
	$p_{sw,out}$	0.97	bar	0.96	bar	-1.03
	$\dot{Q}_{cond}$	4965	W	3707	W	-25.34
Rec. WF Pump	T_{out}	12.35	°C	5.87	°C	-52.47
	p_{out}	8.71	bar	8.70	bar	-0.11
	$\dot{W}_{pump}$	19.01	W	12	W	-36.88
				Average Deviation [%]		**-9.42**

Table 5.16: Full model outputs compared to the experimental outputs for a singly iteration run over the ORC model, where the pressure drop in the orifice is equal to 2.26 [bar].

		Experimental		**Off-design Model**		
Component	Variable	Measured	Unit	Output	Unit	Deviation [%]
Evaporator	$\dot{m}_{evap}$	0.00461	kg/s	0.00461	kg/s	-
	T_{in}	15.37	°C	12.21	°C	-20.56
	p_{in}	8.71	bar	8.85	bar	1.61
	T_{out}	20.51	°C	20.93	°C	2.05
	p_{out}	8.69	bar	8.83	bar	1.61
	$T_{sw,out}$	23.62	°C	24.31	°C	2.92
	$p_{sw,out}$	1.00	bar	0.98	bar	-2.00
	$q_{evap,out}$	0.76	-	0.59	-	-22.37
	$\dot{Q}_{evap}$	4242	W	3379	W	-20.34
Separator	$T_{liq,out}$	20.49	°C	20.92	°C	2.10
	$p_{liq,out}$	8.70	bar	8.83	bar	1.49
	$T_{vap,out}$	20.54	°C	20.92	°C	1.85
	$p_{vap,out}$	8.61	bar	8.83	bar	2.56
Gear Pump/	T_{out}	-	°C	20.93	°C	-
One Way Valve	p_{out}	-	bar	8.85	bar	-
	y_{liq}	-	m	0.320	m	-
Orifice	T_{out}	14.27	°C	14.38	°C	0.77
	p_{out}	6.35	bar	6.57	bar	3.46
Condenser	T_{out}	9.95	°C	5.01	°C	-49.65
	p_{out}	6.31	bar	6.52	bar	-3.33
	$T_{sw,out}$	9.78	°C	8.59	°C	-12.17
	$p_{sw,out}$	0.97	bar	0.96	bar	-1.03
	$\dot{Q}_{cond}$	4481	W	3391	W	-24.32
Rec. WF Pump	T_{out}	11.83	°C	5.97	°C	-49.54
	p_{out}	8.82	bar	8.85	bar	0.34
	$\dot{W}_{pump}$	18.35	W	12	W	-34.60
				Average Deviation [%]		**-8.80**

Table 5.17: Full model outputs compared to the experimental outputs for a singly iteration run over the ORC model„ where the pressure drop in the orifice is equal to 2.46 [bar].

		Experimental		**Off-design Model**		
Component	Variable	Measured	Unit	Output	Unit	Deviation [%]
Evaporator	$\dot{m}_{evap}$	0.00448	kg/s	0.00448	kg/s	-
	T_{in}	15.81	°C	11.85	°C	-25.05
	p_{in}	8.81	bar	8.87	bar	0.68
	T_{out}	20.86	°C	20.99	°C	0.62
	p_{out}	8.79	bar	8.85	bar	0.68
	$T_{sw,out}$	23.88	°C	24.36	°C	2.01
	$p_{sw,out}$	1.00	bar	0.98	bar	-2.00
	$q_{evap,out}$	0.72	-	0.59	-	-18.06
	$\dot{Q}_{evap}$	3908	W	3312	W	-15.25
Separator	$T_{liq,out}$	20.91	°C	20.98	°C	0.33
	$p_{liq,out}$	8.80	bar	8.85	bar	0.57
	$T_{vap,out}$	20.90	°C	20.98	°C	0.38
	$p_{vap,out}$	8.71	bar	8.85	bar	1.61
Gear Pump/	T_{out}	-	°C	20.99	°C	-
One Way Valve	p_{out}	-	bar	8.87	bar	-
	y_{liq}	-	m	0.428	m	-
Orifice	T_{out}	14.07	°C	13.83	°C	-1.71
	p_{out}	6.25	bar	6.39	bar	2.24
Condenser	T_{out}	9.41	°C	5.12	°C	-45.59
	p_{out}	6.22	bar	6.34	bar	1.93
	$T_{sw,out}$	9.42	°C	8.51	°C	-9.66
	$p_{sw,out}$	0.97	bar	0.96	bar	-1.03
	$\dot{Q}_{cond}$	4138.03	W	3316	W	-19.87
Rec. WF Pump	T_{out}	11.52	°C	6.16	°C	-46.53
	p_{out}	8.92	bar	8.87	bar	-0.56
	$\dot{W}_{pump}$	18.77	W	13	W	-30.74
				Average Deviation [%]		**-8.21**

Table 5.18: Full model outputs compared to the experimental outputs for a singly iteration run over the ORC model, where the pressure drop in the orifice is equal to 2.75 [bar].

		Experimental		**Off-design Model**		
Component	Variable	Measured	Unit	Output	Unit	Deviation [%]
Evaporator	$\dot{m}_{evap}$	0.00429	kg/s	0.00429	kg/s	-
	T_{in}	16.29	°C	13.41	°C	-17.68
	p_{in}	8.97	bar	9.00	bar	0.33
	T_{out}	21.41	°C	21.44	°C	0.14
	p_{out}	8.95	bar	8.98	bar	0.34
	$T_{sw,out}$	24.24	°C	24.62	°C	1.57
	$p_{sw,out}$	1.00	bar	0.98	bar	-2.00
	$q_{evap,out}$	0.67	-	0.56	-	-16.42
	$\dot{Q}_{evap}$	3460	W	2982	W	-13.82
Separator	$T_{liq,out}$	21.31	°C	21.44	°C	0.61
	$p_{liq,out}$	8.97	bar	8.98	bar	0.11
	$T_{vap,out}$	21.40	°C	21.44	°C	0.19
	$p_{vap,out}$	8.88	bar	8.98	bar	1.13
Gear Pump/	T_{out}	-	°C	21.44	°C	-
One Way Valve	p_{out}	-	bar	9.00	bar	-
	y_{liq}	-	m	0.321	m	-
Orifice	T_{out}	13.65	°C	13.45	°C	-2.20
	p_{out}	6.12	bar	6.23	bar	1.31
Condenser	T_{out}	9.48	°C	5.28	°C	-44.30
	p_{out}	6.09	bar	6.18	bar	1.48
	$T_{sw,out}$	8.90	°C	8.17	°C	-8.20
	$p_{sw,out}$	0.97	bar	0.96	bar	-1.03
	$\dot{Q}_{cond}$	3651	W	3001	W	-17.80
Rec. WF Pump	T_{out}	11.30	°C	7.88	°C	-43.01
	p_{out}	9.07	bar	8.97	bar	-0.77
	$\dot{W}_{pump}$	21.49	W	14	W	-39.51
				Average Deviation [%]		**-9.01**

Table 5.19: Full model outputs compared to the experimental outputs for a singly iteration run over the ORC model, where the pressure drop in the orifice is equal to 3.11 [bar].

		Experimental		**Off-design Model**		
Component	Variable	Measured	Unit	Output	Unit	Deviation [%]
Evaporator	$\dot{m}_{evap}$	0.00377	kg/s	0.00377	kg/s	-
	T_{in}	17.61	°C	13.93	°C	-20.90
	p_{in}	9.18	bar	9.18	bar	0.00
	T_{out}	22.16	°C	22.10	°C	-0.27
	p_{out}	9.16	bar	9.17	bar	0.11
	$T_{sw,out}$	24.68	°C	25.02	°C	1.38
	$p_{sw,out}$	1.00	bar	0.98	bar	-2.00
	$q_{evap,out}$	0.64	-	0.53	-	-17.19
	$\dot{Q}_{evap}$	2906	W	2481	W	-14.62
Separator	$T_{liq,out}$	21.88	°C	22.10	°C	1.01
	$p_{liq,out}$	9.17	bar	9.17	bar	0.00
	$T_{vap,out}$	22.24	°C	22.10	°C	-0.63
	$p_{vap,out}$	9.09	bar	9.17	bar	0.88
Gear Pump/	T_{out}	-	°C	22.10	°C	-
One Way Valve	p_{out}	-	bar	9.18	bar	-
	y_{liq}	-	m	0.323	m	-
Orifice	T_{out}	13.47	°C	13.08	°C	-2.90
	p_{out}	5.98	bar	6.06	bar	1.34
Condenser	T_{out}	8.66	°C	5.29	°C	-38.91
	p_{out}	5.95	bar	6.01	bar	1.01
	$T_{sw,out}$	8.25	°C	7.64	°C	-7.39
	$p_{sw,out}$	0.97	bar	0.96	bar	-1.03
	$\dot{Q}_{cond}$	3072	W	2492	W	-18.88
Rec. WF Pump	T_{out}	11.16	°C	6.60	°C	-40.86
	p_{out}	9.26	bar	9.18	bar	-0.86
	$\dot{W}_{pump}$	24.10	W	12	W	-50.21
				Average Deviation [%]		**-9.59**

Table 5.20: Full model outputs compared to the experimental outputs for a singly iteration run over the ORC model, where the pressure drop in the orifice is equal to 3.32 [bar].

		Experimental		**Off-design Model**		
Component	Variable	Measured	Unit	Output	Unit	Deviation [%]
Evaporator	$\dot{m}_{evap}$	0.00359	kg/s	0.00359	kg/s	-
	T_{in}	19.16	°C	16.07	°C	-16.13
	p_{in}	9.25	bar	9.27	bar	0.22
	T_{out}	22.39	°C	22.39	°C	0.00
	p_{out}	9.23	bar	9.25	bar	0.22
	$T_{sw,out}$	25.05	°C	25.20	°C	0.60
	$p_{sw,out}$	1.00	bar	0.98	bar	-2.00
	$q_{evap,out}$	0.57	-	0.51	-	-10.53
	$\dot{Q}_{evap}$	2451	W	2261	W	-7.75
Separator	$T_{liq,out}$	22.31	°C	22.39	°C	0.36
	$p_{liq,out}$	9.25	bar	9.25	bar	0.00
	$T_{vap,out}$	22.35	°C	22.38	°C	0.13
	$p_{vap,out}$	9.17	bar	9.25	bar	0.87
Gear Pump/	T_{out}	-	°C	22.39	°C	-
One Way Valve	p_{out}	-	bar	9.27	bar	-
	y_{liq}	-	m	0.325	m	-
Orifice	T_{out}	13.26	°C	12.75	°C	-3.85
	p_{out}	5.85	bar	5.93	bar	1.37
Condenser	T_{out}	7.34	°C	8.05	°C	9.67
	p_{out}	5.83	bar	5.88	bar	0.86
	$T_{sw,out}$	7.77	°C	7.41	°C	-4.63
	$p_{sw,out}$	0.96	bar	0.96	bar	0.00
	$\dot{Q}_{cond}$	2607	W	2277	W	-12.66
Rec. WF Pump	T_{out}	10.98	°C	9.45	°C	-13.93
	p_{out}	9.31	bar	9.27	bar	-0.43
	$\dot{W}_{pump}$	24.63	W	12	W	-51.28
				Average Deviation [%]		**-4.95**

INTERPRETATION & DISCUSSION

As can be seen in Tables 5.13 to 5.20, the energy balance over the OTEC cycle in the measured data shows an error. The evaporator heat transfer rate plus the pump work should be equal to the condenser heat transfer rate. In the measured data, the condenser heat transfer rate is slightly higher than the sum of the evaporator heat transfer rate and the pump work. This difference ranges from 131-276 [W]. This is a worrying phenomenon, indicating that either the measured values are wrong, or the OTEC Demo is not insulated properly and heat is leaking into the system. Looking back at the measured data gathered by Goudriaan [11] and Kuikhoven [25], the same error in the energy balance over the OTEC Demo in Kalina cycle configuration can be seen. For four out of six experimental data sets shown in the report made by Goudriaan, the energy balance difference is between 242-280 [W], which is a similar error as can be seen in the presented ORC configuration data. Considering that the error in the energy balance is similar as it is, the assumption is made that this is caused by the insulation not being perfect, where heat is leaking into the system in the cold side of the cycle.

Below, the results from the off-design ORC model full cycle will be discussed per component.

The evaporator outlet states are what could be expected after the re-evaluation of the two phase heat transfer correlations. The two phase heat transfer correlation proposed by Taboas [33] under-predicts the heat transfer rate in the evaporator and consequentially the vapor quality at the evaporator outlet is lower for the off-design model than the OTEC Demo. The pressure drop correlation proposed by Yan and Lin [27] predicts the two phase pressure drop in the evaporator correctly since it is of similar proportions. Making any claims on how well it would perform on a broader range of evaporator pressure drops is difficult since the pressure drop itself is so low.

The separator outlet states show some interesting results. The results for the model are, logically, saturated liquid and vapor conditions at the respective outlets. For the experimental data, the outlet liquid and vapor states sometimes do not have the same temperature. Since the evaporator outlet state is partially vapor and partially liquid, it is rather strange to see two different temperatures at the separator outlets. The difference in separator outlet temperatures can be explained by two hypotheses:

- The difference in temperature could be caused by the fact that the vapor in the two phase stream coming from the evaporator is slightly superheated and the liquid is still slightly subcooled. When separated in the separator, this temperature difference then becomes measurable in the separator outlet states.
- The difference in the temperature could also be the consequence of the physical location of the temperature sensor that measures the liquid outlet stream coming from the bottom of the separator. This temperature sensor (TI-11 in the P&ID shown in Figure 3.4) is located at the bottom of the separator. This means that some pressure build up from the working fluid liquid column has already occurred at this point, as can be seen by the measured liquid outlet pressure. This increase in pressure causes the liquid temperature at this point to be slightly higher than the saturated liquid temperature.

A combination of these two phenomena could cause the difference in vapor and liquid outlet temperatures for the separator.

The gear pump/one-way valve results, unfortunately, cannot be validated to experimental values. As can be seen in Figure 3.4, there are no sensors that measure the outlet state of the gear pump/ one way valve before the mixing point. One thing that can be evaluated is the required liquid column height to overcome the pressure drop. The results from the OTEC off-design model show that the liquid column height needs to be around 0.30-0.40 [m] for the re-circulation to occur. In reality, for the OTEC Demo, the liquid column height for all experiments was almost up to the separator liquid inlet, which amounts to a liquid column length of around 0.70-0.90 [m]. In the OTEC off-design model, the only pressure losses which need to be overcome by the liquid column height are those created in the evaporator, the separator and the mixing point, for which the latter two are negligible. This means that in the experiments executed, roughly 50% of the pressure drop between the separator liquid outlet and the separator inlet is created in the evaporator. The rest of the pressure drop is piping pressure drop, caused by friction in the pipes and manifolds.

The results for the Orifice are pretty straight forward since they're modeled with the orifice pressure drop as an input to the off-design model.

The results for the condenser in general show quite a deviation from the experimental data. This can be explained by the fact that the vapor mass flow rate coming from the separator in the model is different from the vapor mass flow rate coming from the separator in the OTEC Demo. Since the two phase heat transfer correlation by Taboas under-predicts the heat transfer in the evaporator, the vapor quality at the evaporator outlet in the model is consistently lower than the vapor quality at the evaporator outlet in the OTEC Demo. This causes the mass flow rate of vapor going through the orifice and condenser to be lower in the model compared to the OTEC Demo as well. Consequentially, as can be seen for the data sets with orifice pressure drops ranging from 1.74-3.11 [bar], the condenser outlet stream in the off-design model is often subcooled. The condenser outlet states for the data of the 1.48 and 3.32 [bar] orifice pressure drops are not subcooled, even though the mass flow through the condenser is lower than what it is for the measured data. This means that the two phase heat transfer correlation used in the condenser probably under-estimates the two phase heat transfer rate in the condenser. To create certainty on the performance of the condenser off-design model, a separate validation of the component will need to be executed, which is not the scope of this research.

The deviation in the results for the evaporator heat transfer rate also resonate in the deviation results of the reciprocating working fluid pump. Since the vapor mass flow rate in the model is lower than in the OTEC Demo, the mass flow which the reciprocating working fluid pump has to create is also lower. Additionally, for the experimental data, the temperature increase of the working fluid caused by the reciprocating working fluid pump increases with an increasing pressure differential. This means that the reciprocating working fluid pump efficiency decreases with an increasing pressure differential. This phenomenon is not accounted for in the off-design model.
The combination of these two phenomena cause the pump work calculated by the OTEC off-design model to be lower than the actual pump work, with a greater difference for higher pressure differentials.

In general, the OTEC off-design model for ORC configuration does not predict the working fluid states very accurately. The major error results from the under-prediction of the evaporator heat transfer rate, which leads to a lower vapor mass flow rate, which in turn results in deviations for the condenser and reciprocating working fluid pump. However, the cycle performance following the prediction can be considered conservative. Using the OTEC off-design ORC model in a scaling analysis will most likely lead to a cycle performance that is lower than the performance of a real system.

6

SCALING ANALYSIS

With the now validated OTEC ORC off-design model, a scaling analysis towards a 3 [MW] OTEC power plant can be executed. This information could be useful to Bluerise B.V. as a reference to other simulation tools. In this short chapter, first, the 3 [MW] plant as designed by Bluerise B.V. will be explained, after which the results from the scaling analysis will be displayed and discussed.

The 3 [MW] plant design used as a reference is taken from van Senden [70], which was specifically designed to deliver a net 3 [MW] power output.

6.1. PLANT DESIGN

The 3 [MW] OTEC power plant designed by Bleurise is an ORC OTEC system containing the following components:

- 40 brazed plate heat exchanger evaporators
- 5 column separators
- A Turbine with a generator to generate electricity
- 21 brazed plate heat exchanger condensers
- 2 buffer tanks
- 3 working fluid pumps
- Several cold an warm seawater pumps

In the current scaling analysis, like in the entirety of this report, the focus will be on the working fluid cycle, neglecting the cold and warm water streams outside of the heat exchangers. The power plant PFD can be seen in Figure 6.1, and an isometric 3D depiction of this plant is shown in Figure 6.2.

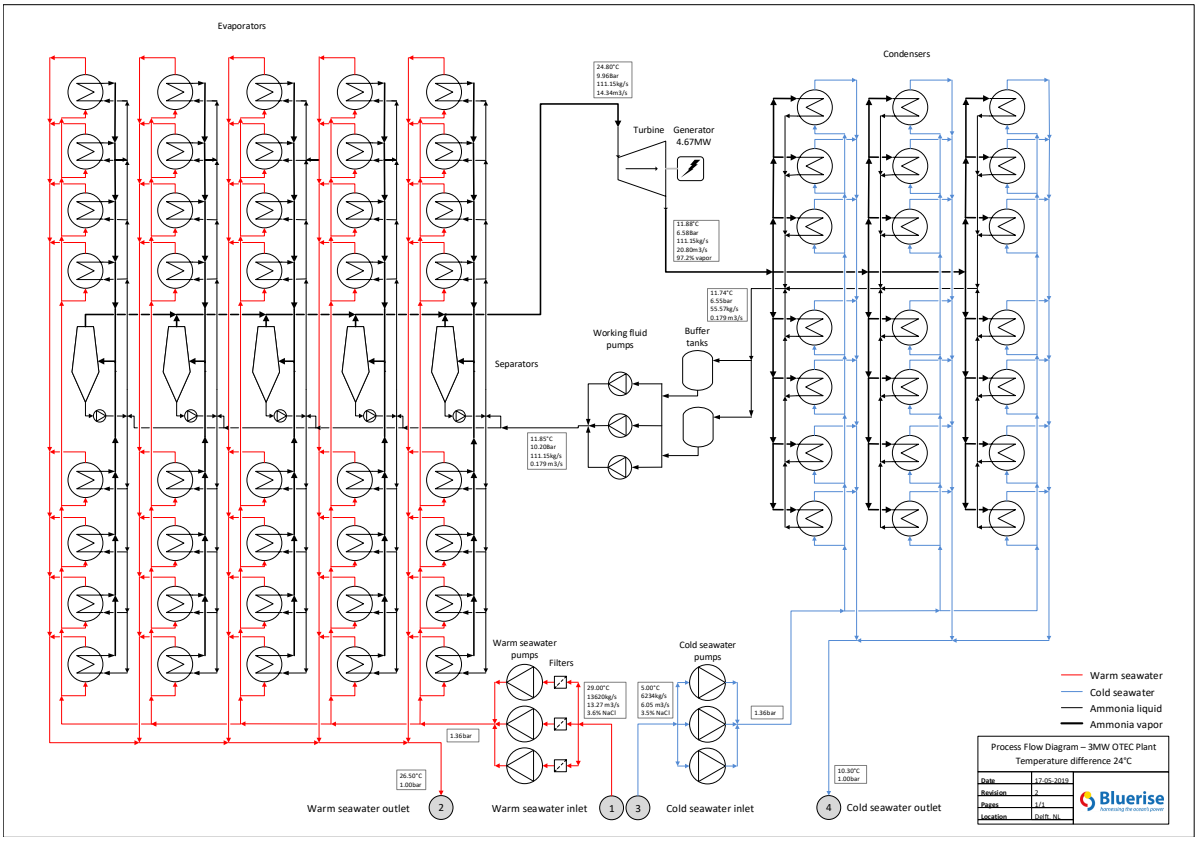

Figure 6.1: PFD for the 3[MW] OTEC power plant designed by Bluerise B.V. Source: [70]

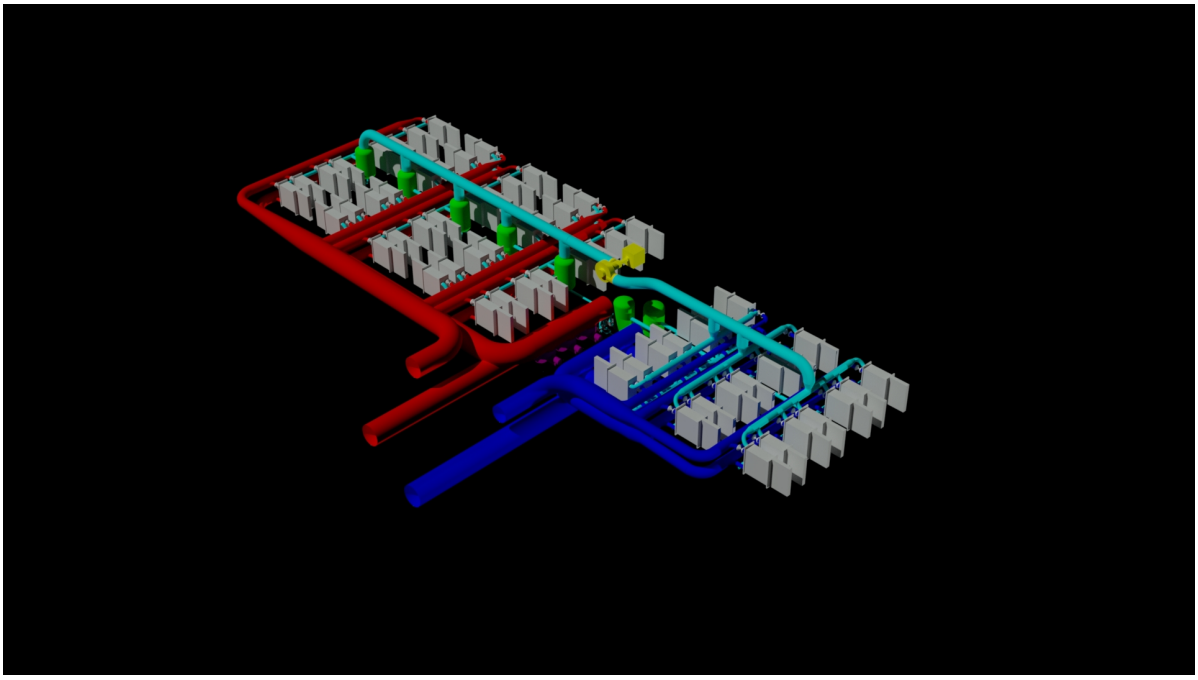

Figure 6.2: Isometric 3D view of the 3[MW] OTEC power plant designed by Bluerise B.V. Source: [70]

The off-design model allows for an easy scaling analysis towards a larger system. The input geometries and flows need to be changed and then the model will calculate the component output states in the same manner as for a smaller OTEC setup.

The heat exchangers used are supplied by a company, which name will not be mentioned here. However, Bluerise B.V. signed a non-disclosure agreement with this company, promising to not spread details about the geometries of these heat exchangers to third parties. For that reason, the exact geometries of these heat exchangers cannot be given in this report. Table 6.1 does show how the evaporator mass flow rates of the working fluid and warm and cold water flows are scaled to the 3[MW] OTEC power plant.

Table 6.1: Scaled mass flow rates of the ammonia and cold and warm seawater streams.

Stream	Mass flow from OTEC Demo [kg/s]	Mass flux from OTEC Demo [kg/m^{2}s]	Total flow passage area in 3[MW] plant [m^2]	Resulting mass flow in 3[MW] plant [kg/s]
Ammonia:				
$dp_{orifice} = 1.48$	0.0486	2.73	45.0	123.51
$dp_{orifice} = 2.00$	0.0466	2.62	45.0	118.41
$dp_{orifice} = 2.48$	0.0448	2.52	45.0	113.96
$dp_{orifice} = 3.11$	0.0377	2.12	45.0	95.92
Warm water	0.300	154.16	45.5	7000
Cold water	0.225	116.62	23.7	2750

Apart from the changes in the heat exchangers, the separator out- and inlet ports change as well. In the 3 [MW] OTEC plant, the separator inlet ports are 0.6 [m] in diameter, the liquid outlet ports are 0.2 [m] in diameter and the vapor outlet ports are 1.0 [m] in diameter. The OTEC off-design model simulates the 5 separators as a single separator with said dimensions.

In the PFD of the power plant, Figure 6.1, additional pumps to drive the liquid re-circulation from the separator bottom back to the evaporator can be seen. In the current scaling analysis these pumps will be neglected and liquid re-circulation is assumed to happen under natural circulation by liquid column driving force. The assumption is that the power required by the gear pumps is very small compared to the water side pumps, so they will not have a significant impact on the performance of the full scale 3 [MW] power plant.

The input conditions used in the scaling analysis can be seen in Table 6.2

Table 6.2: Boundary conditions for the scaled ORC off-design 3[MW] model.

Number of simulations	$dp_{orifice}$ [bar]	T_{warm} [°C]	$\dot{m}_{warm}$ [kg/s]	T_{cold} [°C]	$\dot{m}_{cold}$ [kg/s]
4	varied	27.00	7000	5.0	2750

Similar to the full cycle validation in the previous chapter, the two phase heat transfer correlation proposed by Taboas [33] will be used to calculate the two phase heat transfer rate in the evaporator. The two phase pressure drop correlation proposed by Yan and Lin [27] will be used to calculate the two phase pressure drop in the evaporator.

6.2. SCALING ANALYSIS RESULTS

Table 6.3 shows the resulting stream data of the off-design model for the 3 [MW] OTEC installation. The results were generated by running the full cycle ORC off-design model with the input conditions given in Table 6.2 and the fixed orifice pressure drop.

The convergence criteria used needed to be less strict than in the full cycle validation. Unfortunately, the model was unable to converge to an energy balance value of less than 1% of the condenser heat transfer rate. This required the convergence criteria for energy balance to be set to 3%. For each of the data sets created in Table 6.3, the resulting energy balance error is given.

As stated before, the OTEC off-design model simulates the orifice as an ideal orifice where the outlet pressure is determined by an orifice pressure drop which is given as an input value to the model. After the model has converged and all the stream states are calculated, the model uses the working fluid states around the orifice to calculate the turbine work that could be created from this stream. The turbine work is calculated using equation 2.8. Table 6.3 shows the calculated parameters used in this equation and the consequential turbine work per data set.

The net work created in the cycle forms the basis on which to assess the performance of the cycle. The net work of the cycle is calculated per data set and displayed in the last row of Table 6.3. In Figure 6.3 the work done by the turbine, the working fluid pump and the net work delivered by the cycle are plotted against the pressure drop over the orifice.

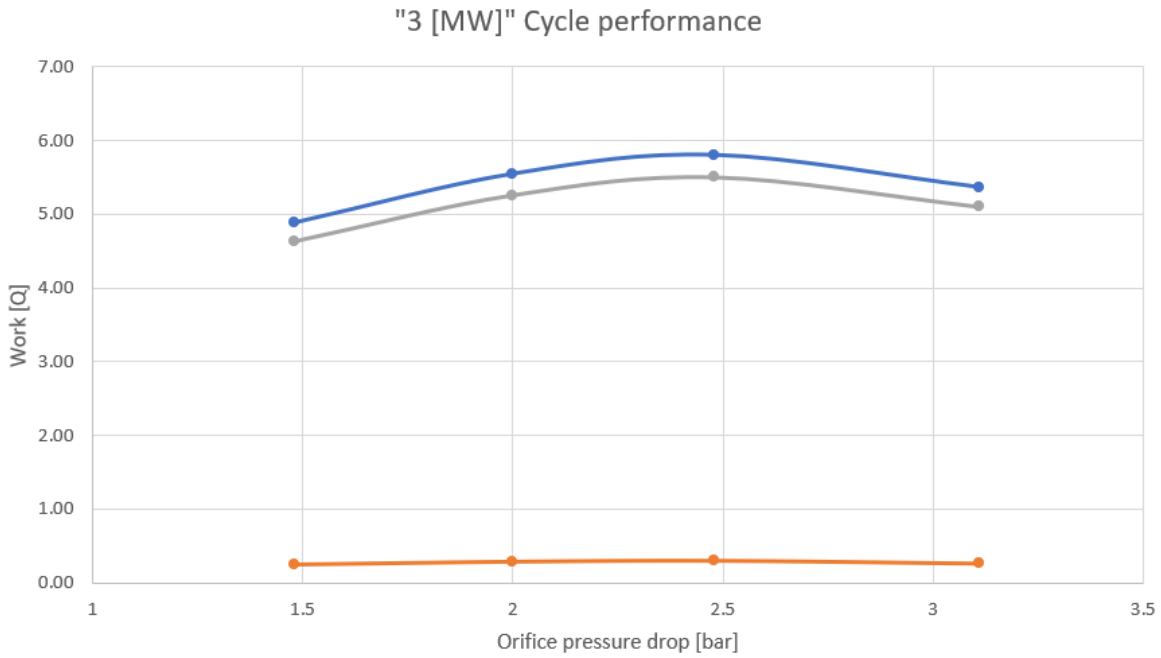

Figure 6.3: Theoretical turbine work, work done by the working fluid pump and consequential net work produced by the 3[MW] OTEC plant versus the pressure drop over the turbine.

Table 6.3: Scaling analysis results from the OTEC off-design model.

Component	Variable	$dp_{orifice}$ 1.48 [bar]	$dp_{orifice}$ 2.00 [bar]	$dp_{orifice}$ 2.46 [bar]	$dp_{orifice}$ 3.11 [bar]
Evaporator	$\dot{m}_{evap}$ [kg/s]	123.51	118.41	113.96	95.2
	T_{in} [°C]	10.10	11.41	14.47	16.52
	p_{in} [bar]	9.12	9.32	9.5	9.76
	T_{out} [°C]	21.87	22.56	23.15	24.04
	p_{out} [bar]	9.10	9.30	9.47	9.74
	$T_{sw,out}$ [°C]	22.88	23.48	24.00	24.82
	$p_{sw,out}$ [bar]	0.90	0.90	0.90	0.90
	$q_{evap,out}$	0.78	0.70	0.62	0.54
	$\dot{Q}_{evap}$ [MW]	120.55	103.1	87.68	63.8
Separator	$T_{liq,out}$ [°C]	21.84	22.52	23.11	24.00
	$p_{liq,out}$ [bar]	9.09	9.29	9.46	9.73
	$T_{vap,out}$ [°C]	21.86	22.56	23.17	24.07
	$p_{vap,out}$ [bar]	9.09	9.29	9.47	9.73
Gear Pump/	T_{out} [°C]	21.84	22.52	23.11	24.00
One Way Valve	p_{out} [bar]	9.09	9.29	9.46	9.73
	y_{liq} [m]	0.698	0.712	0.762	0.750
Orifice	T_{out} [°C]	16.31	15.02	13.75	12.17
	p_{out} [bar]	7.61	7.29	6.99	6.62
Condenser	T_{out} [°C]	5.10	5.07	5.41	5.23
	p_{out} [bar]	7.41	7.09	6.79	6.42
	$T_{sw,out}$ [°C]	15.34	13.78	12.49	10.43
	$p_{sw,out}$ [bar]	0.90	0.90	0.90	0.90
	$\dot{Q}_{cond}$ [MW]	119.33	101.36	86.46	62.70
Rec. WF Pump	T_{out} [°C]	5.66	5.80	6.29	6.32
	p_{out} [bar]	9.13	9.33	9.51	9.77
	$\dot{W}_{pump}$ [MW]	0.26	0.29	0.30	0.27
Turbine	$\dot{m}_{vap}$ [kg/s]	96.34	82.89	70.66	51.80
	η_{is}	0.9	0.9	0.9	0.9
	c_p [J/kgK]	3067.45	3082.00	3095.03	3113.73
	γ	1.46	1.46	1.46	1.47
	$\dot{W}_{turb}$ [MW]	4.89	5.55	5.80	5.37
Energy Balance	$\frac{\dot{Q}_{cond}-\dot{Q}_{evap}-\dot{W}_{pump}}{\dot{Q}_{cond}}$ [%]	-1.24	-2.00	-1.76	-2.19
Net Work	$\dot{W}_{turb}-\dot{W}_{pump}$ [MW]	4.63	5.26	5.50	5.10

6.3. INTERPRETATION & DISCUSSION

The evaporator heat transfer rate is within a range that could be expected. Looking at the vapor quality of the working fluid at the evaporator outlet, the same range of vapor qualities can be seen as were calculated in the OTEC Demo validation.

The pressure drops over the evaporator, calculated with the two phase pressure drop correlation proposed by Yan and Lin, are calculated to be rather low when compared to the manufacturer values. According to the manufacturer, the pressure drop inside the evaporators is significantly higher than what is calculated in the current OTEC off-design model, but unfortunately, that value cannot be disclosed here.
The reason for this difference in pressure drop could be caused by the fact that the manufacturer includes an evaporator inlet and outlet pressure drop. The working fluid flows into and out of the evaporator through the evaporator ports, which causes a significant pressure drop in the working fluid flow. The two phase pressure drop correlation proposed by Yan and Lin does not account for these manifold pressure drops. When calculating and adding the heat exchanger manifolds pressure drop using equation H.3, the pressure drop over the evaporator is still relatively low compared to the manufacturer value. This indicates that the two phase pressure drop correlation proposed by Yan and Lin does underestimate the two phase pressure drop in the evaporator heat exchanger, or that the manufacturer value is a very conservative estimate.

The required liquid column height to overcome the pressure drop is calculated to be around 0.70-0.75 [m]. Considering that the pressure drop calculated in the evaporator heat exchanger model is too low, and the fact that the piping pressure drop is not considered in the OTEC off-design model, the required liquid column height will probably be higher in reality.

The results from the scaling analysis on first look are very promising. With the provided system dimensions, the cycle can produce a net power output between 4.5-5.5 [MW]. Even though this could be considered a very satisfactory result, it has to come with some side notes:

- The net work output of the cycle is mostly determined by the turbine work. In the current case, the turbine work is calculated with equation 2.8, which requires an isentropic efficiency of the turbine to be entered. In this report, an isentropic efficiency of the turbine of 0.9 has consequently been used. When looking at the absolute performance of a 3 [MW] scaled OTEC power plant, the isentropic efficiency of the turbine does play a big role. An isentropic efficiency of 0.9 is believed to be relatively high and could potentially be lower in reality, causing lower turbine work and a lower net work output of the cycle.
- When looking at the study done by van Senden [70], it can be noticed that the seawater pumps for the cold and warm seawater streams require a relatively large power input when compared to the working fluid pump. So even though the net work output of the cycle itself might be as high as 5.5 [MW], this analysis does not include the power lost in pumping 7000 and 2750 [kg/s] of respective warm and cold seawater.

7

CONCLUSIONS & RECOMMENDATIONS

In this chapter, the work that has been done in this thesis report and the created results are shortly summarized and concluded. Finally, some recommendations on improvements and subjects for further research will be given.

7.1. CONCLUSIONS

The main objective of this thesis research was to study how changing the cycle configuration from a Kalina cycle configuration to an ORC configuration would influence the system performance and operating characteristics. This goal has successfully been achieved. The main take away would be based on Figure 5.17, leading to conclude that the performance of the OTEC system does not necessarily suffer from changing the cycle configuration from a Kalina cycle configuration to an ORC configuration.

All accompanying sub-questions have also been answered successfully.

The working mechanism of the OTEC system has successfully been changed from a Kalina cycle configuration to an ORC configuration for both the OTEC Demo and the off-design OTEC model. Interestingly, the performance of the evaporator is independent of the ammonia re-circulation rate through it, for the tested domain of 1.2 to 2.9 re-circulation rate.
The reason for this independence on re-circulation rate was found in the relatively low mass flow rates through the evaporator. At the working fluid flow velocities, pool boiling could be the main heat transfer mechanism, instead of flow boiling. This would cause the heat transfer rate in the evaporator to be independent of the working fluid mass flow rate through the evaporator.

This result allows for a simplification of the ORC configuration. The initial idea was to optimize the re-circulation rate using a gear pump to drive the liquid fraction coming from the separator back to the evaporator. This was supposedly done to achieve a re-circulation mass flow rate that would cause the highest evaporator heat transfer rate to occur. When the re-circulation rate does not influence the evaporator performance, natural re-circulation through liquid column pressure build-up will perform equally well as forced re-circulation using a (gear) pump.

Comparing the evaporator performance of the ORC configuration to the Kalina cycle configuration, one can conclude that the Kalina cycle configuration evaporator performance is higher than the ORC configuration evaporator performance. This evaporator overall heat transfer coefficient for the Kalina cycle configuration is higher than the overall heat transfer coefficient for the ORC configuration, using pure ammonia. From data obtained during the experiments executed by Goudriaan [11] and Kuikhoven [25] it was concluded that the evaporator performance for a mixture of ammonia/ water is higher than the evaporator performance of pure ammonia. The combination of these two conclusions leads to conclude that the evaporator performance in the ORC configuration is lower than the evaporator performance of the Kalina cycle configuration, for any ammonia/ water concentration between 90.7-95.4%.

The full cycle performance, however, does not indicate the Kalina cycle configuration to be necessarily better than the ORC configuration. Based on the results found by Goudriaan [11] and Kuikhoven [25], the full cycle performance of the Kalina cycle configuration was highest using pure ammonia. Based on this finding, a comparison between the Kalina cycle configuration and ORC configuration using pure ammonia was executed.

For both the ORC configuration and Kalina cycle configuration, it was found that the full cycle performance was dependant on the orifice pressure drop since it plays a role in determining the evaporator operating pressure and the turbine power output.

When comparing the ORC configuration to the Kalina cycle configuration, as stated before, one can conclude that the ORC does not perform worse than the Kalina cycle configuration. The net work output of the current OTEC Demo shows that the ORC configuration slightly outperforms the Kalina cycle configuration, using pure ammonia. The main driver for this result is the fact that in the ORC configuration, the working fluid pump has to perform less work. This is a consequence of the fact that for the ORC configuration, the working fluid pump only has to pump the vapor fraction of the working fluid stream coming from the evaporator. The liquid fraction of this stream is re-circulated through natural re-circulation. In the Kalina cycle configuration, these streams are joined before entering the condenser, and as a result, the working fluid pump has to pump the total working fluid mass flow rate.
This result does come with two disclaimers.

- In the current OTEC Demo, the working fluid pump used is a very inefficient reciprocating working fluid pump, with an isentropic efficiency of 8-15% for pure ammonia, see Figure 5.1. The work done by the working fluid pump will be significantly lower if a more efficient pump would be used. Implementing a more efficient pump could cause the currently small difference in net power output between the ORC configuration and Kalina cycle configuration to shift the other way.
- In the full cycle performance analyses done on both the ORC configuration and Kalina cycle configuration, the isentropic efficiency of the turbine is assumed to be 90%. In reality, the turbine of a real OTEC system can be less efficient. Since the Kalina cycle configuration of the current OTEC Demo results in the highest turbine work, the net power output of the ORC configuration will be less influenced by a less efficient turbine. This will result in the net power output of the ORC configuration to be even higher compared to the Kalina cycle configuration.

The combination of these two factors leads to conclude that the full cycle performance difference between the ORC configuration and the Kalina cycle configuration for pure ammonia are very close to one another. The difference in the resulting net work is dependant on the efficiencies of both the turbine and the working fluid pump. When both the turbine and the working fluid pump are not very efficient, an ORC configuration might be more desirable. When both the turbine and the working fluid pump are very efficient, a Kalina cycle configuration might be more desirable.

The OTEC off-design model for the ORC configuration was validated against experimental results gathered on the OTEC Demo. The two phase heat transfer correlation that was used is the correlation proposed by Taboas [33]. The performance of this correlation was found to be not influenced by a changing mass flow rate, where most other correlations were. Unfortunately, the correlation proposed by Taboas still deviates from experimental data and does not predict the heat transfer rate in the evaporator very accurately. The consequence of this deviation is a conservative model, where the heat transfer rate calculated in the evaporator is most likely lower than the heat transfer rate for a real system.

When looking at the scaled off-design model for the 3 [MW] OTEC power plant, a quick conclusion would be to say that with the given plant dimensions, it would be possible to generate a net 3 [MW] power output. But since the turbine performance is based on an estimated isentropic efficiency and the work required by the water pumps is not considered in this analysis, a definitive claim on the performance of this design must be avoided. This result can be used by Bluerise B.V. to compare to other cycle analysis tools.

7.2. RECOMMENDATIONS

Based on the work done in this assignment, some recommendations are given on improvements and topics for further studies.

One recommendation would be towards an improvement of the OTEC Demo. The reciprocating working fluid pump currently used in the cycle is a very robust and reliable pump, which has been working for the past years. But the oscillating working fluid mass flow it generates is detrimental to any flow measurements made in the flow path that follows. Like stated in Section 5.2, the mass flow sensor FI-203 is now useless when it comes to determining the mass flow rate going through the vapor side of the cycle. A recommendation would be to implement a more stable gear pump, but caution has to be taken, since the used gear pumps have shown to be unresistant to ammonia. However, if a solution could be found that creates a (more) stable working fluid flow between the buffer tank and the recuperator/ evaporator, that would greatly enhance the OTEC Demo functionality.

Some more recommendations are directed towards the OTEC off-design model:

- The piping infrastructure of the OTEC system is not taken into account when modeling the OTEC cycles. Pressure drops in the system are primarily caused by the piping infrastructure and are only partially influenced by component pressure drops. The difficulty with modeling the piping infrastructure is the fact that this is most likely never identical between different OTEC installations. Implementing this into the OTEC off-design model in a way that allows for the model to maintain its applicability to many different configurations is a huge challenge, but one worth looking at nonetheless.
- The water side of the OTEC cycle is not considered in the off-design model either. Since recent studies have shown that the water pumps require a much larger power input than the working fluid pump, this is crucial when assessing the performance of a specific cycle design. Adding the water side power requirement would be a great addition to the OTEC off-design model.
- The two phase pressure drop correlation proposed by Yan and Lin [27] does predict the evaporator pressure drop quite accurately for the OTEC Demo, but considering the pressure drop is very low, additional research might be useful. When the OTEC off-design model is scaled to the geometries of a 3 [MW] plant, the calculated pressure drop in the evaporator does not match the manufacturer pressure drop value. Whether this is a consequence of the pressure drop correlation not being accurate or if the manufacturer pressure drop value is very conservative will need to be investigated.
- Finally, the two phase heat transfer correlation used in the final validation of the model and scaling analysis towards a 3 [MW] system is the correlation proposed by Taboas [33]. This correlation underpredicts the heat transfer rate in the evaporator, but was still the correlation with the best fit to the acquired experimental data. Creating a two phase evaporative heat transfer correlation that is based on experimental data using similar mass fluxes would be a great addition to the OTEC off-design model. This two phase heat transfer correlation could be based on pool boiling heat transfer phenomena more than flow boiling heat transfer phenomena, since these are probably more dominant in the measured mass flow rates. Creating a two phase heat transfer correlation for this flow domain requires more experimental data to be gathered.

When the decision is made to implement the ORC configuration using natural re-circulation of the working fluid, a follow-up study on the potential of an ejector used as a mixing point could be interesting. Appendix I shows the basic working principle of an ejector. In short, an ejector uses a certain geometry to reduce the required pressure of one out of two input streams, to create an intermediate pressure level output stream. This component does not have moving parts so is very robust. When natural re-circulation is implemented on a full scale (3 [MW] for example) OTEC system, the required working fluid liquid column height in the separator could be very large. To create this large liquid column height, the separator will either need to be very tall or placed at an elevated level, causing the capital investment costs of the plant to increase. Implementing an ejector could reduce the need for a very large liquid column height, and thus reduce the cost of an OTEC plant. Ejectors do however impose an energy loss on the system, so a performance analysis will have to be executed.

A

PLATE HEAT EXCHANGER DIMENSIONS

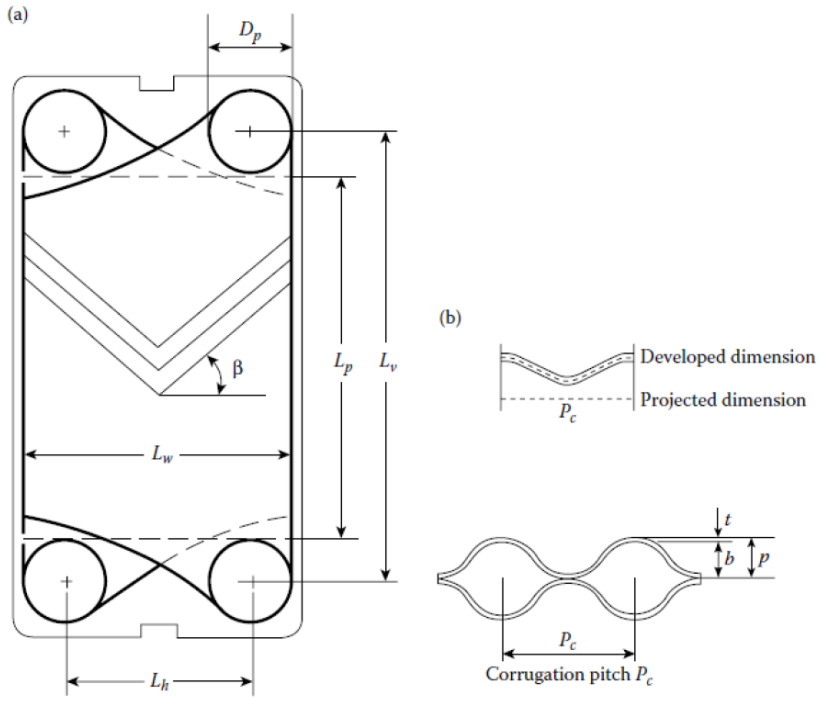

Figure A.1: Relevant plate heat exchanger dimensions.(a) Main dimensions of chevron plate. (b) developed and projected dimensions of a chevron plate cross-section normal to the direction of troughs. Source [11]

The dimensions seen in Figure A.1 are used to calculate the heat transfer area accordingly:

$$A_e = \Phi(L_v - D_p)L_w N_e \tag{A.1}$$

In equation A.1, A_e is the effective area of the heat exchanger in [m^2]. Φ is the surface enhancement factor. L_v is the vertical port to port length , D_p is the port diameter and L_w is the effective width of the plate, all three in [m]. N_e is the effective number of channels [11].
The surface enhancement factor Φ can be calculated as follows:

$$\Phi = \frac{\text{developed area}}{\text{projected area}} = \frac{A_1}{A_{1p}} \tag{A.2}$$

Where A_1 is the single plate heat transfer area and A_{1p} is the projected single plate heat transfer area, both in [m^2].

Two other dimensions that are often used in heat transfer calculations for plate heat exchangers are the equivalent diameter and hydraulic diameter.

$$d_{eq} = 2b \tag{A.3a}$$

$$d_h = \frac{d_{eq}}{\Phi} = \frac{2b}{\Phi} \tag{A.3b}$$

Where b is the plate pitch in [m]. The hydraulic diameter is an expression of the equivalent diameter in which the surface enhancement factor is included.

PLATE HEAT EXCHANGER DIMENSIONS IN THE OTEC DEMO

Some relevant dimensions for the plate heat exchangers used in the OTEC Demo can be seen in Table A.1 Because of proprietary concerns, some dimensions are not allowed to be mentioned in reports, so these have not been mentioned.

Table A.1: Heat exchanger dimensions for the OTEC Demo

Dimension	**Condenser**	**Recuperator**	**Evaporator**
number of passes	1	1	1
total number of channels	17	17	23
number of channels warm	9	9	12
number of channels cold	8	8	11
L_h [m]	0.05	0.05	0.05
L_v [m]	0.25	0.25	0.25
t [mm]	0.4	0.4	0.4
b [mm]	2.02	2.02	2.02
D_p [m]	0.030	0.030	0.030
L_w [m]	0.08	0.08	0.08
total number of plates	18	18	24
A_e [m^2]	0.34	0.34	0.47

B

Evaporation Flow Regimes

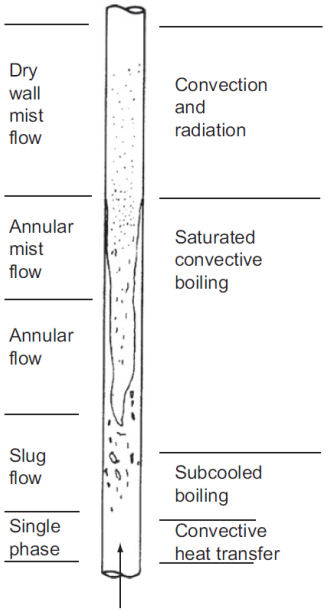

Figure B.1: Flow regimes during evaporation from (subcooled) liquid to (super heated) vapor. Source [36]

According to Sinnott & Towler [36], the following conditions occur as the fluid flows up the tube:

- Single-phase flow region: at the inlet the liquid is below its boiling point and heat is transferred by forced convection.
- Subcooled boiling: in this region the liquid next to the wall has reached the boiling point, but not the bulk of the liquid. Local boiling takes place at the wall, which increases the rate of heat transfer over that given by forced convection alone.
- Saturated boiling region: in this region bulk boiling of the liquid is occurring in a manner similar to nucleate pool boiling. The volume of vapor is increasing and various flow patterns can form.
- Dry wall region: ultimately, if a large fraction of the feed is vaporized, the wall dries out and any remaining liquid is present as a mist. Heat transfer in this region is by convection and radiation to the vapor. This condition occurs when the working fluid is super heated, but doesn't occur in overfed evaporators.

C

DIMENSIONLESS NUMBERS

C.0.1. SINGLE PHASE

The Reynolds number (Re_{eq}) is the non-dimensional ratio of the inertial forces compared to the viscous forces and is typically used to assess the flow regime [11].

$$Re_i = \frac{Gd_{eq}}{\mu_i} \tag{C.1}$$

G is the mass flow rate per cross-sectional area in [kg/m^{2}s]. d_{eq} is the equivalent diameter in [m] and μ_i is the dynamic viscosity of the fluid in [Pa s].

The Prandtl number is the ratio of the momentum diffusivity to the thermal diffusivity [11].

$$Pr_i = \frac{c_{p,i}\mu_i}{k_i} \tag{C.2}$$

$c_{p,i}$ is the specific heat capacity of the fluid in [J/kgK]. k_i is the thermal conductivity of the fluid in [W/mK].

C.0.2. (ADDITIONAL) TWO PHASE

The Boiling number (Bo) is the non-dimensional ratio of the mass of vapor created per surface area of the heat exchanger compared to the mass flow rate per cross-sectional area of the working fluid.

$$Bo = \frac{q"}{G\delta h_{fg}} \tag{C.3}$$

In this equation q" is the heat flux per unit area in [W/m^2]. G is the mass flux per cross sectional area in [kg/m^{2}s]. δh_{fg} is the latent heat of vaporization in [J/kg].

The Bond number (Bd) is the non-dimensional ratio of the gravitational forces compared to the surface tension forces.

$$Bd = \frac{g(\rho_l - \rho_v)d_h^2}{\sigma} \tag{C.4}$$

In this equation σ is the surface tension of the working fluid in [N/m].

The Weber number is the non-dimensional ratio of a fluid's inertia compared to its surface tension.

$$We = \frac{G^2 d_h}{\rho_l \sigma} \tag{C.5}$$

The equivalent Reynolds number is also used in some two phase heat transfer correlations.

$$Re_{eq} = \frac{G_{eq} d_{eq}}{\mu_{liq}} \tag{C.6}$$

In this equation G_{eq} is the equivalent mass flux in [kg/m^{2}s]:

$$G_{eq} = G\left[(1-q) + q\frac{\rho_{liq}}{\rho_{vap}}^2\right] \tag{C.7}$$

In this equation q is the vapor quality and the subscripts indicate liquid or vapor.

D

Single Phase Heat Transfer Correlations

Table D.1: Overview of the selected single phase heat transfer correlations for the plate heat exchanger evaporator

Author	Single phase heat transfer correlation	Validation range
VDI Heat Atlas [54]	$\alpha_{sp} = \frac{\lambda_i}{d_e} 1.615 (\frac{\xi \cdot Re_{VDI,i}}{64} Re_{VDI,i} \frac{Pr_i \cdot d_e}{l_p})^{1/3}$	$60 < Re < 30,000$
Yan et al. [50]	$\alpha_{sp} = \frac{\lambda_i}{d_e} 0.2121 Re_i^{0.78} Pr_i^{1/3}$	$Re > 200$
Sinnott & Towler [36]	$\alpha_{sp} = \frac{\lambda_i}{d_e} 0.26 Re_i^{0.65} Pr_i^{0.4}$	turbulent flow in a typical plate
Donowski & Kandlikar [24]	$\alpha_{sp} = \frac{\lambda_i}{d_e} 0.2875 Re_i^{0.78} Pr_i^{1/3}$	$Re > 200$
Winkelmann [41]	$\alpha_{sp} = \frac{\lambda_i}{d_e} 0.60 Re_i^{0.51} Pr_i^{C}$ $\alpha_{sp} = \frac{\lambda_i}{d_e} 0.22 Re_i^{0.68} Pr_i^{C}$ $C = 0.4$ if fluid is heated $C = 1/3$ if fluid is cooled	$10 < Re < 450$ $450 < Re < 13,000$
Manglik [71]	$\alpha_{sp} = \frac{\lambda_i}{d_e} 0.44 (\frac{100-\beta}{30})^{0.38} Re_i^{0.5} Pr_i^{1/3}$	NOG UITZOEKEN!!!!!
GoudKuik [11]	$\alpha_{sp} = \frac{\lambda_i}{d_e} 0.291 Re_i^{0.72} Pr_i^{0.33}$	$400 < Re < 1800$

E

OTEC Demo

The numbered red boxes in Figure E.1 correspond to the following components [25]:

1. Evaporator - stainless steel plate heat exchanger, type AlfaNova 27-24H.
2. Separator - gravity controlled with a fine mesh for improved separation
3. Valve + orifice - a sharp edged thin plate orifice and a valve represent the turbine
4. Recuperator - stainless steel plate heat exchanger, type AlfaNova 27-18H.
5. Condenser - stainless steel plate heat exchanger, type AlfaNova 27-18H.
6. Warm water pump - centrifugal water pump, type Ebara CDXM 70/07.
7. Buffer tank
8. Working fluid pump - reciprocating ammonia pump, type Bran+Luebbe - ProCam Ds200.
9. Cold water pump - centrifugal water pump, type Ebara CDXM 70/07.

Figure E.1: The initial OTEC DEMO located in the Process & Energy laboratory at Delft University of Technology. Source [25]

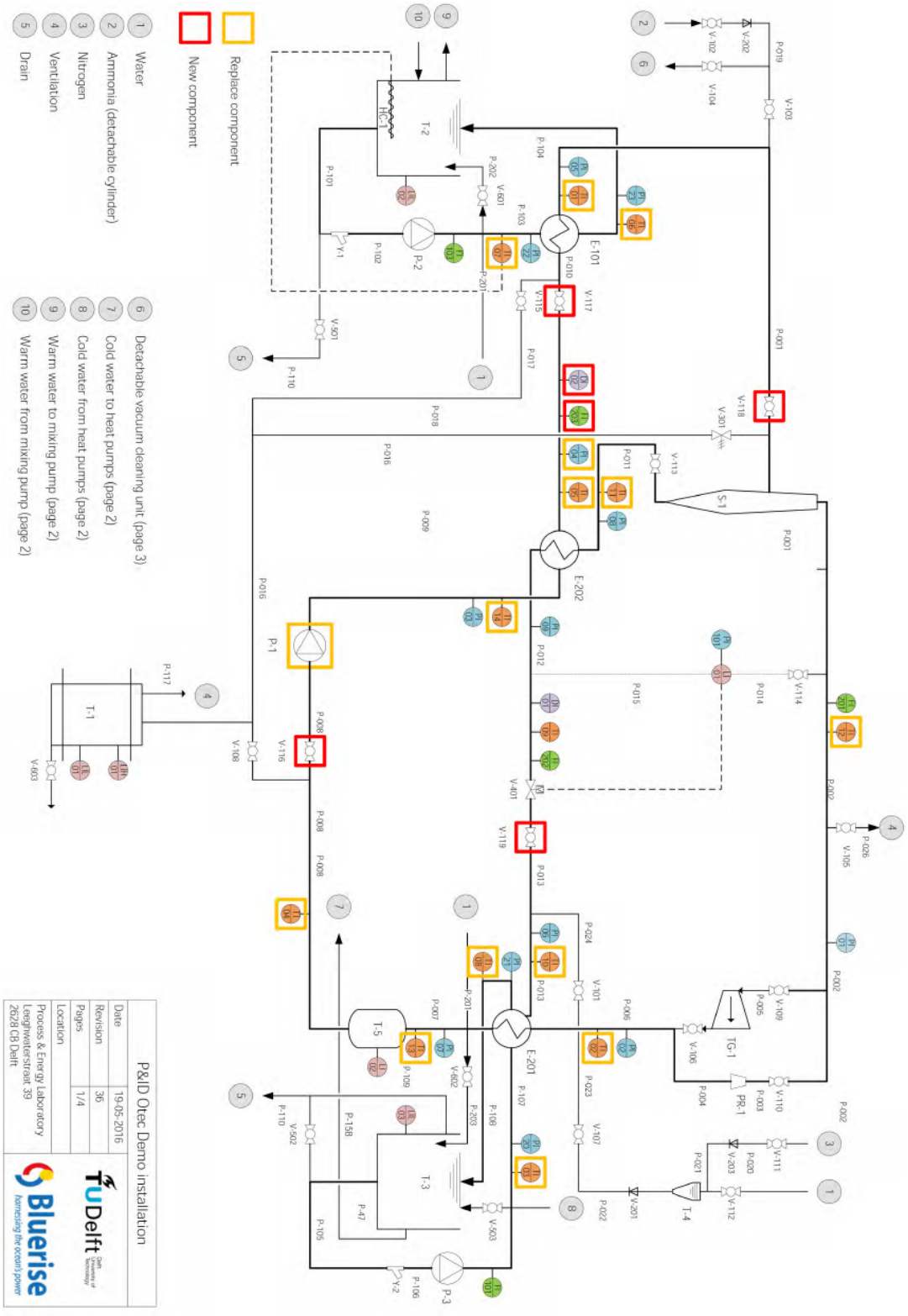

Figure E.2: Piping & Instrumentation Diagram (P&ID) of the initial OTEC DEMO Kalina cycle. Copyright 2017 by Bluerise B.V.

F

P&ID

The components in Figure 3.4, Figure F.1 and Figure F.2 are labelled as:

1. The evaporator is labelled as: E-101
2. The separator is labelled as: S-1
3. The recuperator is labelled as: E-202
4. The brazed plate condenser is labelled as: E-201
5. The gasketed plate condenser is labelled as: E-203
6. The working fluid buffer tank is labelled as: T-5
7. The working fluid pump is labelled as: P-1
8. The warm water pump is labelled as: P-2
9. The cold water pump is labelled as: P-3
10. The gear pump is labelled as: P-6

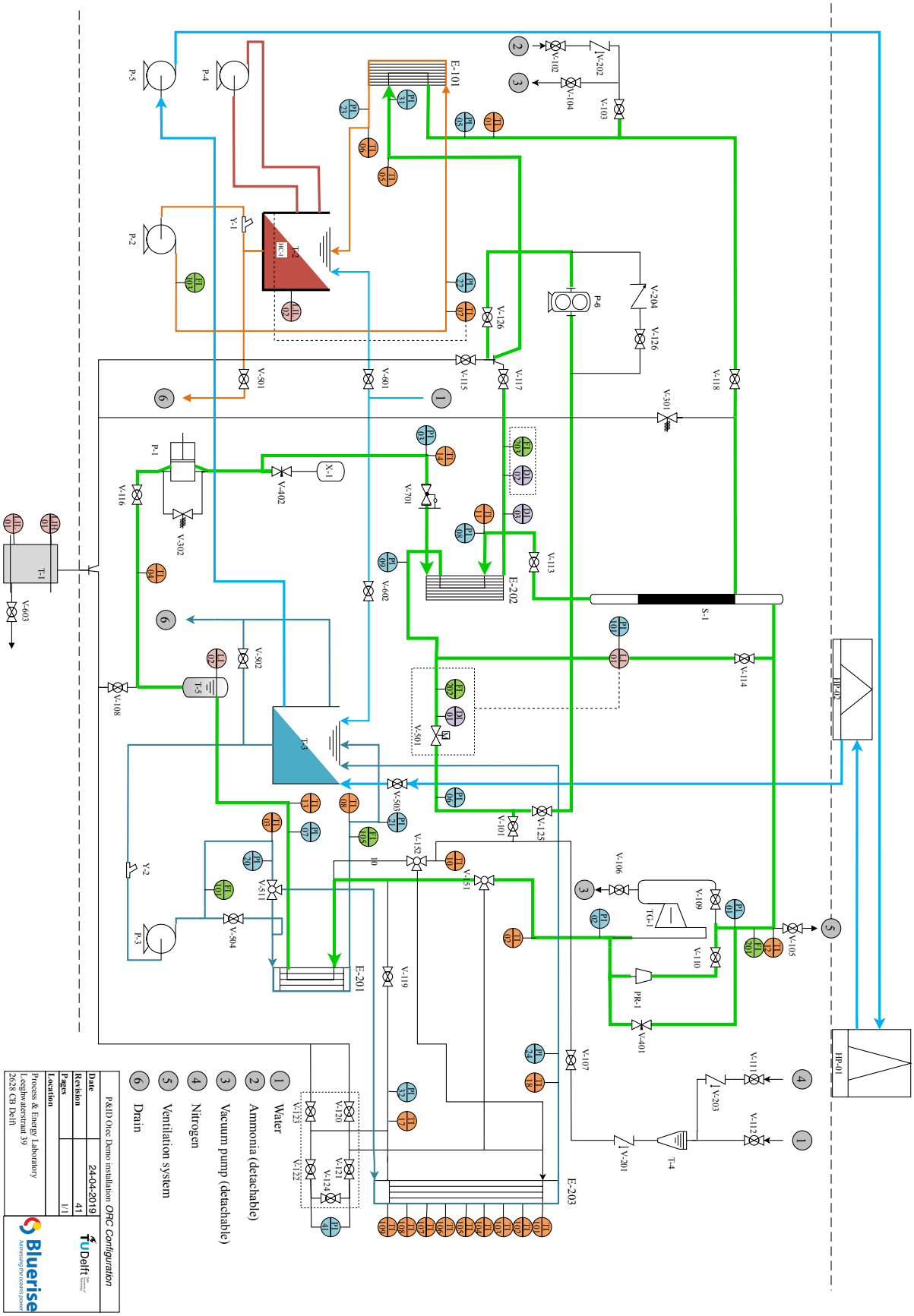

Figure F.1: Piping & Instrumentation Diagram (P&ID) of the OTEC experimental setup where the ORC working fluid path is highlighted in green.

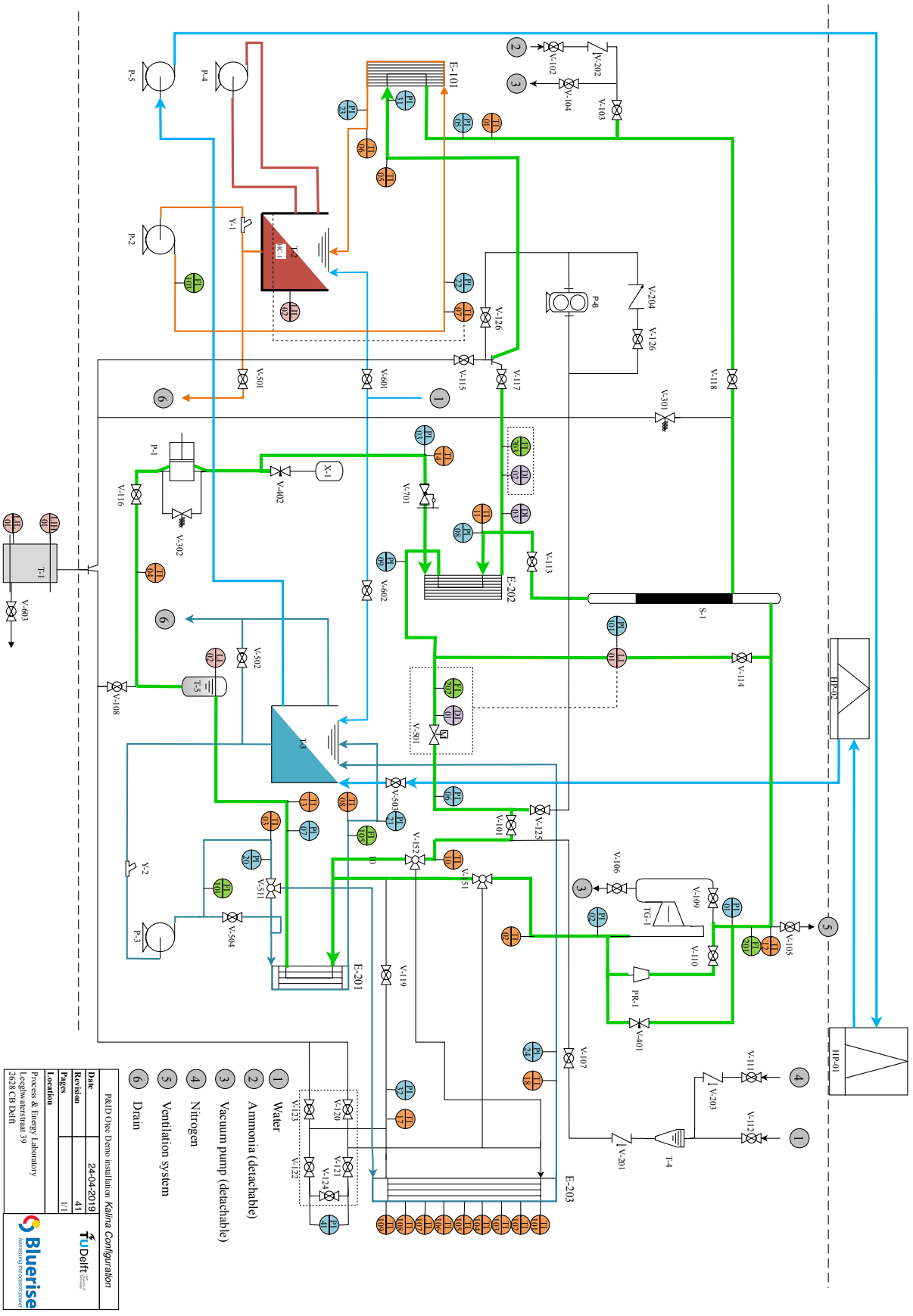

Figure F.2: Piping & Instrumentation Diagram (P&ID) of the OTEC experimental setup where the Kalina cycle working fluid path is highlighted in green.

G

REBOILER GRADING

In this section a selection procedure to choose an evaporator re-circulation method is made. The possible options for the evaporator reboiler method are forced circulation, a thermosiphon or a kettle type reboiler.

Table G.1: Rating several design options for evaporator recirculation

	Importance factor	Forced Circulation	Thermosiphon	Kettle type
Viscous Handling	*1*	9	3	3
Fouling	*1*	9	3	3
Pressure Handling	*3*	8	8	8
C.I.C.	*5*	5	8	3
H.T.C.	*5*	8	8	5
Final Score		**107**	**110**	**70**

All design options have been rated on five criteria, namely: viscous handling, fouling, pressure handling, costs and heat transfer coefficient. All three evaporator re-circulation methods have different advantages and disadvantages which relate to the nature of the process fluid, the operating pressure and the equipment layout.

Forced circulation reboilers are suitable for handling viscous and heavily fouling process fluids. They're suitable for low vacuum operations and for low rates of vaporization. The disadvantage of forced circulation reboilers is the requirement of a pump, which brings in extra costs [36].

Thermosiphon reboilers are the most economical type for most applications, but are not suitable for high viscosity or high vacuum operation. A disadvantage of this type is that the column base must be elevated to provide the hydrostatic head required for the thermosiphon effect. This increases the cost of the column supporting structure [36].

Kettle reboilers have lower heat-transfer coefficients than the other types as there is no liquid circulation. They are not suitable for fouling materials and have a high residence time. In general, these type of reboilers will be most expensive. They are suitable for vacuum operation and for high rates of vaporization [36].

Since ammonia is neither that viscous nor heavily fouling, the importance factor given to these two criteria is 1. The forced circulation method is significantly better considering these two criteria so scores higher than the thermosiphon and kettle type method, which are rated equal on these two criteria.

According to previous work by Goudriaan [11] and Kuikhoven [25], low or extremely high pressures do not occur inside the evaporator. The pressure in the evaporator is at around 8 bar. With this intermediate pressure level, all three systems score the same rating.

The total capital investment costs (C.I.C.) of the system are very important for Bluerise B.V. If these can be kept as low as possible, the cost per unit of energy produced can be kept at a low value, able to compete

with alternative energy sources. This is why the C.I.C have been given an importance factor of 5. The heat exchangers themselves are by far the largest components in the cycle, so the additional elevation costs of the column base for the thermosiphon is considered to have a smaller impact than other cost factors. The additional pump required for the forced circulation technique is considered to have a larger impact, that's why the thermosiphon scores highest on this criteria, followed by the forced circulation. The kettle type reboiler is mentioned to be (in general) the most expensive one of the three [36], so is awarded the lowest rating.

The heat transfer coefficient (H.T.C.) is a very important criteria in the OTEC design. Since higher heat transfer coefficients cause a lower required heat transfer surface area, the costs of the evaporator heat exchanger will also drop. Following up on the information found in Sinott & Towler [36], the Kettle type is given the lowest rating for this criteria. The heat transfer coefficient for forced circulation reboilers and thermosiphon reboilers is assumed to be of similar proportions.

Multiplying the individual scores by the importance factor and adding these together for each reboiler technique gives the final score. The thermosiphon and forced circulation techniques both score very high marks of 110 and 107 respectively. The thermosiphon would be the preferred technique in designing an ORC configuration.

H

Additional Pressure Drop Calculations

The acceleration and gravity contributions may be evaluated as proposed by Vakili-Farahani et al. [39] assuming homogeneous flow:

$$\Delta p_a = G^2 \Delta q \left(\frac{1}{\rho_v} - \frac{1}{\rho_l} \right) \tag{H.1a}$$

$$\Delta p_g = \rho_m g L \tag{H.1b}$$

Where G is the mass flux in [kg/m^{2}s]. Δq is the difference in working fluid quality over the evaporator. L is the height difference between the feed and return lines, which for a plate heat exchanger is the plate length. ρ_m is the two phase mean density in [kg/m^3], determined by:

$$\rho_m = \left(\frac{q}{\rho_v} + \frac{1-q}{\rho_l} \right)^{-1} \tag{H.2}$$

The manifold pressure drop can be evaluated using the correlation by Shah and Focke [72] assuming homogeneous flow:

$$\Delta p_{man} = 0.75 \left[\left(\frac{G^2_{port}}{2\rho} \right)_{in} + \left(\frac{G^2_{port}}{2\rho} \right)_{out} \right] N_{pass} \tag{H.3}$$

I

EJECTOR

A cross-section of an ejector used in an ammonia cycle can be seen in Figure I.1.

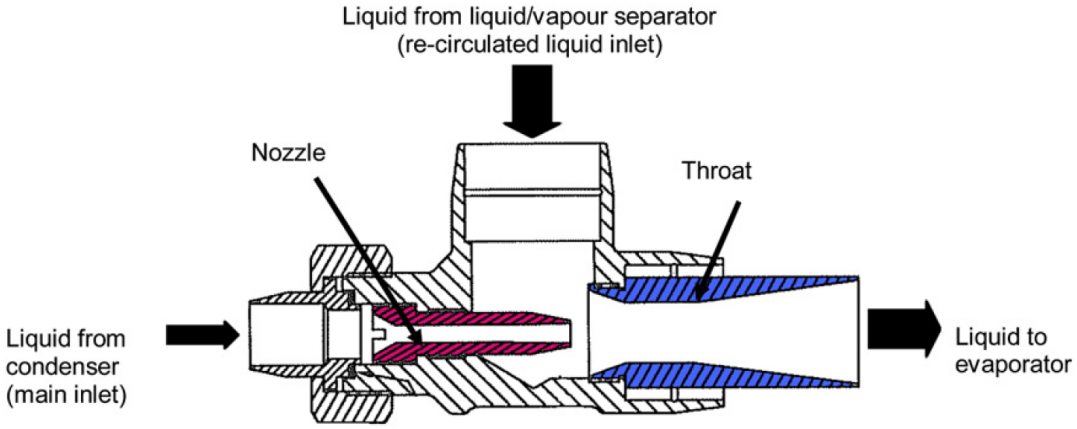

Figure I.1: Cross-section of an ejector used to re-circulate ammonia through a plate heat exchanger evaporator. Source [73]

Gac [74] discussed that the use of an ejector will make the necessity of a gear pump or control valve obsolete. The principal advantage of using an ejector is its simplicity, without moving parts, and strong construction. In addition, ejectors are more economical compared to pumps. Nevertheless, Gac stated that the effectiveness of ejector performance is strongly linked to the quality of its construction, pointing out that in practice the use of ejectors is best applied in systems with relatively constant operating conditions.

Ejectors in general are used to compress a low pressure suction to discharge at an intermediate pressure by utilizing a high pressure motive. Typical pressure and velocity levels throughout an ejector can be seen in Figure I.2. The primary motive stream's high pressure is used to accelerate this stream. This causes a significant pressure drop in the suction chamber, enough to suck in the secondary motive stream. A shock wave can occur in the throat section, causing a stepped increase in pressure. In the diffuser section of the ejector, the mixed working fluid stream is slowed down and thus increases in pressure until the outlet pressure is reached.

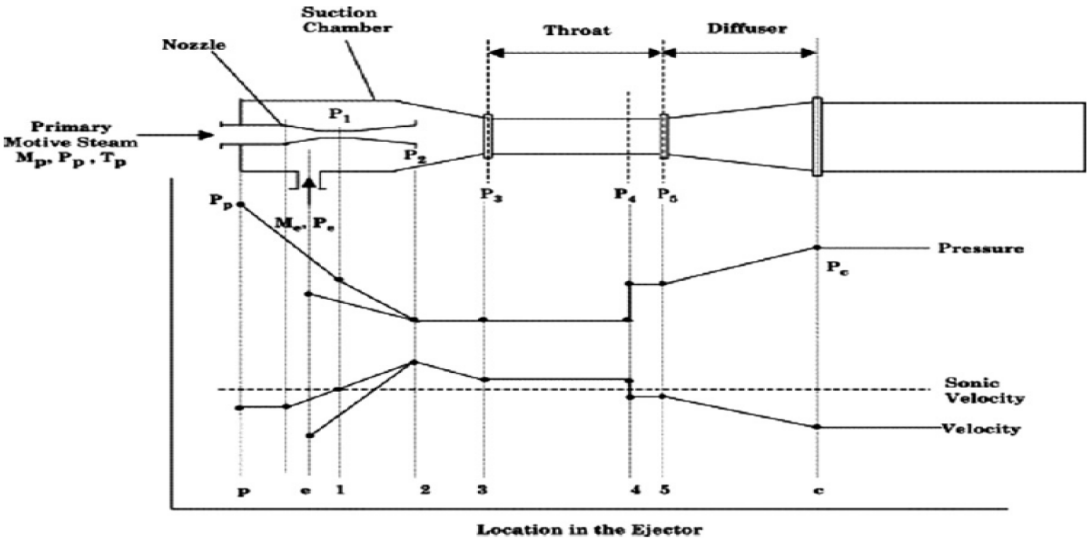

Figure I.2: Typical pressure and velocity levels throughout an ejector. Source [75]

In the ORC an ejector could be used between the pump, column and evaporator to act as a mixing point. A high pressure working fluid coming from the working fluid pump could be used to suck in a low pressure working fluid coming from the column. These streams will mix in the ejector and leave at an intermediate pressure level. Using this method will cause a decreased working fluid column height in the separator column to overcome the evaporator pressure drop. This could be an interesting technique for a large scale ORC OTEC plant, reducing the need for separator column elevation and thus potentially reducing investment costs for the plant.

J

HE Algorithm Old

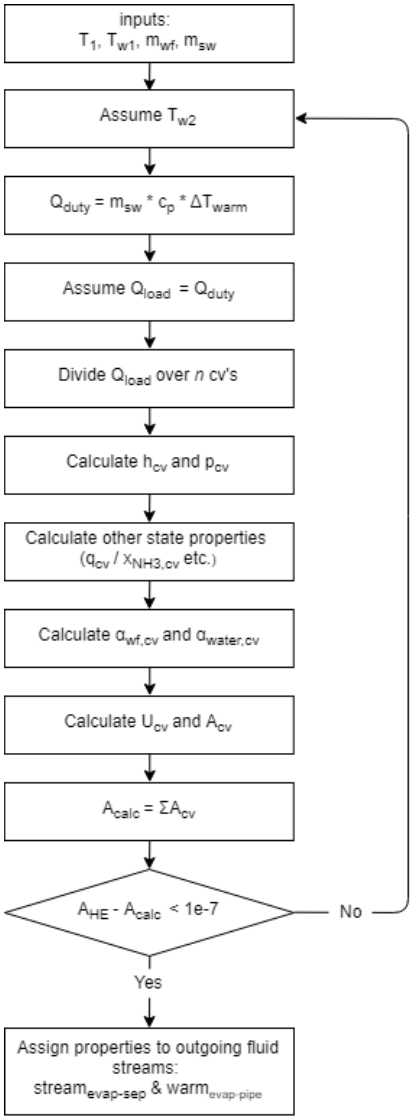

Figure J.1: Heat exchanger algorithm proposed by Kuikhoven [25] and Goudriaan [11]

K

HEAT TRANSFER RATE DEVIATION

Table K.1: Measured evaporator water side heat transfer rate, the calculated working fluid heat transfer rate and the deviation between them, part 1.

$\dot{Q}_{evap,water}$ [W]	$\dot{Q}_{evap,wf}$ [W]	Deviation (%)
1818.31	1816.011	-0.13
2032.616	2030.447	-0.11
2346.287	2343.924	-0.10
2805.76	2803.388	-0.08
3418.162	3416.098	-0.06
4143.526	4141.584	-0.05
4585.555	4583.595	-0.04
5010.889	5009.075	-0.04
5532.517	5530.909	-0.03
5983.751	5982.363	-0.02
4222.405	4220.837	-0.04
4656.452	4655.034	-0.03
5098.119	5096.765	-0.03
5592.316	5591.102	-0.02
5972.23	5971.146	-0.02
3405.735	3404.45	-0.04
2618.567	2614.58	-0.15
2953.619	2949.748	-0.13
3171.323	3167.767	-0.11
3712.102	3708.414	-0.10

Table K.2: Measured evaporator water side heat transfer rate, the calculated working fluid heat transfer rate and the deviation between them, part 2.

$\dot{Q}_{evap,water}$ [W]	$\dot{Q}_{evap,wf}$ [W]	Deviation (%)
4238.843	4235.251	-0.08
4764.11	4760.604	-0.07
5272.337	5268.691	-0.07
5607.969	5604.192	-0.07
5777.217	5773.523	-0.06
5658.617	5654.949	-0.06
5888.134	5884.6	-0.06
3562.562	3556.69	-0.16
4096.806	4091.025	-0.14
4536.581	4531.654	-0.11
5143.236	5138.223	-0.10
5477.065	5471.252	-0.11
2076.594	2075.614	-0.05
2141.001	2139.947	-0.05
2458.365	2457.212	-0.05
2938.688	2937.078	-0.05
3267.828	3266.345	-0.05
3505.075	3503.42	-0.05
4031.249	4029.39	-0.05
4434.246	4432.286	-0.04
4935.845	4933.636	-0.04
5412.787	5410.462	-0.04
5675.856	5673.28	-0.05
5889.083	5886.496	-0.04
2363.979	2363.655	-0.01
2775.108	2774.721	-0.01
3414.252	3413.232	-0.03
3995.921	3994.558	-0.03
4041.696	4040.216	-0.04
4622.879	4618.14	-0.10
4891.302	4886.347	-0.10
5159.381	5154.758	-0.09
5421.551	5417.123	-0.08

L

Evaporator Heat Transfer Validation

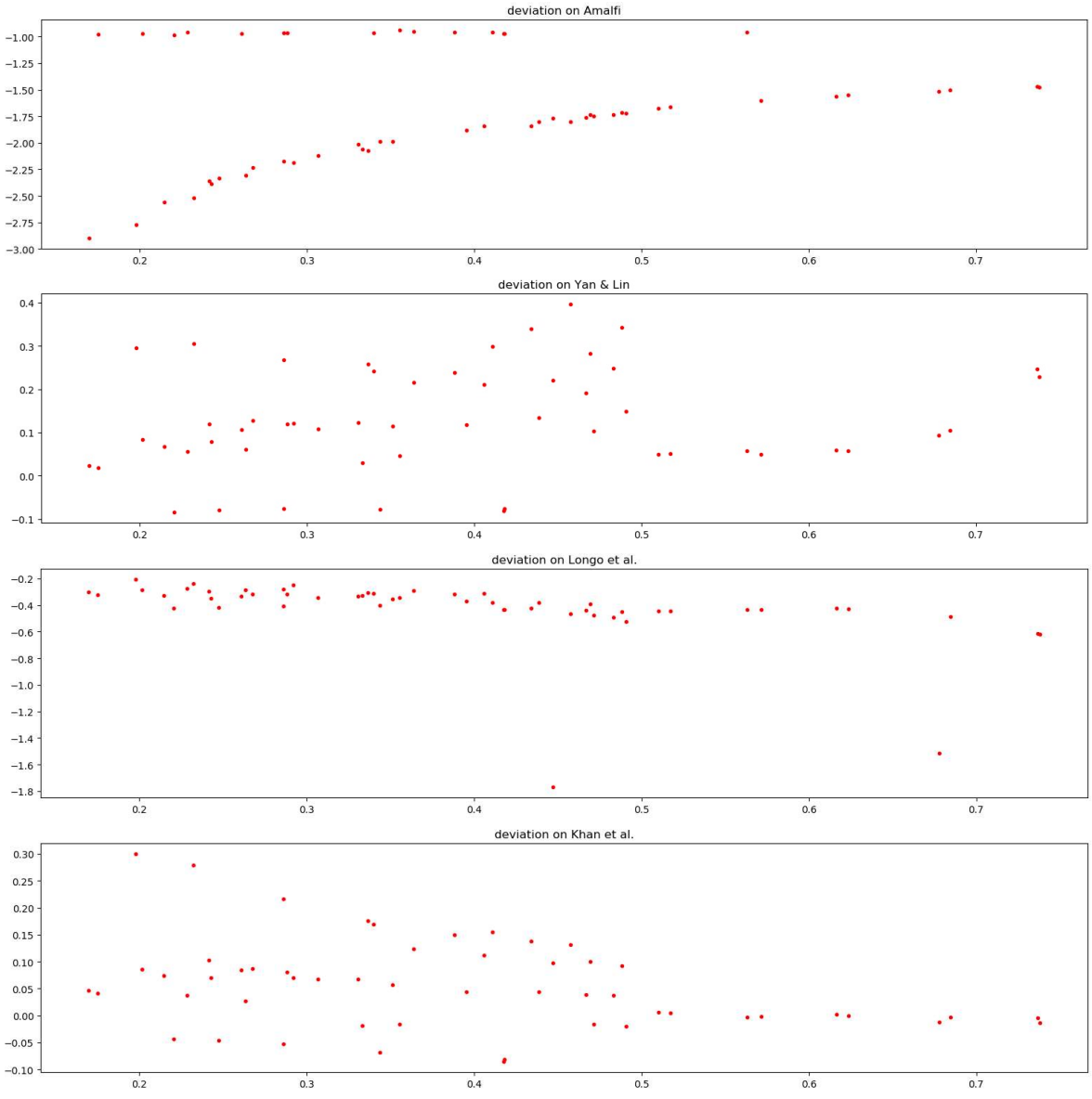

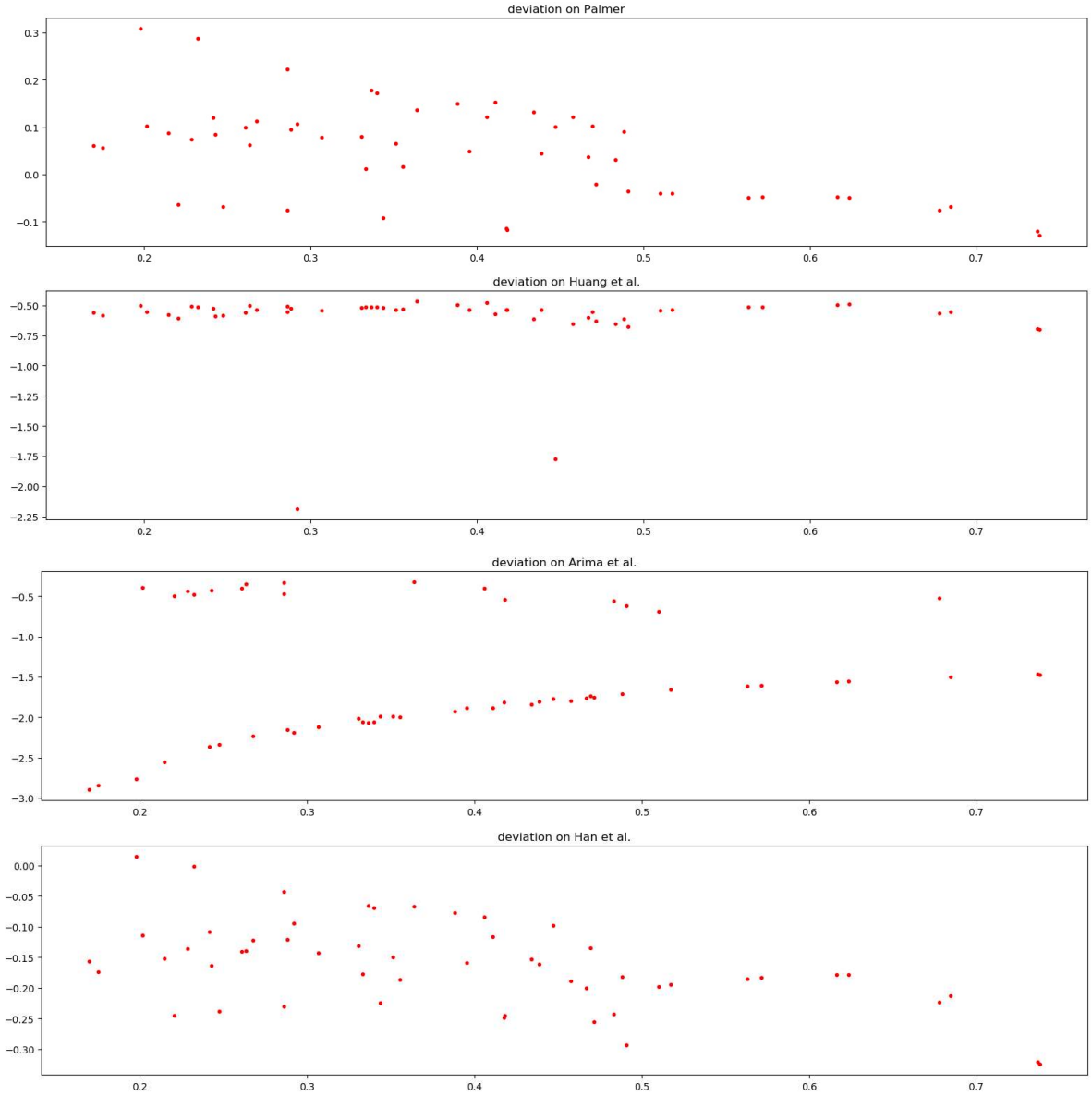
deviation on Palmer
deviation on Huang et al.
deviation on Arima et al.
deviation on Han et al.

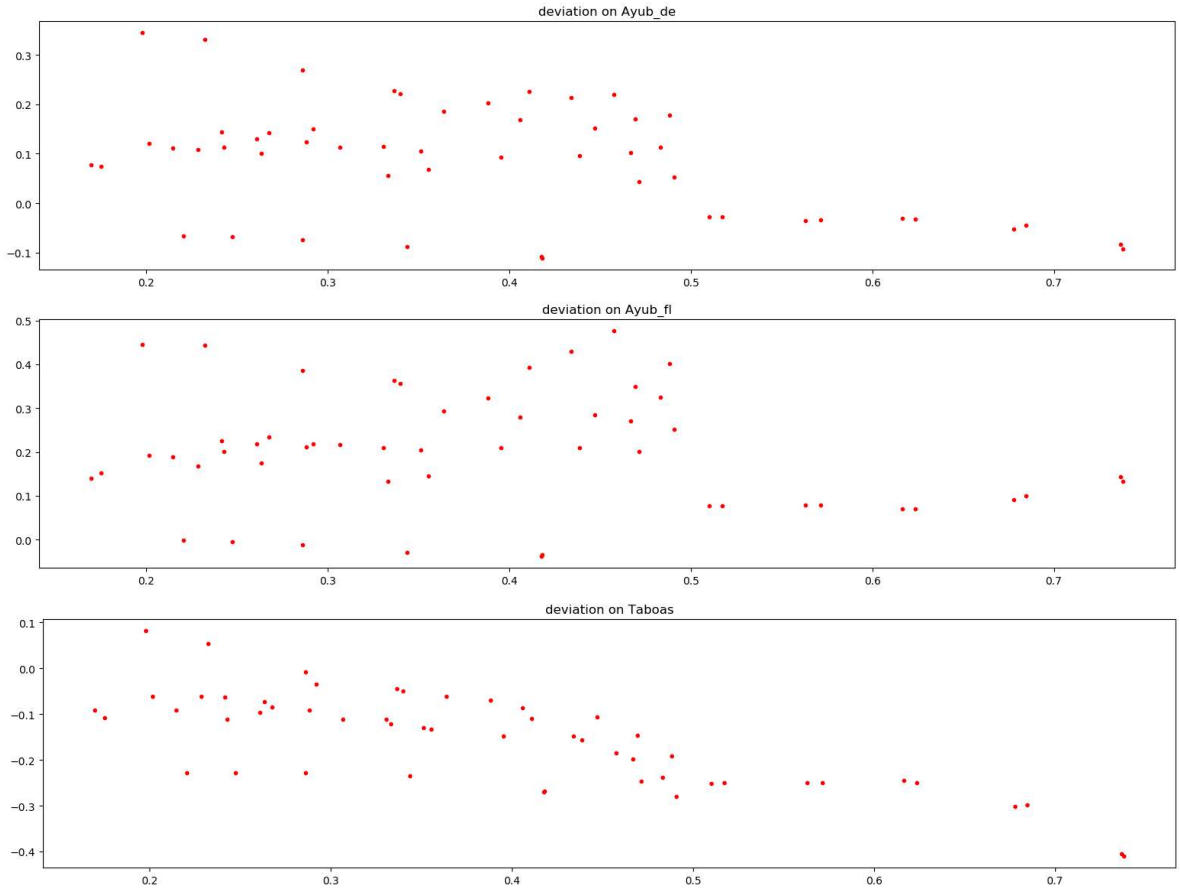
deviation on Ayub_de
0.3
0.2
0.1
0.0
−0.1
0.2
0.3
0.4
0.5
0.6
0.7

deviation on Ayub_fl
0.5
0.4
0.3
0.2
0.1
0.0
0.2
0.3
0.4
0.5
0.6
0.7

deviation on Taboas
0.1
0.0
−0.1
−0.2
−0.3
−0.4
0.2
0.3
0.4
0.5
0.6
0.7

M

Evaporator Pressure Drop Validation

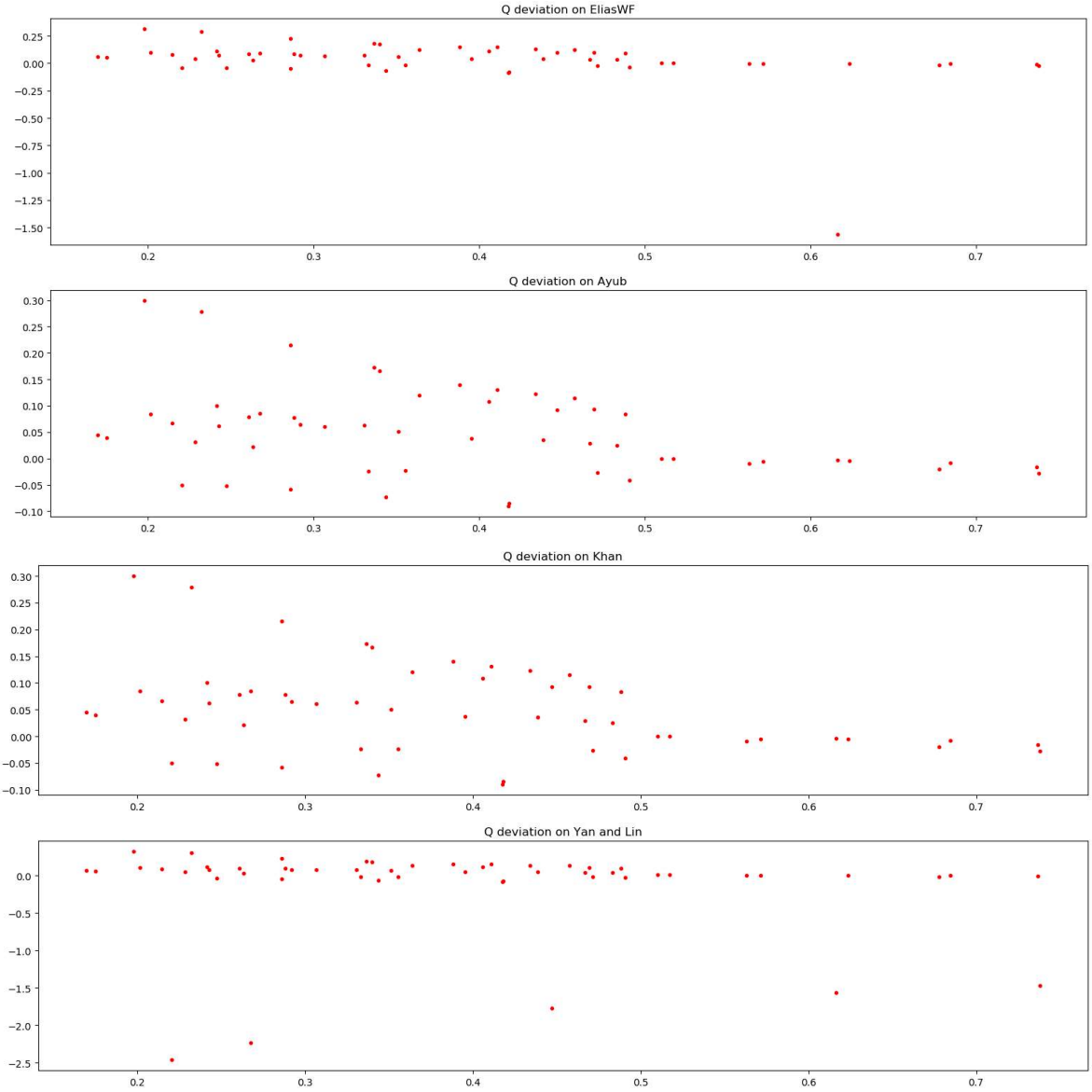

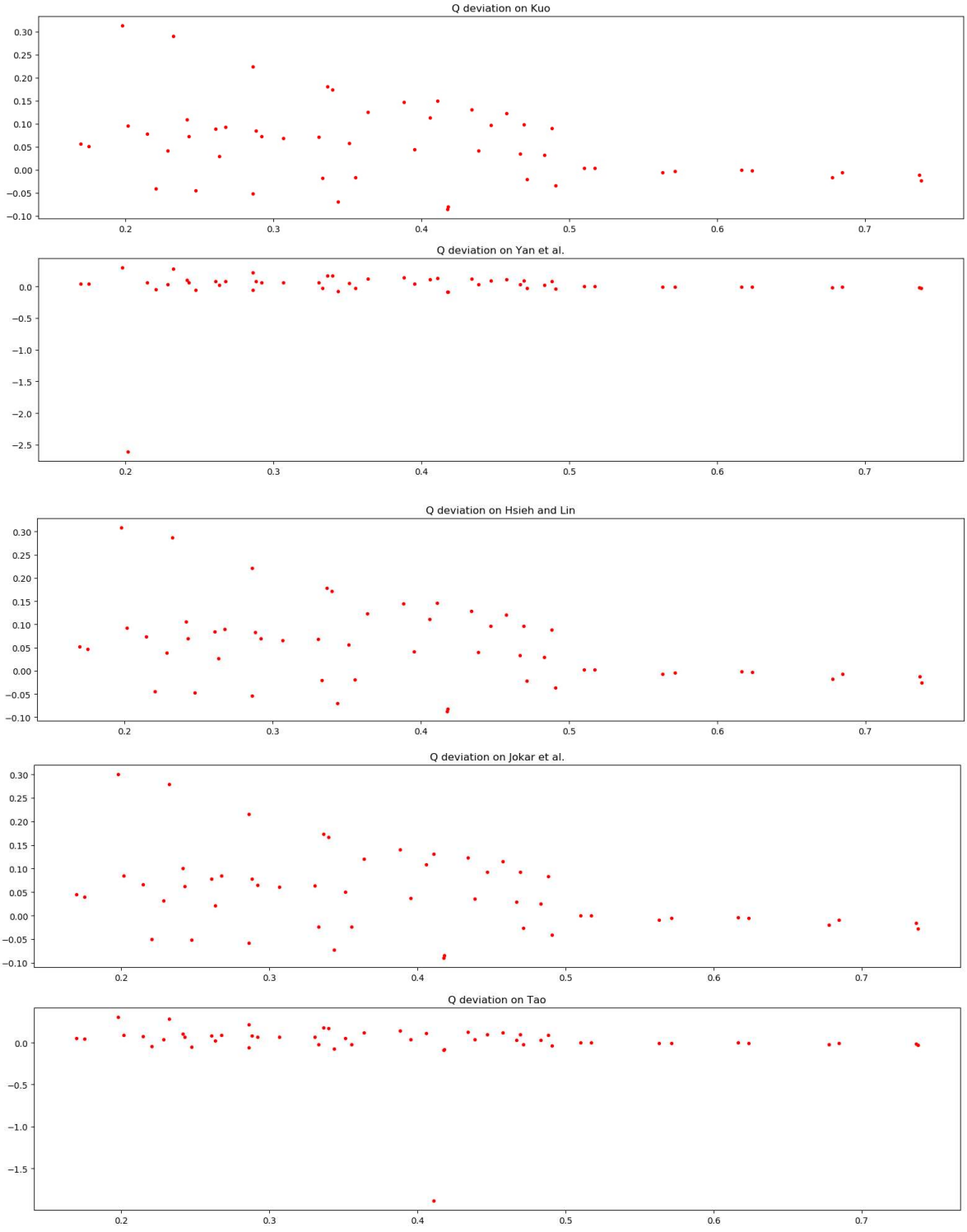
Q deviation on Kuo
Q deviation on Yan et al.
Q deviation on Hsieh and Lin
Q deviation on Jokar et al.
Q deviation on Tao

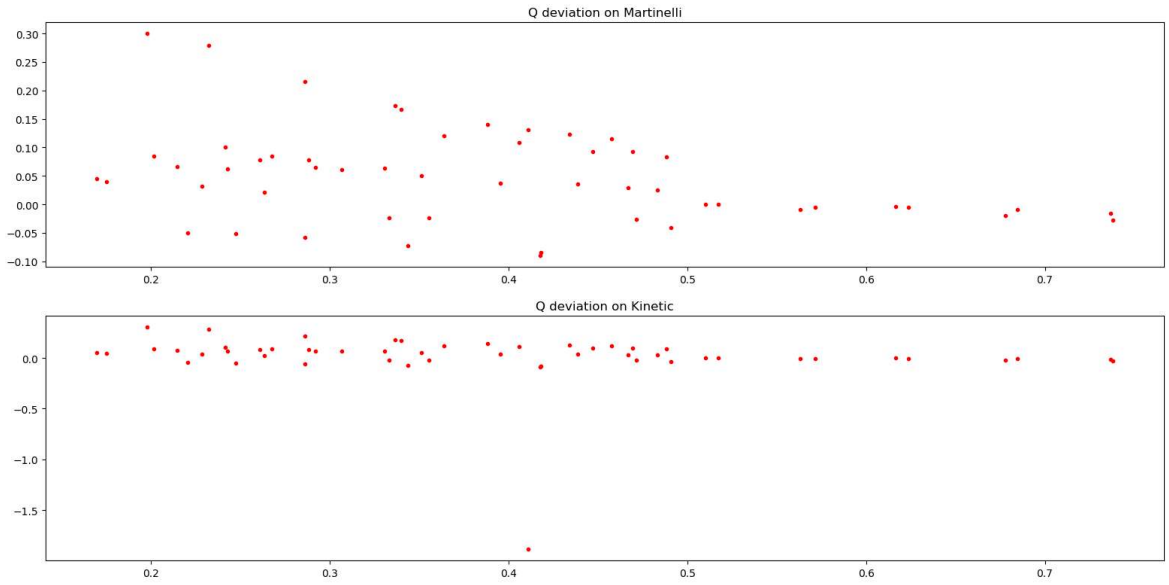
Q deviation on Martinelli
0.30
0.25
0.20
0.15
0.10
0.05
0.00
−0.05
−0.10
0.2
0.3
0.4
0.5
0.6
0.7

Q deviation on Kinetic
0.0
−0.5
−1.0
−1.5
0.2
0.3
0.4
0.5
0.6
0.7

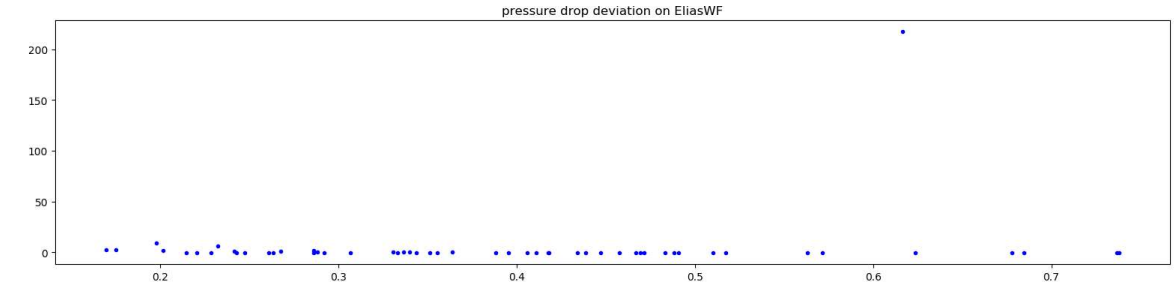
pressure drop deviation on EliasWF
200
150
100
50
0
0.2
0.3
0.4
0.5
0.6
0.7

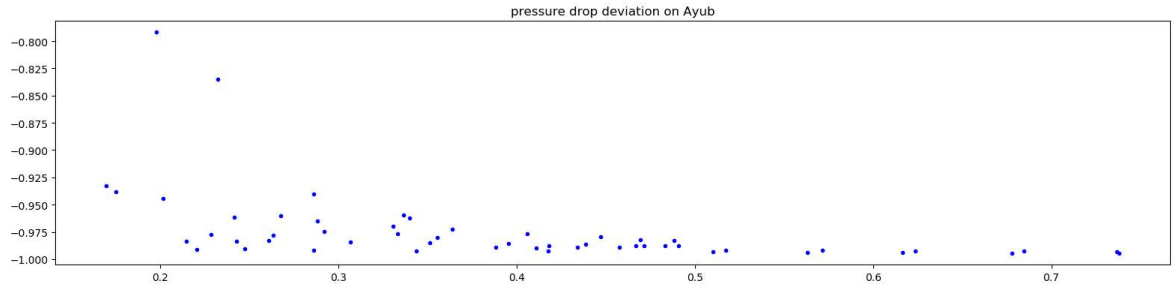
pressure drop deviation on Ayub
−0.800
−0.825
−0.850
−0.875
−0.900
−0.925
−0.950
−0.975
−1.000
0.2
0.3
0.4
0.5
0.6
0.7

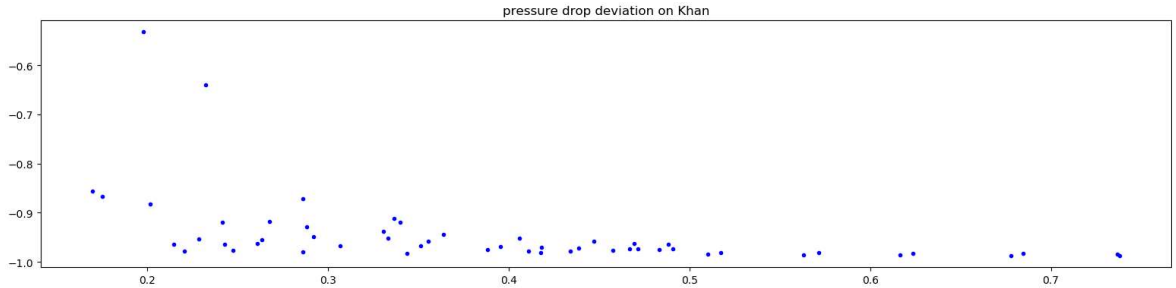
pressure drop deviation on Khan
−0.6
−0.7
−0.8
−0.9
−1.0
0.2
0.3
0.4
0.5
0.6
0.7

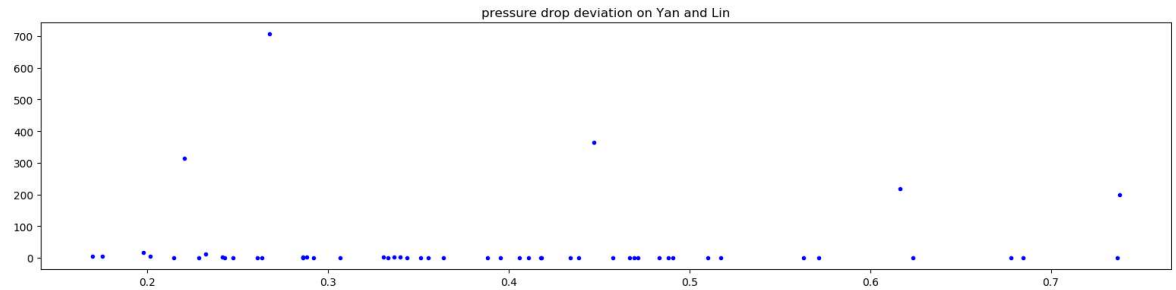
pressure drop deviation on Yan and Lin
700
600
500
400
300
200
100
0
0.2
0.3
0.4
0.5
0.6
0.7

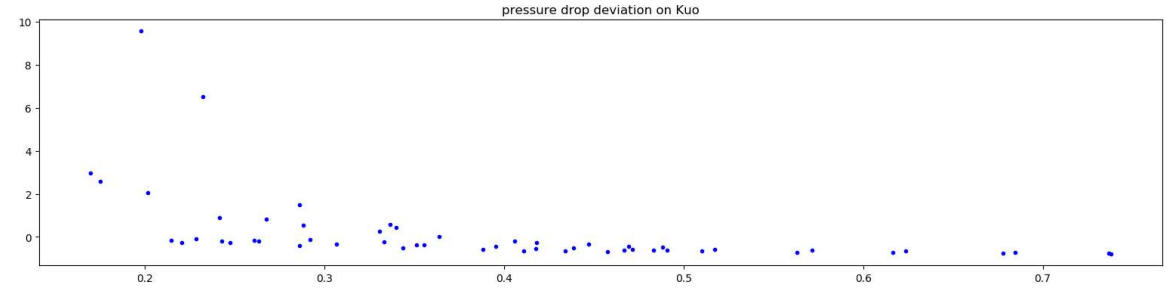
pressure drop deviation on Kuo
10
8
6
4
2
0
0.2
0.3
0.4
0.5
0.6
0.7

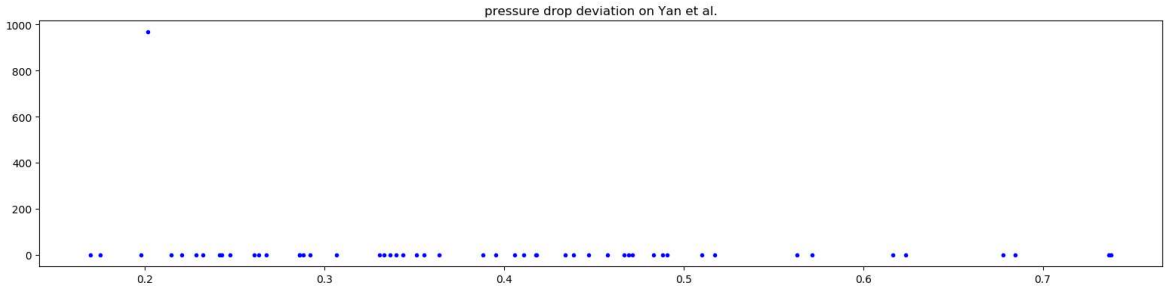
pressure drop deviation on Yan et al.
1000
800
600
400
200
0
0.2
0.3
0.4
0.5
0.6
0.7

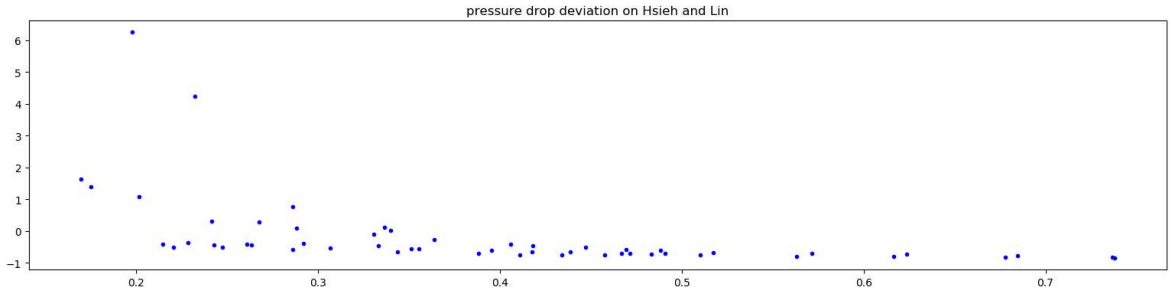
pressure drop deviation on Hsieh and Lin
6
5
4
3
2
1
0
−1
0.2
0.3
0.4
0.5
0.6
0.7

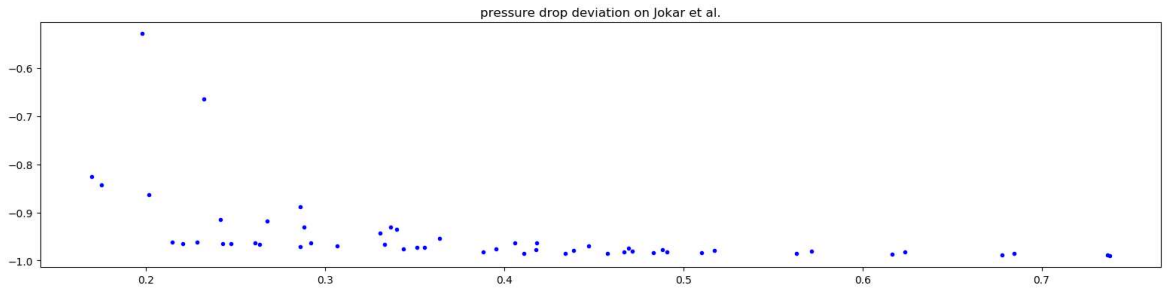
pressure drop deviation on Jokar et al.
−0.6
−0.7
−0.8
−0.9
−1.0
0.2
0.3
0.4
0.5
0.6
0.7

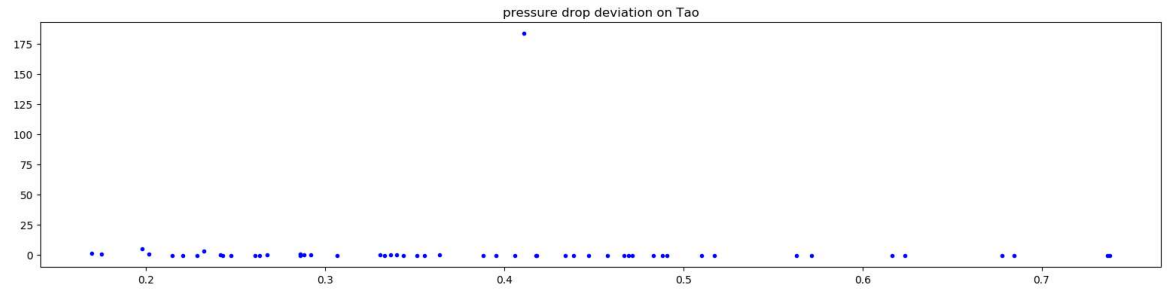
pressure drop deviation on Tao
175
150
125
100
75
50
25
0
0.2
0.3
0.4
0.5
0.6
0.7

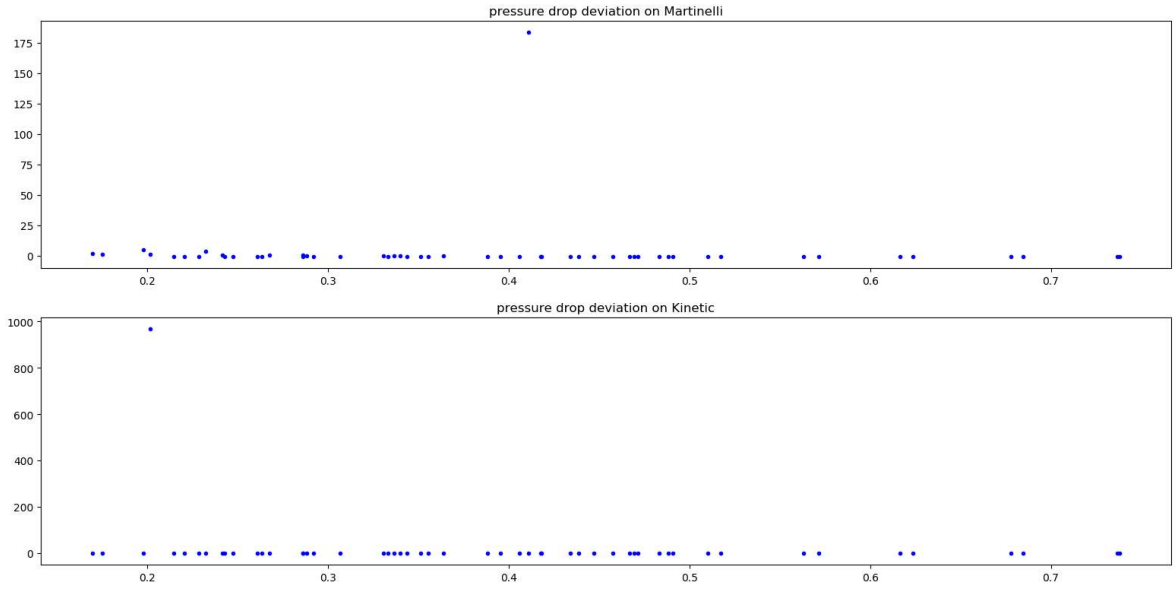
pressure drop deviation on Martinelli
175
150
125
100
75
50
25
0
0.2
0.3
0.4
0.5
0.6
0.7
pressure drop deviation on Kinetic
1000
800
600
400
200
0
0.2
0.3
0.4
0.5
0.6
0.7

N

Re-circulation Experiments: Temperature Profiles

Table N.1: Heat transfer rate to heat the working fluid from subcooled to saturated conditions compared to the total evaporator heat transfer rate, for the executed re-circulation experiments.

p_{evap} [bar]	$q_{evap,out}$	$\frac{\dot{Q}_{sl}}{\dot{Q}_{evap}}$ [%]
8.58	0.85	2.70
8.58	0.60	3.07
8.58	0.57	2.97
8.58	0.55	3.06
8.58	0.49	3.56
8.58	0.41	4.11
8.58	0.36	3.56
8.58	0.34	3.38

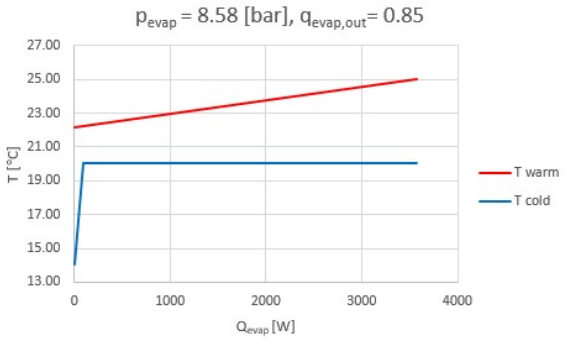
p_{evap} = 8.58 [bar], $q_{evap,out}$= 0.85
T [°C]
Q_{evap} [W]
T warm
T cold

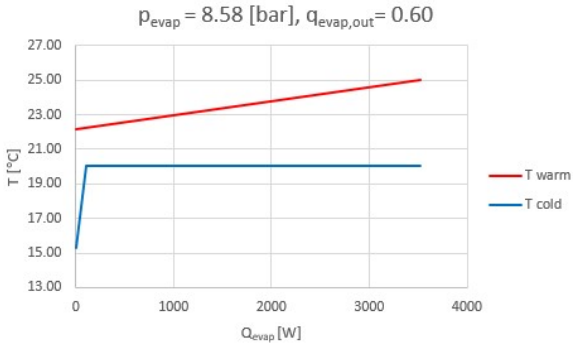
p_{evap} = 8.58 [bar], $q_{evap,out}$= 0.60
T [°C]
Q_{evap} [W]
T warm
T cold

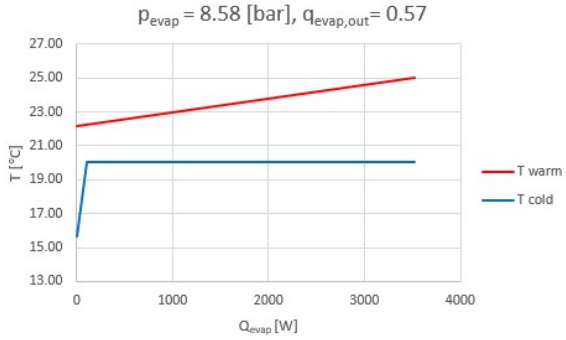
p_{evap} = 8.58 [bar], $q_{evap,out}$= 0.57
T [°C]
Q_{evap} [W]
T warm
T cold

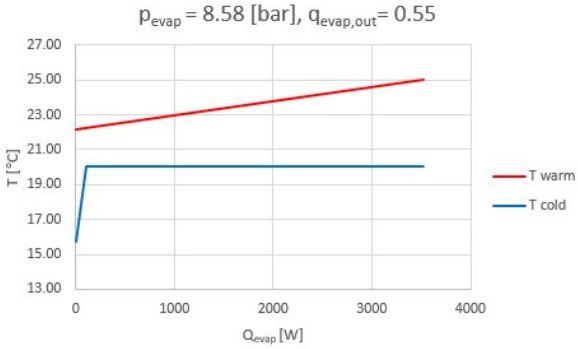
p_{evap} = 8.58 [bar], $q_{evap,out}$= 0.55
T [°C]
Q_{evap} [W]
T warm
T cold

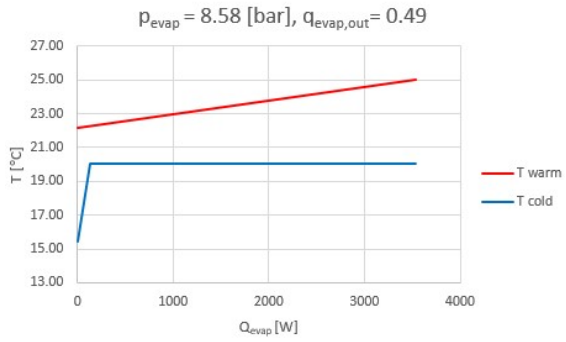
p_{evap} = 8.58 [bar], $q_{evap,out}$= 0.49
T [°C]
Q_{evap} [W]
T warm
T cold

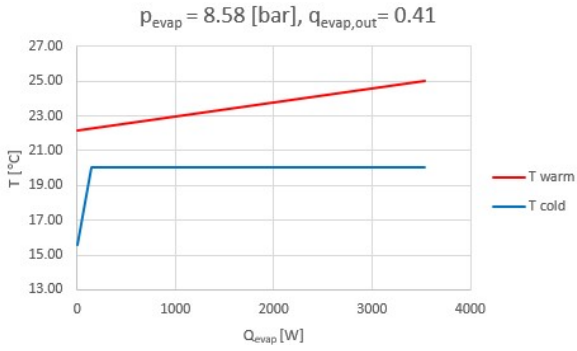
p_{evap} = 8.58 [bar], $q_{evap,out}$= 0.41
T [°C]
Q_{evap} [W]
T warm
T cold

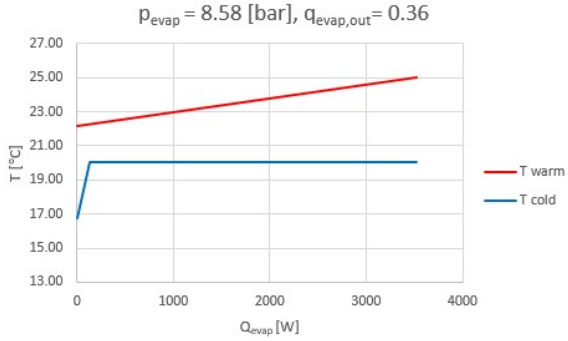
p_{evap} = 8.58 [bar], $q_{evap,out}$= 0.36
T [°C]
Q_{evap} [W]
T warm
T cold

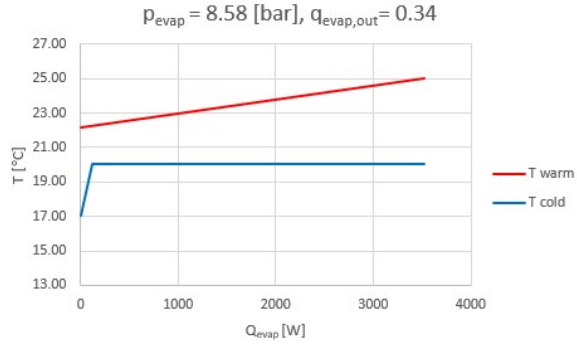
p_{evap} = 8.58 [bar], $q_{evap,out}$= 0.34
T [°C]
Q_{evap} [W]
T warm
T cold

BIBLIOGRAPHY

[1] T. F. Stoker, D. Qin, G.-K. Platter, M. Tignor, S. K. Allen, J. Boschun, A. Nauels, Y. Xia, V. Bex, and P. M. Midgley, *Climate Change 2013: The Physical Science Basis* (2013).

[2] J. Glenn, T. Gordon, and E. Florescu, *State of the Future,* Washington DC , 1 (2014).

[3] A. W. Harmsen, *Improving, testing and ver-ification of a small-scale OTEC research plant*, Tech. Rep. (2016).

[4] F. C. Geschiere, *OTEC condenser heat exchanger analysis*, Tech. Rep. (2018).

[5] P. André Van Strijp, *Impact of turbine performance on the operating conditions of a MW OTEC plant*, Tech. Rep.

[6] E. Ganic and J. Wu, *Comparative study of working fluids for otec power plants*, Tech. Rep. (Illinois University, Chicago (USA), 1979).

[7] R. . Mancini, J. K. Jensen, W. B. Markussen, and B. Elmegaard, *Comparison of Heat Transfer and Pressure Drop Correlations for Evaporation of Zeotropic Mixtures in Plate Heat Exchangers,* (2018), 10.18462/iir.gl.2018.1261.

[8] H. Arima, J. H. Kim, A. Okamoto, and Y. Ikegami, *Local boiling heat transfer characteristics of ammonia in a vertical plate evaporator,* International Journal of Refrigeration **33**, 359 (2010).

[9] *REFPROP,* .

[10] I. Bell, J. Wronski, S. Quoilin, and V. Lemort, *Coolprop,* .

[11] R. J. Goudriaan, *Performance analysis of ammonia and ammonia-water as working uids for Ocean Thermal Energy Conversion power plants*, Tech. Rep. (2016).

[12] M. Dahlgren, *Experimental study of transport phenomena in the condenser of an OTEC-Cycle,* (2018).

[13] B. Palm and J. Claesson, *Plate Heat Exchangers : Calculation Methods for Singleand Two-Phase Flow Plate Heat Exchangers : Calculation Methods for Single- and Two-Phase Flow,* **7632** (2006), 10.1080/01457630500523949.

[14] C. Panchal, D. Hillis, and A. Thomas, *Convective boiling of ammonia and Freon 22 in plate heat exchangers,* NASA STI/Recon Technical Report N **83** (1983).

[15] H. R. Engelhorn and A. M. Reinhart, *Investigations on heat transfer in a plate evaporator,* Chemical Engineering and Processing **28**, 143 (1990).

[16] B. Osterberger R. Slipcevic, *Nucleate Boiling Heat Transfer in Plate Heat Evaporator,* Ki Klima - Kalte Heizung (1990).

[17] O. Pelletier, *Propane as Refrigerant in Residential Heat Pumps*, Trita-REFR (Division of Applied Thermodynamics and Refrigeration, The Royal Institute of Technology, 1998).

[18] W. S. Kuo, Y. M. Lie, Y. Y. Hsieh, and T. F. Lin, *Condensation heat transfer and pressure drop of refrigerant R-410A flow in a vertical plate heat exchanger,* International Journal of Heat and Mass Transfer **48**, 5205 (2002).

[19] L. Margat, B. Thonon, and L. Tadrist, *Heat Transfer and Two-Phase Flow Characteristics during Convective Boiling in a Corrugated Channel,* in *Compact heat exchangers for the process industries: proceedings of the International Conference on Compact Heat Exhangers for the Process Industries,* edited by R. K. Shah, K. J. Bell, S. Mochizuki, and V. V. Wadekar (1997) pp. 323–329.

[20] D. Han, K. Lee, and Y. Kim, *Experiments on the characteristics of evaporation of R410A in brazed plate heat exchangers with different geometric configurations,* (2003), 10.1016/S1359-4311(03)00061-9, arXiv:arXiv:1011.1669v3 .

[21] Zeigarnik and Y. Albertovich, *Forced Convection Boiling,* Thermopedia (2011), http://dx.doi.org/10.1615/AtoZ.f.forced$_c onvection_b oiling$.

[22] V. Gudjonsdottir, *Analysis of external influences on an OTEC cycle,* (2015).

[23] Y. Yan and T. Lin, *Evaporation Heat transfer and pressure drop of R-134a inside a plate heat exchanger,* ASME International Mechanical Engineering Congress and Expostion **6**, 115 (2001).

[24] S. G. Kandlikar and V. Donowski, *Correlating Evaporation Heat Transfer Coefficient of Refrigerant R-134A in a Plate Heat Exchanger,* (2015).

[25] L. J. Kuikhoven, *Influence of the ammonia concentration on the performance of OTEC power cycles*, Tech. Rep. (2017).

[26] R. L. Amalfi, F. Vakili-Farahani, and J. R. Thome, *Flow boiling and frictional pressure gradients in plate heat exchangers. Part 2: Comparison of literature methods to database and new prediction methods,* International Journal of Refrigeration **61**, 185 (2016).

[27] Y. Yan and T. Lin, *Evaporation Heat Transfer and Pressure Drop of Refrigerant R-134a in a Plate Heat Exchanger,* **121** (2015).

[28] G. A. Longo and A. Gasparella, *Heat transfer and pressure drop during hydrocarbon refrigerant condensation inside a brazed plate heat exchanger,* International Journal of Refrigeration **33**, 944 (2007).

[29] M. S. Khan, T. S. Khan, M.-c. Chyu, and Z. H. Ayub, *Evaporation heat transfer and pressure drop of ammonia in a mixed configuration chevron plate heat exchanger,* International Journal of Refrigeration **41**, 92 (2014).

[30] S. C. Palmer, W. V. Payne, P. A. Domanski, S. C. Palmer, and W. V. Payne, *Evaporation and Condensation Heat Transfer Performance of Flammable Refrigerants in a Brazed Plate Heat Exchanger Brazed Plate Heat Exchanger,* (2000).

[31] J. Huang, T. J. Sheer, and M. Bailey-mcewan, *Heat transfer and pressure drop in plate heat exchanger refrigerant evaporators,* **5** (2012), 10.1016/j.ijrefrig.2011.11.002.

[32] Z. H. Ayub, *Plate Heat Exchanger Literature Survey and New Heat Transfer and Pressure Drop Correlations for Refrigerant Evaporators,* Heat Transfer Engineering **24**, 3 (2003).

[33] F. Taboas, M. Valle, M. Bourouis, and A. Coronas, *Assessment of boiling heat transfer and pressure drop correlations of ammonia / water mixture in a plate heat exchanger,* International Journal of Refrigeration **5** (2012), 10.1016/j.ijrefrig.2011.10.003.

[34] P. A. van Strijp, *Pieter André van Strijp*, Tech. Rep. (TU Delft, 2018).

[35] M. J. Moran, H. N. Shapiro, D. D. Boettner, M. B. Bailey, and M. J. F. of engineering thermodynamics Moran, *Principles of engineering thermodynamics*, 7th ed. ([Singapore] : Wiley, 2012).

[36] G. Towler and R. Sinnott, *Chemical Engineering Design*, second edi ed. (Elsevier Ltd., 2013).

[37] S. Arneth and J. Stichlmair, *Characteristics of thermosiphon reboilers,* **0729**, 385 (2001).

[38] R. W. Lockhart and R. C. Martinelli, *Proposed correlation of data for isothermal two-phase, two-component flow in pipes,* Chemical Engineering Progress **45**, 39 (1949).

[39] F. Vakili-Farahani, R. Amalfi, and J. Thome, *Two Phase Heat Transfer and Pressure Drop within Plate Heat Exchangers,* in *Encyclopedia of Two Phase Heat Transfer and Flow II: Special Topics and Applications. Volume 2: Boiling Using Enhanced Surfaces, Plate Heat Exchangers and Two Phase Devices* (1987) Chap. Chapter 4, pp. 145–215.

[40] H. Martin, *A theoretical approach to predict the performance of chevron-type plate heat exchangers,* Chemical Engineering and Processing: Process Intensification **35**, 301 (1996).

[41] D. Winkelmann, *Condensation of pure refrigerants and their zeotropic mixtures in plate heat exchangers,* Deutscher Kälte-und Klimatetechnischer Verein (2010).

[42] H. Kumar, *The Plate Heat Exchanger: construction and design.* in *First U.K. National Conference on Heat Transfer* (Elsevier, 1984) pp. 1275–1288.

[43] W. W. Focke, J. Zachariades, and I. Olivier, *The effect of the corrugation inclination angle on the thermohydraulic performance of plate heat exchangers,* International Journal of Heat and Mass Transfer **28**, 1469 (1985).

[44] B. Thonon, *Design method for plate evaporators and condensers,* BHR Group Conference Series Publication **18**, 37 (1995).

[45] T. S. Khan, M. S. Khan, and Z. H. Ayub, *Single-Phase Flow Pressure Drop Analysis in a Plate Heat Exchanger,* Heat Transfer Engineering **38**, 256 (2017).

[46] Z. jian LUAN, G. min ZHANG, M. cheng TIAN, and M. xiu FAN, *Flow resistance and heat transfer characteristics of a new-type plate heat exchanger,* Journal of Hydrodynamics **20**, 524 (2008).

[47] Z. H. Ayub, *Plate Heat Exchanger Literature Survey and New Heat Transfer and Pressure Drop Correlations for Refrigerant Evaporators,* **7632** (2010), 10.1080/01457630304056.

[48] T. S. Khan, M. S. Khan, M.-c. Chyu, and Z. H. Ayub, *Experimental investigation of evaporation heat transfer and pressure drop of ammonia in a 60 chevron plate heat exchanger,* **5** (2012), 10.1016/j.ijrefrig.2011.10.018.

[49] W. S. Kuo, Y. M. Lie, Y. Y. Hsieh, and T. F. Lin, *Condensation heat transfer and pressure drop of refrigerant R-410A flow in a vertical plate heat exchanger,* International Journal of Heat and Mass Transfer **48**, 5205 (2005).

[50] Y.-Y. Yan, H.-C. Lio, and T.-F. Lin, *Condensation heat transfer and pressure drop of refrigerant R-134a in a plate heat exchanger,* International Journal of Heat and Mass Transfer **42**, 993 (1999).

[51] Y. Y. Hsieh and T. F. Lin, *Evaporation heat transfer and pressure drop of Refrigerant R-410A flow in a vertical plate heat exchanger,* International Journal of Heat and Mass Transfer **125** (2003), 10.1016/j.ijheatmasstransfer.2005.07.023.

[52] A. Jokar, M. H. Hosni, and S. J. Eckels, *Dimensional analysis on the evaporation and condensation of refrigerant R-134a in minichannel plate heat exchangers,* Applied Thermal Engineering **26**, 2287 (2006).

[53] X. Tao and C. A. Infante, *Heat transfer and pressure drop during condensation in plate heat exchangers : assessment of correlations and a new method,* , 1 (2018).

[54] P. Stephan, S. Kabelac, M. Kind, H. Martin, D. Mewes, and K. Schaber, , 2nd ed. (Springer, 2010).

[55] D. Chisholm, *A theoretical basis for the Lockhart-Martinelli correlation for two-phase flow,* International Journal of Heat and Mass Transfer **10**, 1767 (1967).

[56] B. Thonon, A. Feldman, L. Margat, and C. Marviilet, *Transition from nucleate boiling to convective boiling in compact heat exchangers,* **20**, 592 (1997).

[57] A. J. Holt, B. J. Azzopardi, and M. W. Biddulph, *Calculation of two-phase pressure drop for vertical upflow in narrow passages by means of a flow pattern specific model,* Chemical Engineering Research and Design **77**, 7 (1999).

[58] K. Mishima and T. Hibiki, *Some Characteristics of Air-Water Two Phase Flow in Small Diameter Vertical Tubes,* (1996).

[59] Y. Koizumi, M. Monde, N. Nagai, M. Shoji, and Y. Takata, *Chapter 1 - Outline of Boiling Phenomena and Heat Transfer Characteristics,* in *Boiling Research and Advances* (2017).

[60] R. Radermacher and Y. Hwang, *Vapor Compression Heat Pumps* (CRC Press Tayor & Francis Group, 2005).

[61] W. R. van Wijk, A. S. Vos, and S. J. D. van Stralen, *Heat Transfer to Boiling Binary Liquid Mixtures,* Chem. Engng. Sci. (1956).

[62] D. Jung and R. Radermacher, *Prediction of evaporation heat transfer coefficient and pressure drop of refrigerant mixtures,* (1993).

[63] E. Djordjevic and S. Kabelac, *Flow boiling of R134a and ammonia in a plate heat exchanger,* International Journal of Heat and Mass Transfer **51**, 6235 (2008).

[64] K. Koyama, H. Chiyoda, H. Arima, and Y. Ikegami, *Experimental study on thermal characteristics of ammonia flow boiling in a plate evaporator at low mass flux,* International Journal of Refrigeration **8**, 0 (2014).

[65] O. Dumont, R. Dickes, R. Daccord, S. Quoilin, and V. Lemort, *Modelling of organic Rankine cycle power systems in off-design conditions : An experimentally-validated comparative study,* **123** (2017).

[66] T. Morisaki and Y. Ikegami, *Performance Evaluation of Heat Exchangers in OTEC Using Ammonia/Water Mixture as Working Fluid,* Open Journal of Fluid Dynamics **3**, 302 (2013).

[67] S. M. W. J. R. Couper, W. R. Penney, J. R. Fair, *Chemical Process Equipment: Selection and Design,* Organic Process Research & Development **9**, 373 (2005).

[68] E. Jones and G. Tsatsaronis, *SciPy: Open source scientific tools for Python,* (2001).

[69] D. KARABOĞA, *A Simple and Global Optimization Algorithm for Engineering ProblemBs: Differential Evolution Algorithm,* Turkish Journal of Electrical Engineering and Computer Science **12**, 53 (2014).

[70] J. van Senden, *Design of 3MW OTEC Power Plant,* (2019).

[71] A. Muley and R. M. Manglik, *Experimental Study of Turbulent Flow Heat Transfer and Pressure Drop in a Plate Heat Exchanger With Chevron Plates,* Journal of Heat Transfer-transactions of The Asme - J HEAT TRANSFER **121**, 110 (1999).

[72] R. Shah and W. Focke, *Plate heat exchangers and their design theory,* Heat Transfer Equipment Design , 227 (1988).

[73] J. A. Dopazo and J. Fernández-Seara, *Experimental evaluation of an ejector as liquid re-circulator in an overfeed NH3 system with a plate evaporator,* International Journal of Refrigeration (2011), 10.1016/j.ijrefrig.2010.12.023.

[74] A. Gac, *Automatisme des systemes frigorifiques,* Supplement à la Revue Gènèrale du Froid Janvier (1974).

[75] B. Elhub and M. A. A. AZIZ, *Review of ejector design parameters and geometry for refrigeration and air conditioning application,* Computer Applications in Environmental Sciences and Renewable Energy , 13 (2014).